Airborne contamination in the indoor environment and its implications for dose

Andersson, Kasper Grann; Roed, Jørn; Byrne, M.A.; Hession, H.; Clark, P.; Elahi, E.; Byrskov, A.; Hou, Xiaolin; Prip, Henrik; Olsen, S.K.; Roed, T.

Publication date:
2004

Document Version
Publisher's PDF, also known as Version of record

Risø-R-1462(EN)

Airborne contamination in the indoor environment and its implications for dose

K.G. Andersson, J. Roed, M.A. Byrne*, H. Hession*, P. Clark+, E. Elahi+, A. Byskov#, X.L. Hou, H. Prip, S.K. Olsen, T. Roed#

* National University of Ireland, Galway, Ireland
+ Imperial College of Science, Technology and Medicine, London, UK
# Rigshospitalet, Copenhagen, Denmark

Risø National Laboratory
Roskilde
Denmark
April 2004

Authors: K.G. Andersson, J. Roed, M.A. Byrne, H. Hession, P. Clark, E. Elahi, A. Byskov, X.L. Hou, H. Prip, S.K. Olsen, T. Roed
Title: Airborne contamination in the indoor environment and its implications for dose
Department: Radiation Research Department

Risø-R-1462(EN)
April 2004

Abstract:

Previous work has indicated that radiation doses from deposition on human skin, hair and clothing may contribute significantly to the dose received after a major nuclear accident, such as that, which happened at Chernobyl in 1986. The available data was, however, sparse and associated with considerable variation, clearly showing a need for further investigations to verify preliminary conclusions, examine processes in greater detail and identify important factors causing the observed parameter variation. For instance, the impacts of thermophoresis, electrophoresis, skin moisture and wind speed on the deposition of contaminant aerosol were examined, and since the previous measurements had indicated that elemental iodine could be a particularly problematic contaminant, experimental work was additionally undertaken to examine the process of deposition of this species to skin. Since both clearance and percutaneous penetration of deposited contaminants could play important roles in determining doses, experimental programmes were dedicated to the identification of parameters of interest in these contexts. Also doses from contamination on different surfaces in the indoor environment have in the past traditionally been neglected, and a theoretical approach, based on measurements, was developed for accurate prediction of these doses under different conditions. Also resuspension of deposited matter and its role in dose formation, by subsequent deposition or inhalation, was investigated through experiments. Contact transfer of contaminants from an indoor surface to human skin may give yet another contribution to dose and also the relevant parameters in this direction were examined experimentally. The ultimate goal of the investigations was to enable the determination of the various contributions to dose in a contaminated indoor environment. A model methodology was developed and an example of its use was given. It was found that after a major nuclear accident, doses from indoor deposition to humans, deposition on indoor surfaces and inhalation in the indoor environment would all be important to consider.

ISSN 0106-2840
ISBN 87-550-3317-2
87-550-3318-0(Internet)

Contract no.:
FIKR-CT-2000-00043

Group's own reg. no.:
1415505-18

Sponsorship:
CEC FP5

Cover :

Pages: 100
Tables: 28
Figures: 53
References: 94

Risø National Laboratory
Information Service Department
P.O.Box 49
DK-4000 Roskilde
Denmark
Telephone +45 46774004
bibl@risoe.dk
Fax +45 46774013
www.risoe.dk

Contents

Preface

This report constitutes the final report of the CEC FP5 project 'Quantification of the distribution of radiation doses received by humans through the various pathways in a contaminated indoor environment' (acronym: INDOOR DOSE) under the Research and Training Programme in the field of nuclear energy, contract FIKR-CT-2000-00043.

The project follows up on work initiated by the partners under the FP4 project contract FI4PCT950019, and measurement techniques developed in that project partially form the basis for the investigations made in the INDOOR DOSE project. Whereas the FP4 project generated data of a predominantly generic nature, much of the INDOOR DOSE project work has been dedicated to improving the understanding of influences of various factors, thus advancing the background for modelling of doses received from contamination of humans. Moreover, investigations have been made in INDOOR DOSE, which enable detailed evaluations of other contributions to dose in a contaminated indoor environment, whereas the FP4 project solely considered doses from contaminant deposition on humans. The scope of this project is thus both considerably wider and more detailed than that of the previous.

The authors wish to acknowledge the contributions to the work by Dr. S.A.M. Hotchkiss and Professor A.J.H. Goddard at Imperial College, and Dr. Kevin McNamara at Galway.

Summary

The reported work was carried out under four work packages, together aimed at improving the knowledge of the mechanisms that determine the contributions to dose in a contaminated indoor environment.

The overall objective of the first of these work packages was to examine experimentally the processes and parameters that govern the deposition of radioactive contaminants to humans. The influence on aerosol deposition of a series of physical parameters (e.g., related to electrostatics, temperature differences, surface moisture and movement) was examined. Some mechanisms, such as thermophoresis, seem to generally be of a minor importance, whereas for instance the surface moisture of skin seems to have significant influence. Studies of deposition of aerosol to human hair were carried out, and here distinction was made between deposition velocities to distal and proximal ends of hair strands. This enabled detailed beta dosimetric modelling assessments. An experiment series was designed to investigate the deposition of elemental iodine to skin of hairless rats. This experiment confirmed earlier assumptions on elemental iodine deposition. Wind-tunnel studies employing fluorescent tracers were carried out to simulate outdoor deposition to humans. A strong influence of air velocity and turbulence intensity on the deposition velocity was recorded.

The investigations in the second work package had the objective of examining the clearance and penetration of contaminants deposited to humans. A specially designed fluorescence scanning system was used to examine the natural clearance rates of various types of contaminant aerosol on humans. Particles in the >2 µm range were generally found to have very short half-lives on human skin (hours-days), whereas particles in the 1 µm range appear to remain on the skin until it sheds from the surface of the body. Using in vitro techniques employing a confocal microscope for particle visualisation, the effects of particle penetration into skin pores and hair follicles were studied. In these experiments, no particle penetration through the epidermis was recorded. However, vigorous flexing of skin is believed to have the potential to effect dermal particle penetration. The penetration of aerosol through clothing and onto skin was examined and found to be of very little significance.

The third work package was aimed at investigating the redistribution of contamination in the indoor environment. One objective was here to examine the characteristics of resuspended indoor contaminant particles. Experiments have been conducted to determine the changes that occur in the size distribution of the deposited contaminant particles and the bearing that this would have on the deposition to humans of the subsequently resuspended particles. In other experiments, the focus was on determining resuspension factors from realistic mechanical impact in the indoor environment. Further, a series of experiments have been carried out to determine the relative importance of the various body surfaces in contributing to elevated breathing zone concentrations of contaminants. Another mechanism that may be responsible for indoor contaminant redistribution is contact transfer. A series of measurements showed that this mechanism is significant even for small particles in the 0.1 µm range. Surface moisture generally enhances transfer, and the transfer to dry gloves was found to vary considerably according to the material characteristics of the contaminated surface.

The fourth work package integrates the experimental findings in a model methodology that can be applied to estimate the various contributions to dose in the indoor environment. The model methodology comprises formulae and parameters for estimation of doses from deposition on humans, inhalation of contaminants, deposition on surfaces in the indoor environment and skin contact transfer, and incorporates the influences of resuspension. An example is used to illustrate the methodology in relation to a situation involving a large nuclear power plant accident. In this case, doses from deposition on both skin and indoor surfaces, as well as from inhalation, proved significant. Resuspension and contact transfer were found to generally play a less significant role in connection with accident scenarios of the modelled type. However, in other perceivable contamination scenarios, also these may be important to consider. Generally, elemental iodine and the radiocaesium isotopes contribute most to the doses received in the scenario. The methodology is applicable in forming more detailed modules for the assessment of implications of indoor contamination in European standard models for nuclear

accident consequence assessment. At the same time, many of the project findings will have relevance also for situations involving non-radioactive exposure of humans in an indoor environment.

Introduction

Background

In nuclear preparedness, there has traditionally been very little focus on the contributions to dose from contamination in the indoor environment. Studies of doses received in living areas have with a few exceptions been restricted to only cover contributions from contaminant inhalation, contaminant consumption and external exposure from sources outside dwellings. In those few studies, where contaminants on surfaces (e.g., indoor walls, ceiling, floor) within the indoor environment have been considered (Andersson et al., 1995), the dose estimates were generally based on crude point kernel calculations, and only related to the deposition of one radionuclide – ^{137}Cs. Moreover, since then, important knowledge has arisen concerning the behaviour of radio-contaminants in the indoor environment. In the reported work, state-of-the-art knowledge has been applied together with detailed Monte Carlo dose calculations to determine the doses that may be received in various indoor geometries from a wide range of contaminants that could be relevant to for instance a major nuclear power plant accident.

One potentially important contribution to dose in the indoor environment, which has in the past attracted very little attention is that from contaminant deposition on the human body (skin, hair and clothing). In the European FP4 project FI4PCT950019, preliminary studies of the parameters governing such doses were made. The focus was then on the development of experimental methods for evaluating aerosol deposition velocities on skin, hair and clothing rather than actual data generation to establish parameters. Nevertheless, important data were generated, albeit for a limited range of conditions, which confirmed that skin deposits can constitute a significant proportion of whole body dose, but also highlighted the extreme complexity of the deposition processes. Based on the developed techniques, the consortium partners have in the INDOOR DOSE project, as reported in this publication, carried out further experimentation to identify parameter sets that would be valid under realistic circumstances, thereby also clarifying the reasons for the considerable variation in the deposition velocities recorded under the previous contract, where the influences of a number of specific factors were not distinguished. In the earlier work, dosimetric modelling also showed that the clearance rate of particles from skin (which may be influenced by the penetration of particles into the skin structure) is an important determinant of dose, and the very limited data that had previously been produced on this topic was therefore extended and refined in the INDOOR DOSE project. In addition, earlier modelling had also highlighted the significance of doses associated with deposition of elemental iodine on skin, relative to particle deposition, but gaseous deposition onto human body surfaces had never been experimentally investigated. Therefore, an experimental study of this topic was undertaken under the INDOOR DOSE project. Further, the role of indoor resuspension in contributing to aerosol deposition on the human body and also to increasing inhalation doses was identified as a topic that clearly merited further investigation. Work packages in the INDOOR DOSE project were therefore specifically dedicated to the investigation of these phenomena.

Together with available data from the literature, the experimental data generated in INDOOR DOSE formed the foundation for the ultimate project goal: a holistic model of radiation doses received through the various pathways in a contaminated indoor environment, with relevance both to acute accident scenarios, and to the industrial environment.

Generally applied methodologies

The generally applied technique for assessment of deposition velocities involves the emission in a test room with human volunteers of tracer aerosol of well-defined sizes. Tracer particles larger than 1 µm in diameter are produced by labelling commercially available monodisperse silica spheres (Phas Sep Spherisorb, Deeside Ind. Park, Queensferry, Clwyd, UK) with neutron activatable tracers (primarily dysprosium). The particles are emitted using a Palas RBG 1000 Powder Dispersion Generator. The submicroneous particles are generated by nebulisation of indium 2,4-pentanedionate powder dispersed in alcohol. Test persons enter the room after the tracer aerosol has been released and mixed well in the room by other personnel. The period of exposure is one hour. A Berner Low Pressure Impactor is applied to examine the size distributions of the emitted particles, which have generally been found to be relatively stable and well defined. After the aerosol deposition to human skin, sampling is performed by three consecutive thorough wipes of a well defined area of the exposed skin with ethanol-soaked Whatman 542 filter paper. This latter part of the technique has been validated through comparison with scanning measurements of fluorescent particles directly on the skin (Fogh et al., 1999). The amounts of indium and dysprosium on the filter paper samples are determined in a gamma spectrometer after sample neutron activation. The deposition velocities of the particles represented by the tracers can then be found from the tracer mass on the samples and the time-integrated air concentration in the test room over the deposition period, according to the formula:

$$V_d = \frac{Tracer\ \ mass\ \ per\ \ unit\ \ of\ \ area}{Average\ \ air\ \ concentration\ \cdot\ Exposure\ \ time\ \cdot\ Wiping\ \ efficiency}$$

The whole technique is described in greater detail by Fogh et al. (1999). The same types of tracer particles were applied in studies of contaminant particle resuspension.

The techniques applied in studies of clearance and percutaneous penetration represent further developments of the techniques established under the previous contract and are described in detail under the relevant sections of this report.

1 Deposition of contaminants on humans

Under contract FI4PCT950019, a series of experiments were carried out to describe the general parameters in relation to the deposition phase. It was found in connection with these experiments that deposition velocities of a given type of particles to essentially the same type of human surface could vary considerably. Part of the work on deposition under the INDOOR DOSE project was thus dedicated to determining the possible sources of variation and their relative significance. The investigations are useful for the identification of skin deposition parameters that would be likely to apply to the 'average' person living/working in an exposed area, and conversely also to estimate significantly different values for critical population groups.

Contaminants deposited on outer and inner (distal and proximal) parts of the hair strand will lead to significantly different beta doses. To facilitate detailed modelling of these beta dose contributions, deposition parameters were under this contract studied separately for the different parts of the hair strand.

The deposition velocity of elemental iodine to live skin was studied for probably the first time ever, as it was found under the previous contract that elemental iodine could be a very significant contributor to dose from skin contamination after a major nuclear accident.

Finally, the effect of outdoor conditions (notably wind speed) on deposition to humans was studied, to provide a link between the observations made under indoor conditions and parameter deviations attributable to outdoor conditions.

1.1 Influences of physical parameters on deposition velocities to human skin

Previous work carried out under the contract F14PCT950019 has shown deposition velocities to skin to be high compared with those to other surfaces in the indoor environment. The influence of several physical parameters might be significant in this context, and a series of experiments were carried out to investigate into the effect that these parameters have on the recorded deposition velocities to human body surfaces.

According to Ficks law, the contributions to particle flux (j_p) due to diffusion, sedimentation and 'external' forces (e.g., thermophoresis, electrophoresis) can be added (Friedlander, 1977):

$$j_p = -D \nabla N + \nu N + \nu_{ext} N,$$

where D is the diffusion coefficient, N is the particle number concentration, ν is the drift velocity due to sedimentation, and ν_{ext} is the drift velocity due to 'external' forces. According to Stokes law (Friedlander, 1977), the drift velocity due to sedimentation can be expressed by:

$$\nu = \frac{\rho_p d_p^2 C}{18\eta} g ,$$

where ρ_p is the particle density, d_p is the particle diameter, C is the slip correction factor, g is the gravitational constant, and η is the kinematic velocity. As the particle flux is directly proportional to the deposition velocity ($V_d = j_p/N$), the sum of the individual contributions to deposition velocity from the various mechanisms gives the total deposition velocity.

In the following the influences of some of the ‘external’ forces will be discussed.

1.1.1 Influence of electrophoresis

The influence on V_d of e.g., electrophoresis at various field strengths can thus be theoretically compared with the contributions to V_d of sedimentation and diffusion (neglecting any influence of turbulence). Figure 1.1.1 shows a typical picture (Otani et al., 1989; Opiolka et al., 1994). As can be seen, the influence of even strong electrostatic fields is of very little importance for supermicroneous particles.

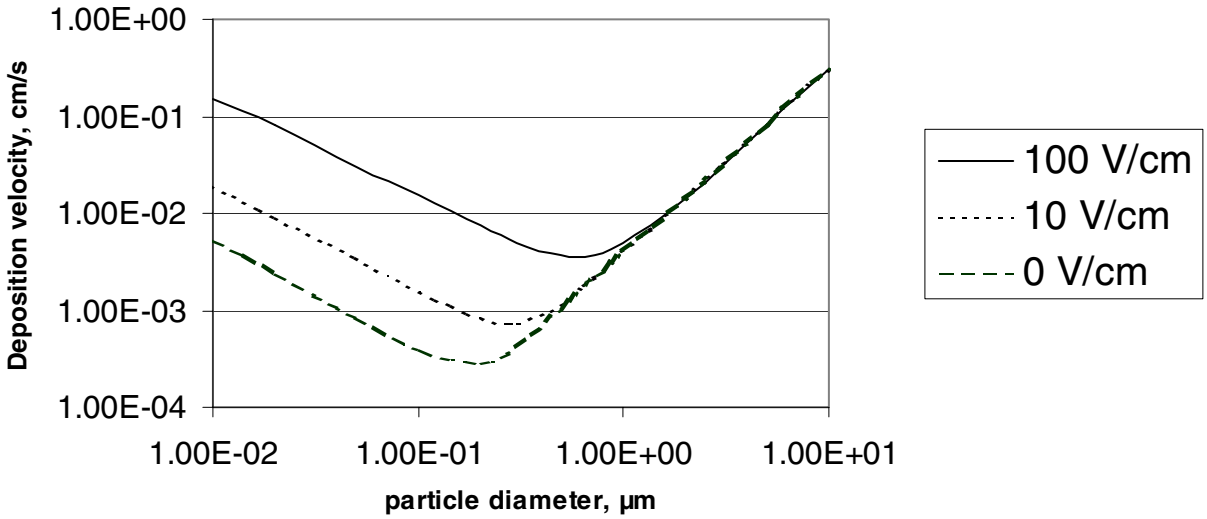

Fig. 1.1.1. A theoretical example of particle deposition velocities versus particle size for particles with single negative charges in various electrostatic fields.

The electrophoretic influence on particles in air is in the indoor environment governed by differences between the triboelectric voltage potentials on the various indoor surfaces, including humans. In two experiments, these voltages were continuously measured on sampling surfaces (primarily test persons) as well as some other surfaces, under 'normal' indoor environment conditions, using a JCI 140 Static Monitor for non-contact measurement of surface voltage. The office, furniture and number and approximate location of test persons corresponded to the conditions in the numerous office experiments conducted under the previous contract.

Some typical values of surface voltage, as measured in one of the experiments, are given in Table 1.1.1. As can be seen, the surface voltages ranged from some -250 to +270 V. In most cases, the voltages were within -50 to +50 V, but associated with large fluctuations within the 1-hour measurement period. Often surfaces starting with a negative potential will become positive over few minutes and vice versa. In another experiment the corresponding surface potentials on the same test persons increased rather consistently over the measurement period, from a value within the range of -10 to -40 volts at the beginning to a value of -2 to -12 volts at the middle of the experiment and to a value of +1 to +17 volts at the end. Also the voltage potentials of other surfaces in the environment were measured, and on these comparatively low positive or negative values were recorded. A PC monitor was found to have the highest potential (ca. 30-40 V).

The electrostatic fields generated by surface voltage differences were in the conducted experiments on average over the experiment period generally less than 1 V cm^{-1}. Particle size measurements made during the experiments using a Berner low-pressure impactor confirmed that of the two particle groups examined, one had a typical aerodynamic diameter of ca. 0.7 µm, whereas that of the other was ca. 2.5 µm. At these particle sizes, and with low electrostatic fields, the influence on particle deposition velocity of electrophoresis is expected to be of very

little significance compared with other influences (see Fig.1.1.1), and changes in voltage differences on surfaces in the experiments were for none of the two particle sizes found to lead to any significant changes in deposition velocities recorded to the test persons.

Table 1.1.1. Triboelectric surface voltages (in kV) on various body part of volunteers throughout an office experiment. Voltage measurement intervals are given in brackets.

Surface	V (2-4 min.)	V(16-18 min)	V(24-26 min)	V(34-36 min)	V(43-45 min)	V(52-55 min)
KGA Left Arm	-0.15	0.03	0.02	0	0.01	0
KGA Left Hand	-0.06	0	0	-0.02	-0.01	-0.01
KGA Head Left side	0.08	0.02	0.01	0	-0.01	-0.01
KGA Head Right side	0.01	0.01	-0.02	-0.06	-0.1	-0.09
KGA Right Arm	-0.04	0	0	0	0.01	-0.06
KGA Right Hand	-0.09	-0.03	0	-0.04	-0.05	-0.25
Chr Left Arm	-0.09	-0.06	-0.07	-0.07	-0.18	-0.1
Chr Left Hand	-0.07	-0.01	-0.07	-0.01	-0.09	-0.04
Chr Head Left side	0.02	-0.17	0.04	0.04	-0.07	0.27
Chr Head Right side	0.02	-0.15	0.06	0.05	-0.09	0.09
Chr Right Arm	-0.25	-0.1	-0.11	-0.11	-0.11	-0.1
ChrRight Hand	-0.12	-0.04	-0.07	-0.08	-0.04	-0.05

In a separate experiment series, the influence of a TV screen was examined. Here the surface voltage was during the experiment 11-13 kV (in comparison with, e.g., only ca. 30 V on a modern computer screen). This was found to significantly affect the deposition velocity of the 0.7 µm particles to the hand and arm of a volunteer near the screen, whereas the deposition velocity of the 2.5 µm particles was unaffected. This is qualitatively in good agreement with the theoretical considerations presented above in Figure 1.1.1. For the larger particles the deposition will to a greater extent be gravity-driven, whereas the submicron particles would be expected to be much more susceptible to electrophoretic influences. Figure 1.1.2, representing averages of four deposition measurements, gives an impression of the potential impact of sitting near a TV screen during aerosol deposition. Even a TV that is not switched on typically has a surface voltage of several kV.

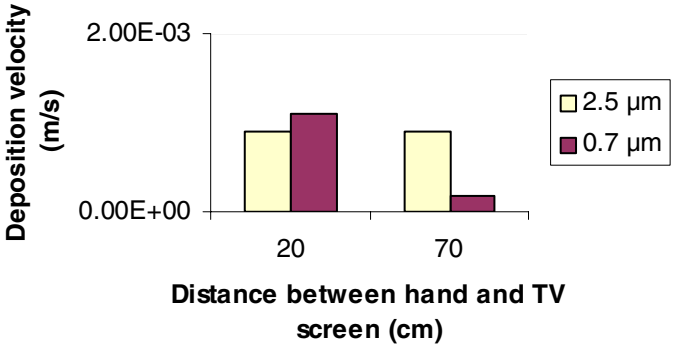

Fig. 1.1.2. Deposition velocities of 0.7 and 2.5 µm particles on a test person near a TV screen with a surface voltage of 11-13 kV (averages of 4 samples; standard deviations of 15-30 %). One hand of a volunteer was fixed at a distance of 20 cm and the other hand at a distance of 70 cm from the TV screen, thus eliminating personal differences in, e.g., surface moisture.

It might be expected that also the deposition on clothing could be influenced by triboelectrification. A series of experiments were carried out to investigate the triboelectric influence on particle deposition to different types of fabric. Some of the samples were worn by test persons, whereas others were carefully kept grounded throughout the duration of the experiment. Various synthetic fibre fabrics were investigated, together with samples of pure cotton, 50 % cotton and 50 % polyester and pure wool. However, because of their conductive properties, clothes made of wool, silk, cotton, and most other natural fibres usually retain very little charge due to rapid leakage to ground through the body (Holdstock, 1997), and not even clothing pieces containing synthetic fibres were in these experiments found to retain much charge. The corresponding measurements of deposition velocities did not reveal any influence of triboelectrification.

1.1.2 Influences of temperature differences

Temperatures may influence aerosol movement and deposition in different ways.

Transport of particles generated by positive or negative temperature gradients (thermophoresis) may cause enhanced deposition to colder surfaces and reduced deposition to warmer surfaces. The thermophoretic velocity can be expressed theoretically on the following form (Camuffo and Bernardi, 1996):

$$V_T = -B\frac{k_a}{p}\frac{dT}{dl},$$

where B is a coefficient accommodating particle size (by Knudsen number), and including the thermal conductivities k_a and k_p of respectively particle and air, p is the atmospheric pressure and dT/dl is the temperature gradient (temperature difference per unit of distance).

The elevated temperatures of human skin surfaces, compared to those of practically the rest of the indoor environment, would, according to theory (Tsai & Liang, 2001), lead to thermophoretic *repulsion* of particles approaching the skin. This is therefore not the explanation for the higher deposition velocities on skin compared with other surfaces in the indoor environment. Also, according to theory, the influence of thermophoresis on particle deposition would generally be expected to be very limited for particles greater than ca. 0.5 µm (Camuffo and Bernardi, 1996; Opiolka et al., 1994), and even relatively high temperature gradients of the order of 10 °K cm^{-1} would in any case lead to modest thermophoretic velocities (typically of the order of 10^{-3} - 10^{-4} cm s^{-1} for particles in the 0.1-0.2 µm range, where the effect is greatest).

A series of tests were carried out to examine the possible influence on skin deposition velocity of seasonal variations in the difference between human skin temperature and indoor air temperature. Part of this test was made under summertime conditions, where the difference between the skin temperature of volunteers and ambient air was ca. 5 °C. The other part was carried out under wintertime conditions, where the corresponding temperature difference was ca. 10 °C. The temperature differences are thus higher in the latter experiment, and as consistency was sought in all details of the experiments (including furnishing and positions of test persons), temperature gradients would be expected to be somewhat greater in that experiment. However, these natural variations were not found to have any significant bearing on the deposition of 0.7 and 2.5 µm particles.

It should be stressed that this does not imply that temperature differences are without importance in connection with deposition. Turbulence due to convection may be important in the vicinity of heat sources. An experiment has been carried out to examine the deposition to 8 cloth patches fixed at different distances from a radiator. Throughout this experiment the temperature profile between the radiator and the patches was carefully measured, and also the humidity and wind velocity were recorded. In this case, the elevated temperature was only found to have significant impact on deposition to humans (represented by cotton patches) very near the heat source. Figure 1.1.3 shows the measured temperature profile (average over the experiment period), generally declining with increasing distance. The temperatures were measured in the exact locations of the cotton patches.

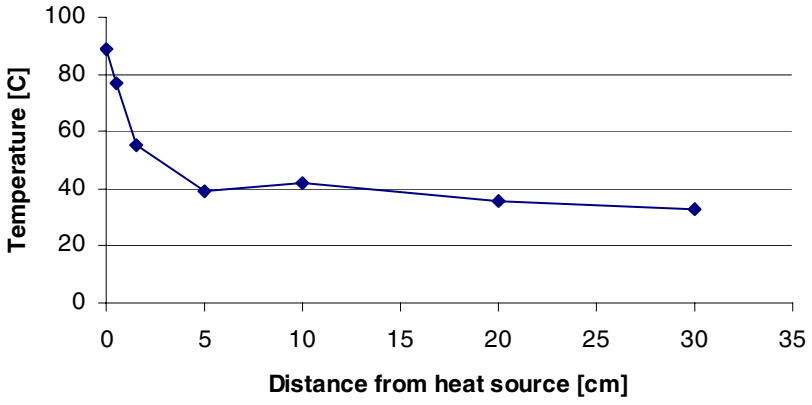

Fig. 1.1.3. Average temperature as a function of distance from the radiator in the experiment.

Figure 1.1.4 shows a graphical representation of the recorded deposition velocities of 0.7 µm aerosol to patches at different distances from the radiator. Figure 1.1.5 shows a corresponding representation of deposition velocities of 2.5 µm aerosol.

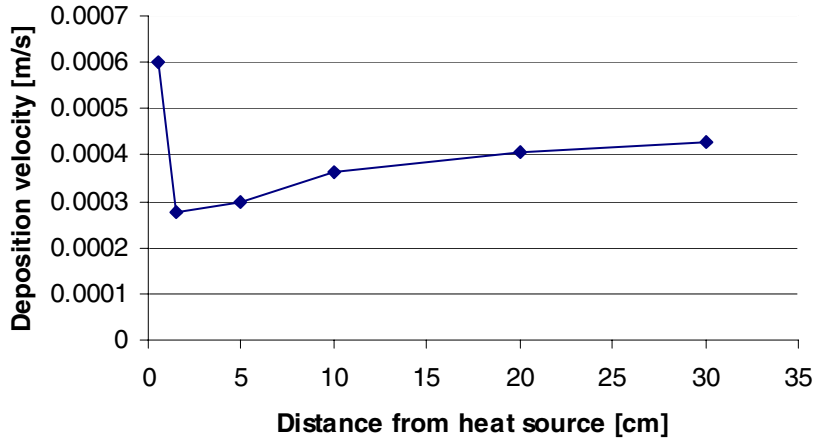

Fig. 1.1.4. Deposition velocity of 0.7 µm particles versus distance from the radiator.

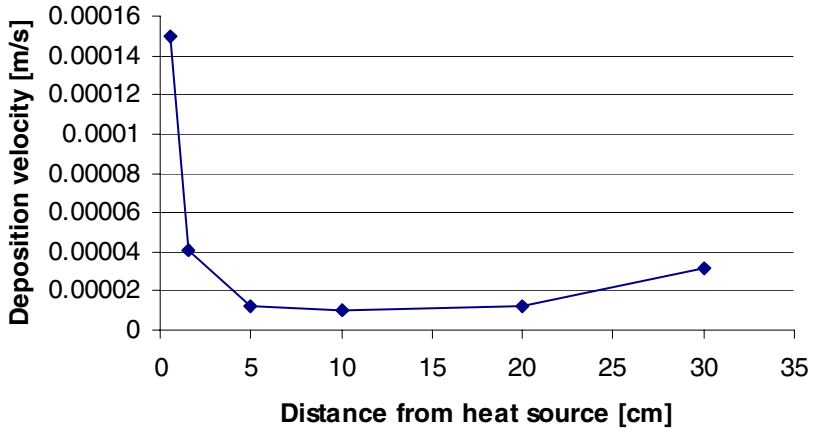

Fig. 1.1.5. Deposition velocity of 2.5µm particles versus distance from the radiator.

As can be seen from Figures 1.1.4 and 1.1.5, the distance between a radiator and a person would have to be extremely small for the radiator temperature to significantly influence aerosol deposition to the person.

1.1.3 Influence of skin moisture

Skin surface moisture (the hydrolipidic surface film consisting of sebum and other excreted moisture components) might influence deposition to humans in several ways. One mechanism has to do with diffusion of water vapour and dry air molecules close to the moist surface, and is termed diffusiophoresis (Tierney and Quarini, 1997; Hollander and Pohlmann, 1991). This mechanism is associated with a hydrodynamic Stefan flow either enhancing deposition by condensation or reducing it by evaporation (Canuffo and Bernardi, 1996). A possibly more important mechanism, particularly for particles in the supermicron range, is the enhanced adhesion of the particles to a moist surface.

In an experimental series, the correspondence between skin moisture and deposition velocity to skin has been examined. Particles (0.7 µm and 2.5 µm) labelled with neutron activatable tracers were emitted into the air of the

test room, in order to determine the deposition velocities to skin of the same two volunteers that participated in the experiments carried out at Riso during the previous contract. Throughout the experiment the skin surface moisture of the volunteers was measured using a Corneometer CM 825, manufactured by CK electronic GmbH, Cologne, Germany. The moisture measurement principle of this instrument is based on capacitance of the skin surface, exploiting the great differences between the dielectric constant of water (81) and those of other substances (generally <7).

A number of different factors influence the skin surface moisture. For instance, increasing air humidity and/or room temperature will increase transpiration. Also direct light has this effect, by heating the skin. Further, the water balance of the person, and the examined body part, as well as physical and emotional strain are important factors influencing an individual's skin surface moisture variations. In addition to this, skin surface moisture may permanently differ between individuals, due to differences in, e.g., age, life style and consumption habits. 'Normal' skin surface moisture values are highly variable between individuals (Blichmann and Seerup, 1988).

The output of the Corneometer is given in arbitrary units on a scale between 0 and 130. For legs and arms, values below 35 are according to the apparatus manual characterised as 'very dry', values between 35 and 50 are characterised as 'dry', and values above 50 as 'sufficiently moistured'. Table 1.1.2 shows the values of the skin surface moisture on hands and arms of the two volunteers over the experimental series, which was carried out under summer conditions. It should be noted that based on measurements on other volunteers, CLF's individual skin moisture range in general represents ordinary levels, whereas that of KGA is rather unusually high.

Table 1.1.2. Average Corneometer readings on the two test persons during the experiment series carried out in the Summer of 2001. Standard deviations and numbers of replicates are given in brackets.

Test person	Arms	Hands
KGA	74 (22 %, 6)	99 (10 % ,6)
CLF	47 (4 %, 6)	35 (2%, 6)

Table 1.1.3 shows the aerosol deposition velocities to the two volunteers in the experimental series. The observed differences in deposition velocities to the two test persons are in-line with the observations made during a large number of experiments in the past (Fogh et al., 1999).

Table 1.1.3. Deposition velocities to hands and arms of the two test persons during the experiment series. Averages of four replications (standard deviations as percentages are given in brackets).

Test person and surface	V_d (m s^{-1}) for 0.7 µm particles	V_d (m s^{-1}) for 2.5 µm particles
KGA, arm	0.0007 (11 %)	0.0086 (21 %)
CLF, arm	0.0001 (36 %)	0.0038 (39 %)
KGA, hand	0.0006 (16 %)	0.0049 (25 %)
CLF, hand	0.0001 (30 %)	0.0011 (35 %)

As can be seen, there is a clear correspondence between surface moisture and deposition velocity to the test persons of both submicroneous and supermicroneous particles, probably due to enhanced adhesion on moist surfaces.

1.1.4 Influence of physical movement

In an experiment, the influence of physical movement of test persons (at walking speed) was synthesised using a ventilator blowing on one side of a volunteer, whilst measuring deposition of 0.7 and 2.5 µm aerosols to both sides of the volunteer. At the same time, the air velocity was measured in 3 positions around the volunteer with hot wire anemometers connected to a DANTEC 54N10 multichannel flow analyser. In this experiment, as in all other experiments, test persons were sitting still throughout the measurement period.

Table 1.1.4 shows the results (avg. of 2 sample sets) of the experiment. The measured air velocities at the positions of the arms of the test person correspond to ordinary walking speeds. In the middle of the room, the air velocity was on average found to be 0.20 m s^{-1}.

Table 1.1.4. Deposition velocity to skin of a test person of 0.7 µm and 2.5 µm particles at different air velocities.

Parameter	Left arm of test person	Right arm of test person
V_d (0.7 µm) (m s^{-1})	0.00031	0.00066
V_d (2.5 µm) (m s^{-1})	0.0035	0.0049
Air velocity (m s^{-1})	1.04	2.76

The shown figures for 0.7 µm particles are in good agreement with previously reported results of wind tunnel experiments (Fogh et al., 1999). It is perhaps surprising that the influence of air velocity on skin deposition of 2.5 µm particles in this experiment appears to be rather limited. Large particles would to a greater extent be expected to impact on the test person rather than follow the air stream around the person. However, this deposition though impaction may be hampered by the highly turbulent airflow around the arm that was closest to the ventilator.

1.2 Deposition to hair - for dosimetric assessment

Under the contract FI4PCT950019 only very few measurements were made to quantify the deposition velocity of particulate contaminants to hair. Most of these measurements employed synthetic hair (wigs), thus introducing a possible source of error in relation to for instance material/ electrostatic influences. The results were then thought to be too sparse to facilitate definite determination of representative deposition velocities. Also, it has been recognised that particle deposition velocities to distal and proximal parts of the hair strand could well be significantly different, as the air movement would be different. Further, in relation to radiation dose, beta radiation from contamination on the outer hair layers would be attenuated through the mass of the inner hair layers. Therefore, it was important to carry out a series of measurements that could help to gain an insight into the possible differences in deposition velocity to the different, more or less 'sheltered' parts of the hair strand.

The tracers particles applied in this study and their emission method were of the same types as have been applied in many other parts of the project. Indium and dysprosium labelled silica spheres were emitted in the test room and impactor measurements were made during the emission to ascertain the adequate monodispersity of the aerosol. A new sampling protocol was developed for the study. Here the exposed hair strands were cut a close as possible to the head of the volunteer. The hair strand samples were then carefully cut at the middle, thus obtaining a 'distal' and a 'proximal' part. Three volunteers participated in these experiments. The volunteers were all male and had relatively short hair, which was, however, visibly different in texture. The experience from previous experiments where all the hair on a test person was cut, was utilised to determine the deposition velocity to the hair samples from the tracer concentrations on the samples. From measurements it was estimated that the total mass of the test person's hair was some w=15 g. The total area covered by this hair was found to be a=0.09 m^2. If

the time-integrated tracer air concentration over the experiment is c, and m_t is the tracer mass per unit of hair sample mass, the total deposition velocity to the hair could be found as:

$$V_d = \frac{w \cdot m_t}{a \cdot c}.$$

Table 1.2.1 shows the results of the sampling in four different experiments.

Table 1.2.1. Measured deposition velocities of 0.7 µm and 2.5 µm particles to distal and proximal parts of human hair.

	V_d, distal part of hair [ms^{-1}]		V_d, proximal part of hair [ms^{-1}]	
	0.7 µm	2.5 µm	0.7 µm	2.5 µm
Average	0.00026 (30)	0.0018 (22)	0.00012 (12)	0.0008 (8)
Std.dev.	0.00012	0.0008	0.00008	0.0005

Generally, the above deposition velocities for 2.5 µm particles to the distal part of the hair are in-line with results obtained during the previous project, whereas the deposition velocities for 0.7 µm particles are significantly lower than what had previously been found (Fogh et al., 1999). However, the new estimates are based on a more extensive sampling programme, and the standard deviations on the figures are here relatively smaller.

1.3 Elemental iodine deposition

Our goal was to find the deposition velocity of elemental iodine on human skin. As a substitute for human skin, we chose to use live hairless rats, as 'guinea pigs'. Further, we wanted to find the deposition velocity to human hair and clothing. As will be described later on, we used filter paper as reference to be able to compare our measurements with standard measurements made under more correct conditions for obtaining deposition velocities from measurements.

1.3.1 Methods

Four exposure chambers have been constructed for the iodine deposition experiments. These are made of glass, and are 30 cm high, 20 cm wide and 30 cm long. Two holes of 10 mm in diameter were drilled in two walls of each chamber (5 cm from the top). During the experiments, air in the chamber is sucked through one of these holes by a pump, via a glass tube filled with active charcoal, at a flow rate of 0.5 l min^{-1}. This maintains sufficient fresh air in the chamber for the survival of the test animal. Another hole of 10 mm in diameter was drilled 8 cm from the floor. Air samples are taken from this hole for the determination of the iodine concentration in the air. There is a small hole (5 mm) in the middle of the lid on the top of the chamber. A steel basket containing an iodine crystal is suspended in the exposure chamber through this hole. A small fan is fixed at the middle of the inner surface of the top cover, blowing sideward, to help distributing the iodine homogeneously in the chamber. The top cover can be removed in order to place experimental materials and the test animal in the chamber. It is sealed during the experiment to avoid loss of iodine from the gap between the top cover and walls. The iodine in the air is collected by sucking air from the chamber through a glass tube of 15 cm length and 6 mm in diameter. Half a gramme of active charcoal (18-35 mesh, Merck) is filled into the glass tube (3.5 cm length) to trap elemental iodine in the air sample. The elemental iodine is released to the chamber air by natural sublimation of an iodine crystal. The iodine concentration in the air will rapidly increase and become stable after some time

when the sublimation rate of iodine from iodine crystal is equal to the deposition rate of iodine to the inner surface of the chamber and the rate of loss from sucking. Therefore, the time reaching a stable iodine concentration in the chamber air depends on the weight and type of the iodine crystal and the shape and material of the chamber. It will therefore be experimentally measured. Air samples (300 ml) are collected in the active charcocal by sucking air through an active charcocal tube using syringes, at the time of 5 min, 10 min, 20 min, 30 min, 40 min, 60 min, 1.5 h, 2.0 h, 3.0 h, 4.0 h, and 5.0 h. In addition, some air samples are collected from the upper hole to investigate the homogeneity of iodine in the chamber air. The active charcoal is immediately transferred and sealed in a 1 ml polyethylene vial for neutron activation analysis of iodine.

1.3.2 Experiments

1.3.2.1. Clothing, filter paper and water surface exposure

One objective of the experiments was to determine elemental iodine deposition on clothing. Also the deposition velocities to water and filter paper were investigated (for reference). Clothing samples were mounted on a wall. The parts of the clothing samples that were subjected to analysis were cut immediately after the experiment and measured 8 cm^2. Filter papers of 55 mm in diameter (hardened ashless, Whatman 542) and clothes (40mm in diameter, white cotton) were attached to walls (4 sides), floor and ceiling of the chamber (one side exposed to air). Further, 20 ml of tap water in a glass beaker of 90mm in diameter was placed on the chamber floor. A 1.1 gramme iodine crystal in a steel basket was used for suspension in the chamber, the fan was switched on, and air in the chamber was sucked with a pump. The temperature in the chamber was measured to be 22±0.5 °C and the humidity was 65±5%. After 4 hours exposure, the filter paper or cloth was transferred and sealed in a 1 ml polyethylene vial. Also 1.0 ml water was transferred and sealed in a 1.0 ml polyethylene vial.

An epithermal neutron activation analysis was developed for the determination of iodine in different materials. The samples (charcoal, filter paper, clothes, water, - and also skin and hair) sealed in the polyethylene vial were irradiated for 20 min in an epithermal neutron irradiation channel (an irradiation channel lined with cadmium of 0.75 mm thickness) in a miniature neutron source reactor (MNSR) in the China Institute of Atomic Energy at an epithermal neutron flux is 1.0×10^{10} n cm^{-1} s^{-1}. The irradiated samples were measured using an HpGe detector after 3 min. decay. A detection limit of iodine is 20 ng for active charcoal and skin, and 5 ng for hair, water, and clothes, which is sufficient for this study.

1.3.2.2. Rat skin exposure

An experiment series was performed to examine the significance of deposition of elemental iodine to skin surfaces (back, belly skin and ears of a rat).

Figure 1.3.1 shows the principles of the exposure experiment set-up. A hairless rat was placed in a ca. 1 m^3 chamber. The rat was fitted with a collar to prevent it from licking its body and thereby removing the deposited iodine. The collar was a special soft type normally used for birds. This type was used instead of the standard type collar to avoid discomfort for the rat during the experiment. This goal was achieved, as the rats were calm and confident during the time of the experiment. The experiment was done in a fume cupboard. This will create some draught that may cool the floor of the chamber and create unpleasant conditions for the rat, and therefore a floor heating system was created so that the floor temperature remained at a comfortable range during the experiment.

An iodine crystal was attached to the ceiling of the chamber, and equipped with a grille preventing the rat from reaching it. A fan near the iodine crystal helped to distribute the iodine homogeneously in the chamber.

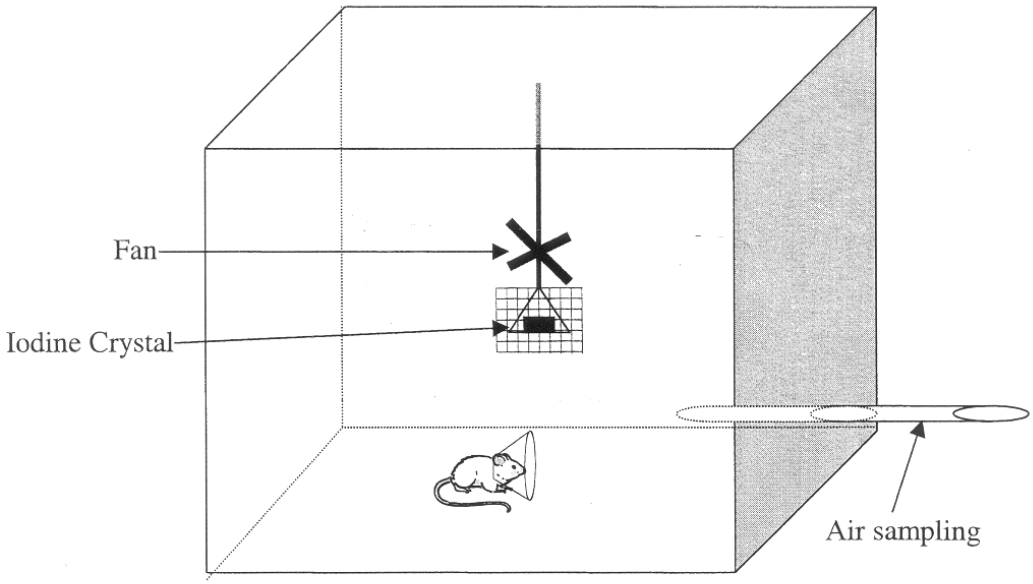

Fig. 1.3.1. Iodine exposure experiment set-up.

The air sampling principle is illustrated in Figure 1.3.2.

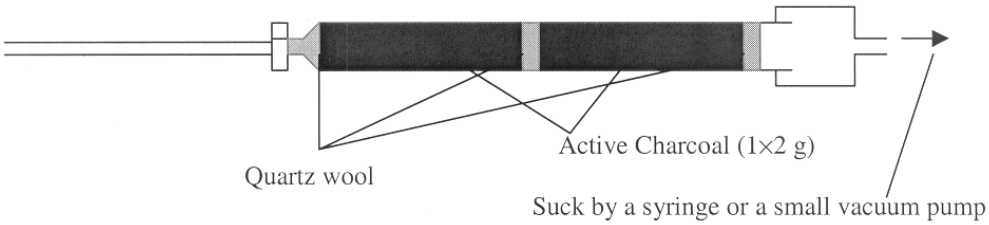

Fig. 1.3.2. Principle for suction of air and trapping of elemental iodine on active charcoal.

Elemental iodine air samples were collected by passing air samples from the chamber through a column of active charcoal. The air sampling was carried out throughout the entire experiment period (ca. 1-4 hours).

The 'hairless' rats were to our surprise not hairless as hairless mice are, so we had to shave the rats to remove the fur. Only part of the skin was shaved. This did not hurt the animals. They actually seem to feel that it was a sort of petting. Using only partial shaving, however, gave us an opportunity to measure on hairless and non-hairless parts of the rats. After exposure and dissection the samples of the skin were immediately sealed and cooled in order to prevent the iodine from escaping and to avoid rot.

The samples were brought as hand luggage to China accompanied by one of the team members, who also took part in the analysis of the neutron activated samples.

Fig. 1.3.3 shows the actual experiment set-up.

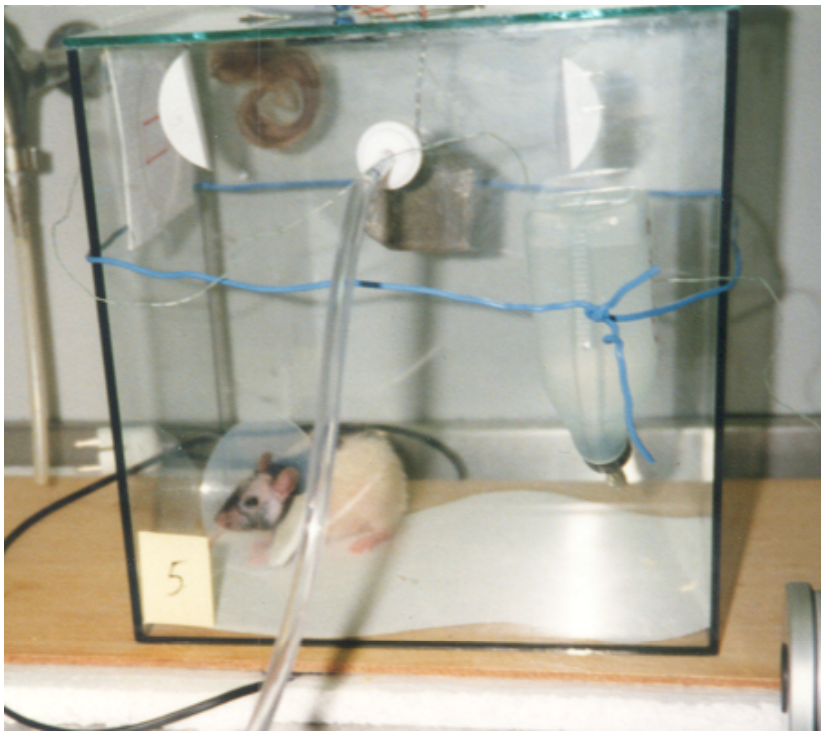

Fig. 1.3.3. The laboratory rat during the experiment in the exposure chamber

In the middle of the picture a grey square can be seen. This is the iodine crystal in its cage. To the right of this, the rat's drinking facility can be seen. The mixing fan was attached to the surface of the top 'lid' of the chamber (a flat, black object can be seen faintly in the picture). Also filter paper samples were exposed, as can be seen (half-circular white objects). On the left wall, a piece of cotton clothing can be seen, mounted in a template that protected against deposition on the reverse side. The lightweight collar around the rat's neck does not prevent it from drinking and moving around. The rat was at this point already coloured by the deposition of the yellow iodine.

1.3.2.3. Exposure of hair

Human hair was prepared, which was fixed in the chamber (the curly object at the top left shown in Fig. 1.3.3), to investigate the deposition of iodine on the hair.

1.3.3 The concept of deposition velocity for gases (e.g., elemental iodine)

The general equation governing the concentration in air of a pollutant is the following:

(1) $$\frac{\partial \chi}{\partial t} = \frac{-\partial(u_i \chi)}{\partial x_i} + \frac{\partial}{\partial x_i} D \frac{\partial \chi}{\partial x_i} + S - k\chi - \frac{\partial(-v_g \chi)}{\partial z},$$

where χ is the concentration, t is time, u_i is the wind speed in all three directions, normally denoted u, v and w, where w is the wind speed in the z direction. This is perpendicular to the horizontal surface. x_i is the length in the three directions x, y and z. D is the molecular diffusion coefficient for χ. S is the local sources and sinks and k is the chemical reaction rate, whereas v_g is the gravitational settling velocity.

Reynolds decomposition splits the concentration and the wind velocities into mean values and fluctuation. It is:

(2) $\chi = \overline{\chi} + \chi' \quad (\overline{\chi'} = 0)$ and

(3) $u_i = \overline{u}_i + u_i' \quad (\overline{u_i'} = 0)$

where the over-bar denotes a time average.

Assuming that S=0 and k=0, inserting in equation 1 and averaging over time gives:

(4) $$\frac{\partial \overline{\chi}}{\partial t} = -\frac{\partial(\overline{u}_i \overline{\chi})}{\partial x_i} - \frac{\partial(\overline{u_i' \chi'})}{\partial x_i} - \frac{\partial(\overline{u_i} \partial \overline{\chi'})}{\partial x_i} + \frac{\partial}{\partial x_i}(D \frac{\partial \overline{\chi}}{\partial x_i}) - \frac{\partial(v_g \overline{\chi})}{\partial z}$$

The first term on the right hand side is the advective transport. The second term is the correlation between the concentration and the wind speed. This is the divergence of the turbulent flux also called turbulent diffusion. The 3rd term is 0, as $\overline{u_i'} = 0$. The 4th term is the molecular diffusion and the 5th term is the flux due to gravitational settling. This term is 0 when only gases are considered.

All this will later be related to deposition velocities. We are therefore only interested in vertical fluxes under steady state conditions and horizontal homogeneity. The mean horizontal wind speed is considered to be 0. Then equation 4 will be reduced to (in the cases of gases):

(5) $$\frac{d(\overline{w'\chi'})}{dz} = \frac{d}{dz}(D \frac{d\overline{\chi}}{dz})$$

In order to find the vertical flux, we integrate equation 5 from the surface to a reference height, h.

(6) $$\int_0^h \frac{d(\overline{w'\chi'})}{dz} dz = \int_0^h \frac{d}{dz}(D \frac{d\overline{\chi}}{dz}) dz$$

(7) $$\overline{w'(h)\chi'(h)} - \overline{w'(0)\chi'(0)} = D \frac{d\overline{\chi(h)}}{dz} - D \frac{d\overline{\chi(0)}}{dz}$$

At the surface the vertical turbulent transport approaches 0, and if h is well above the surface the vertical turbulent transport will be many orders of magnitude greater than the molecular diffusion transport. Then we can disregard the two comparatively small terms leading to an expression for the vertical gas flux:

(8) $$\overline{F} = \overline{w'(h)\chi'(h)} = -D \frac{d\overline{\chi(0)}}{dz}$$

The flux can also (Panofsky and Dutton, 1984) be expressed as a turbulent diffusion.

(9) $$\overline{F} = \overline{w'\chi'} = -K_\chi \frac{d\overline{\chi}}{dz}$$

The diffusion coefficient $K_\chi \approx K_M$, where K_M is the diffusion coefficient for momentum. The flux of the momentum will in analogy be

(10) $\overline{F}_M = -K_M \frac{d\overline{\rho_a u}}{dz} = -K_M \rho_a \frac{d\overline{u}}{dz}$,

where ρ_a is the air density.

The flux of the momentum downwards must be equal to the surface stress τ (positive in downward direction). Inserting this in equation 10 gives

(11) $\tau = K_M \rho_a \frac{d\overline{u}}{dz}$

$\Downarrow$

(12) $K_M = \frac{\tau}{\rho_a}(\frac{d\overline{u}}{dz})^{-1}$

u_*^2 is defined as:

$u_*^2 = \frac{\tau}{\rho_a}$, and inserting this in equation 12 gives:

(13) $K_M = u_*^2(\frac{d\overline{u}}{dz})^{-1}$

If K_M is proportional to the product of u_*, the eddy velocity, and z, the eddy size, then

(14) $K_M \approx \kappa u_* z$, where

κ is the von Karman constant ($\kappa \approx 0.4$).

Then by inserting equation 14 in equation 13 gives:

(15) $\kappa u_* z \approx u_*^2(\frac{d\overline{u}}{dz})^{-1}$

Substituting '≈' with '=' we get

(16) $\frac{d\overline{u}}{dz} = \frac{u_*}{\kappa z}$

Integrating this expression from z_0 to z gives

(17) $\int_{z_0}^{z} d\overline{u} = \int_{z_0}^{z} \frac{u_*}{\kappa z} dz$, where z_0 is the height where the wind speed is 0. The integration gives:

(18) $\overline{u}(z) - \overline{u}(z_0) = \frac{u_*}{\kappa}(\ln(z) - \ln(z_0)) = \frac{u_*}{\kappa}\ln(\frac{z}{z_0})$

$\Downarrow$

(19) $\overline{u}(z) = \frac{u_*}{\kappa}\ln(\frac{z}{z_0})$

Now and then it is necessary to define a new arbitrary using a displacement height L. L is defined in the following way: in the logarithmic wind profile $\overline{u}(L + z_0) = 0$. This displacement is often used in places where

the roughness elements are tall. The mean height of the roughness elements is called H. L is typically 0.6H. z_0 is normally called the roughness height. In this case equation 19 will be transformed to

$$(20) \qquad \overline{u}(z) = \frac{u_*}{\kappa} \ln(\frac{z-L}{z_0}) .$$

In the same way we can formulate an equation for the mean concentration as

$$(21) \qquad \overline{\chi}(z) - \overline{\chi}(z_0) = \frac{\chi_*}{\kappa} \ln(\frac{z-L}{z_0}) .$$

where $\chi_* u_*$ is defined so that $\chi_* u_*$ is the vertical particle flux.

The profile of the wind speed and the concentration is given in Figure 1.3.4 (a and b), where the dotted lines give the theoretical profile according to the equation and the full line a real profile within the roughness elements. As can be seen from the figures $\overline{u}$ is 0 at the ground surface, whereas χ is only zero when the surface absorb al the gas. This is in certain circumstances the case for elementary iodine.

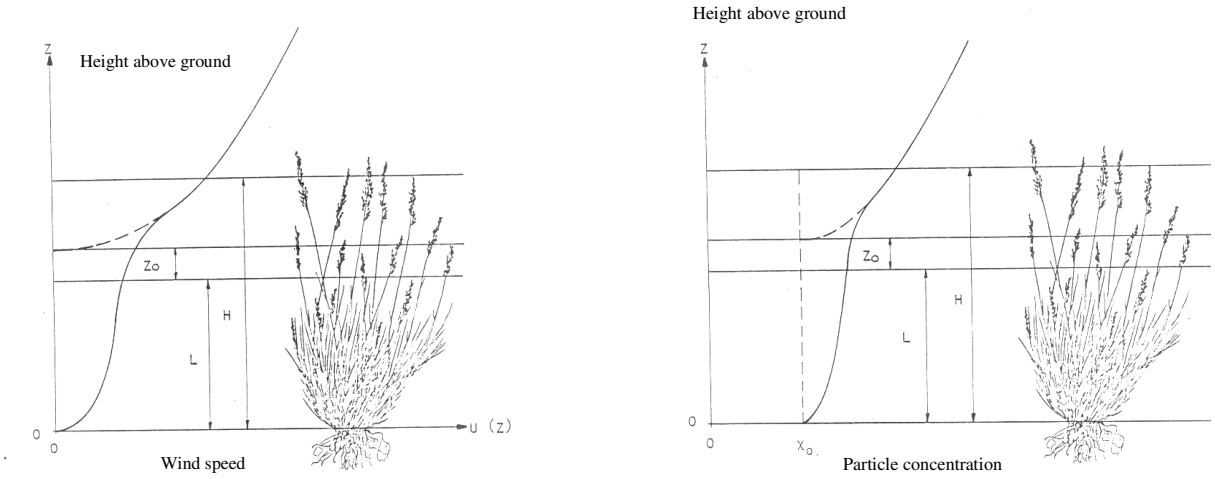

Fig. 1.3.4. (a) Variation of wind speed above ground (left) and (b) variation of particle concentration above ground (right).

Deposition velocity is defined as

$$(22) \qquad v_d(z) \equiv -\frac{\overline{F}_\chi}{\overline{\chi}(z)} .$$

$\overline{F}_\chi$ is the mean flux of gas or particles in the z direction at the height z. $\overline{F}_\chi$ is constant in the z-direction. As can be seen from the expression, $v_d(z)$ is a function of z, and as the concentration, $\overline{\chi}$, will in the vicinity of the surface rise with height, then $v_d(z)$ will decrease with height. The gradient of $\overline{\chi}$ will be smaller with height, and consequently the variation in $v_d(z)$ will be less with height. Normally, the deposition velocity is measured at 1 m height.

Using some manipulations it can be shown that

$$(23) \qquad v_d(z) = \frac{1}{\frac{\bar{u}}{u_*^2} + \frac{1}{u_* \kappa} \ln\left(\frac{z_0}{z_{0\chi}}\right) + \frac{\chi_0}{u_* \chi_*}}$$

where $z_{0\chi}$ is the roughness length for gas. This brings us to the concept of the resistance model. We can view the deposition as a series of resistances in the following way:

$$(24) \qquad v_d(z) = \frac{1}{r_a + r_b + r_c}$$

where r_a is the atmospheric resistance, r_b is the laminar boundary layer resistance and r_c is the surface resistance. The different terms can be recognized in equation 23, respectively as the three terms in the denominator.

A laminar boundary layer will build up from a change in the surface roughness and will at a certain distance build up to a sufficient height so that deposition velocities found using different measuring techniques can be compared. This layer's formation is dependent on the roughness elements. The building up of a sufficient layer will require a distance of many meters where the wind conditions are stable. The conditions under which we are measuring 'deposition velocities' in the chamber with the rats, as described, do not fulfil this condition and can therefore not directly be compared to other measured deposition velocities. One more condition that is required to make a comparable deposition velocity measurement is that the source should be at a long distance from the target. Also this is not fulfilled.

As there is no atmospheric resistance (r_a) in this case, this would tend to result in high deposition velocities in our measurements compared to standard measurements.

To overcome some of these problems simultaneous deposition velocity measurements or deposition velocity measurements made under the same conditions were in all cases carried out on filter paper. Filter paper can be used as a reference as it has been used in numerous measurements where deposition velocities to different surfaces have been measured. By relating our 'deposition velocities' to filter papers with those measured to filter papers in other more conceptionally correct measurements we can obtain a correction factor for our measurements to other surfaces. This factor can be used for correcting our 'deposition velocities' measured on skin, clothes, etc. to those measured under correct conditions. This enables us make estimates of deposition velocities to skin surfaces etc. of elemental iodine, which can be used as parameters in models, including our own.

1.3.4 Results

In Fig. 1.3.5 the build-up of a stable elemental iodine air concentration through natural sublimation in the test chamber is illustrated. These data were recorded using charcoal traps, as described above. The curve can be approximated with the expression $\chi = 13.8\ \mu g\ l^{-1} \cdot (1\text{-}e^{-(0.031 \cdot t)})$, with an R squared value of 0.955.

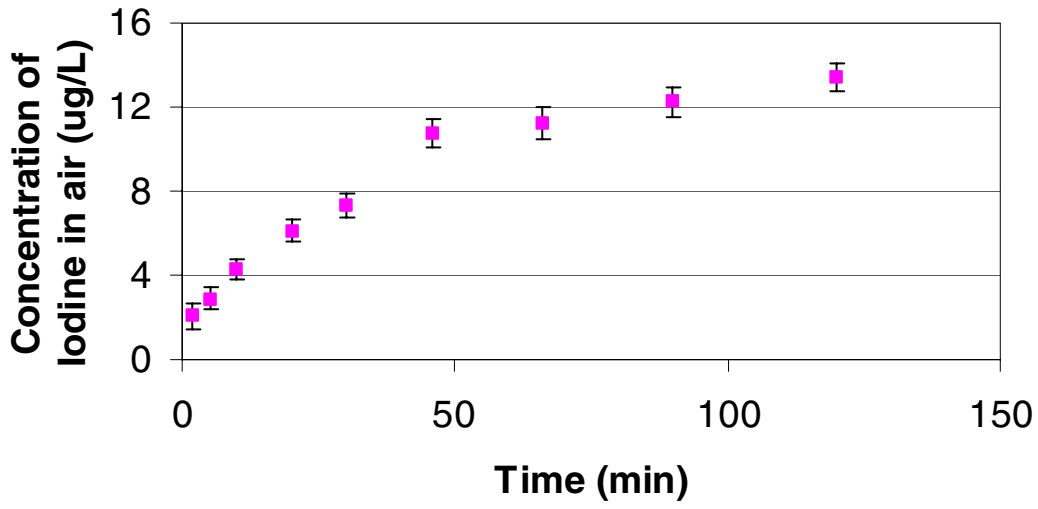

Fig. 1.3.5. Air concentration of naturally sublimated elemental iodine in the test chamber as a function of time.

1.3.4.1. Skin

The measured 'deposition velocities' to the skin of the rats in the experiment are shown in Table 1.3.1. Each figure is the average of 5 individual experiments with different rats. An additional experiment was carried out with a rat that was *not* exposed to elemental iodine, to have a background reference. The samples taken from the unexposed rat generally contained less than 3 % of the iodine on the corresponding samples from the exposed rats. The background is thus not of a magnitude that could significantly influence the results of the iodine exposure measurements.

Table 1.3.1. 'Deposition velocities' of elemental iodine measured on rats in the experiment series.

Rat experiment no.	'v_d' on ear [m s^{-1}]	'v_d' on belly [m s^{-1}]	'v_d' on back with hair [m s^{-1}]	'v_d' on back without hair [m s^{-1}]
1	$8.4\ 10^{-4}$	$7.7\ 10^{-5}$	-	$8.2\ 10^{-4}$
2	$5.7\ 10^{-4}$	$7.7\ 10^{-5}$	$6.2\ 10^{-4}$	$4.9\ 10^{-4}$
3	$5.2\ 10^{-4}$	$5.9\ 10^{-5}$	$7.6\ 10^{-4}$	$6.3\ 10^{-4}$
4	$2.1\ 10^{-4}$	$3.8\ 10^{-5}$	$3.3\ 10^{-4}$	$2.5\ 10^{-4}$
5	$1.7\ 10^{-4}$	$7.4\ 10^{-5}$	$2.0\ 10^{-4}$	$2.5\ 10^{-4}$
Avg (stdev.)	$4.6\ 10^{-4}$ (60 %)	$7.0\ 10^{-5}$ (28 %)	$4.8\ 10^{-4}$ (52 %)	$4.9\ 10^{-4}$ (51 %)

As can be seen, the 'deposition velocities' on the different parts of the rat were not found to be significantly different, with the exception of the belly. The experiments were carried out in the daytime, where the rats are least active (and thus least likely to cause mechanical disturbance in the iodine deposits), and the low deposition velocity on the belly reflects that the animals were lying on the belly most of the time. No significant difference was found between deposition velocities to shaved and unshaved parts of the back of the rats. The ears are without any hair growth.

In each rat experiment, two filter paper samples were also exposed. The 'deposition velocities' that were recorded on those smooth samples were on average 4.5 10^{-5} m s^{-1}, with a standard deviation of 3.1 10^{-5} m s^{-1} (for comparison, the deposition velocity to a water surface was in on of the experiments recorded to be 6 10^{-5} m s^{-1}). This is almost exactly one order of magnitude less than the deposition velocities recorded on the rats in the same experiment.

Probably the reference surface, to which most experiments on elemental iodine deposition have been made, is cut grass. Naturally, the deposition velocity will here vary somewhat, according to density and the length of the grass, and thereby the roughness of the surface. However, a typical deposition velocity on a grass surface is of the order of 0.5-1.5 10^{-2} m s^{-1} (Hawley, 1964; Hawley, 1966; Cline, 1965). After the Chernobyl accident, Roed (1990) found that the deposition velocity of elemental iodine to smooth surfaces, such as walls and windows were under 'natural' conditions about an order of magnitude lower than that to a grassed surface. The elemental iodine deposition velocity to filter paper would be comparable to that. Combining this with the finding that the experimentally derived rat 'deposition velocities' were about one order of magnitude higher than the corresponding to filter paper, it follows that the elemental iodine deposition velocity to skin would under realistic conditions be estimated to be of the same order as the typical elemental iodine deposition velocity to grass, i.e., 10^{-2} m s^{-1}. This is exactly the value that was assumed in the modelling performed under the previous contract, thus verifying the validity of these calculations.

1.3.4.2. Hair

Using the usual assumption, that the total mass of hair on a head is 15 g, and the total area of the head that is covered by hair is 0.09 m^2 (Fogh et al., 1999), it was found from the exposed pieces of hair in four individual experiments that the 'deposition velocity' of elemental iodine to hair in the chamber was 8.8 10^{-4} m s^{-1}. Based on the above findings used to calculate deposition velocities to skin under realistic conditions, it can be seen that a realistic estimate of the elemental iodine deposition velocity to hair would be of the order of 20* 8.8 10^{-4} m s^{-1} = 1.7 10^{-2} m s^{-1}. For modelling purposes we had under the previous contract assumed a deposition velocity of 10^{-2} m s^{-1}. As the long curly hair strands applied in the exposure chamber experiments may well constitute a rougher surface than hair on a human head, which is likely to some extent to follow the shape of the head, we found no reason to change the estimate of 10^{-2} m s^{-1} for hair.

1.3.4.3. Clothing

Deposition to fabric sample mounted on a chamber wall was investigated in four of the experiments. The fabric was in all cases slightly ribbed, thin cotton T-shirt material. The experiments showed an average 'deposition velocity' of 5.5 10^{-4} m s^{-1}, with a standard deviation of 39 %. This is practically the same as was found for the skin in these experiments (see above). A realistic estimate of the elemental iodine deposition velocity to cotton clothing is therefore also of the order of 10^{-2} m s^{-1}. The validity of the parameter value assumed in modelling under the previous contract is thus verified.

1.4 Outdoor deposition to humans

The aim of this study is to gain knowledge about the deposition velocity as a function of the aerodynamic diameter and the dependence of deposition velocity on the mean velocity and turbulence intensity.

1.4.1 Wind Tunnel Description

The boundary layer wind tunnel at the Department of Civil Engineering in NUI Galway is a low speed, open-return and open working section type tunnel. The test section is 1.99m high and 2.44m wide. The overall length of the tunnel is 15.75m. The wind tunnel consists of an inlet and contraction section, followed by a working section of 9.90m, and then a fan section and a diffuser. The wind speed range is 0 to 7m/s. The fan is driven by a hydraulic system. Power is provided by a 20HP AC electric motor, which in turn drives a variable speed hydraulic pump, which is controlled manually to vary the wind speed. The maximum pressure is 200 Bar corresponding to 960 revolutions per minute.

The first about 6.3m of the working section is used to place the turbulence-generating devices and roughness elements for simulation the required flow characteristics of the approaching flow. The instruments and models are located on a turntable whose centre is downwind of the working section at a distance of 7.6m.

1.4.2 Simulation of the Boundary Layer

Naturally grown boundary layers can be simulated in those wind tunnels with long test-sections. For example, Cermak states that a wind tunnel without any boundary layer thickening devices installed at the entrance or at any sections of the working section can form a boundary layer thickness of approximate 50 cm at a distance of 15 m from the entrance of the boundary layer development section. Since the limitation of length, the artificial simulation technique by Counihan & Armitt (1968) method was used to thicken turbulent boundary layer to be simulated in the short wind tunnel. This method consists of spire arrays, perforated trip and roughness element. Their dimensions and configuration is shown in Table 1.4.1.

Table 1.4.1. Dimensions and configuration of boundary layer thickening devices.

	Element description	Distance from the elemental frontal edge to the outlet of honeycomb (m)	Length of section (m)	Element geometry (mm)	Density (%)
1	Perforated trips	0.33		2440 wide 65 high	
2	4 Spires	0.35		1270 high 220 bottom	
3	Roughness elements with staggered arrangement	0.70	5.3	38mm high 34 mm wide 34 mm deep	5
4	Carpet	6.0	0.37		

Fig. 1.4.1. View of the roughness configuration in BLWT of NUI, Galway

1.4.3 Characterisation of Flow

The vertical profiles of mean velocity and turbulence intensity are obtained using TSI hot-film anemometer system (Model 1054) at a sampling frequency 5000Hz and sampling time of 50 s. The moveable rig was used to move the hot-film probe to the specified height. During the measurement, a FCO14 Micromanometer system was used to monitor the variation of wind velocity at a reference height of 1.2 m. This instrumental system consists of a pitot static tube placed just ahead of the measured site at a height of 1.2 m, the pressures from the pitot tube are measured by transducer and the voltage signals was sent to the data acquisition system.

Figure 1.4.2 is a plot of the mean wind speed and turbulence intensity with height for the roughness configuration as viewed in Figure 1.4.1. This profile was used while the experiments were carried out. Measurements took place at a height of 10cm and a mean wind velocity of 3m/s to represent outdoor conditions equivalent to medium to strong winds as measured near ground level. The turbulence intensity at this height was measured to be 18.4%.

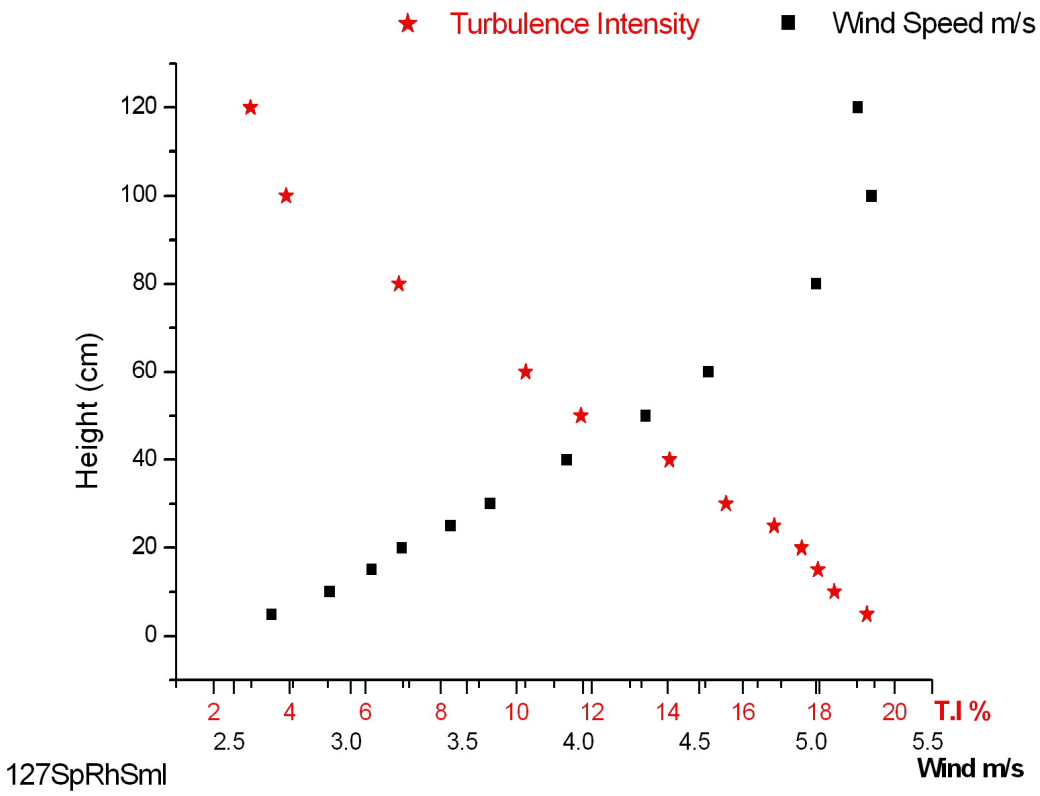

Fig. 1.4.2. Mean wind speed and turbulence intensity with height.

An experimental investigation of aerosol deposition onto actual human body surfaces in the wind tunnel was ruled out for several reasons. The cross-section of the wind tunnel is such that a human would significantly affect the pattern of airflow in the tunnel and thus accuracy of the simulation would be poor. Also, the experiments required a duration of several hours to generate detectable deposits on the test surfaces; therefore use of human volunteers was impractical.

A cylinder was used as the deposition surface for the deposition experiments. Rapp (1973) concluded that for conditions of low air velocity an upright cylinder was a reasonable approximation to the human body. However, in the higher air velocity conditions of the wind tunnel experiments, the most significant contribution to aerosol deposition may arise from inertial impaction, in which case the physical form of the phantom would be the most important consideration. Biomechanical modelling studies (Semwal and Hallauer, 1994) have shown that cylinders are good approximations to the human form. Thus, the cylinder was considered an accurate phantom for the wind tunnel studies of aerosol deposition onto human body surfaces in simulated outdoor conditions.

The test surface used was latex, the same of which was used for the clearance experiments and was chosen due to their low background fluorescence, which would allow for the least interference with the fluorescent signal from the deposited particles. Measurements of aerosol deposition onto the surfaces of the cylinder were made for 3 different particle sizes. After the deposition period, the test surfaces were removed from the cylinder and analysed with a fluorescent scanning system. The fluorescent scanning system consists of an array of blue LEDs (480nm peak) and a Starlight Express HX516 CCD camera was used to detect the fluorescent signal of the deposited particles. This system was also used in the clearance experiments. The particle concentration and size distribution of the aerosol in the wind tunnel was measured continuously to ensure a consistent concentration of aerosol in the wind tunnel using a Met One particle counter.

1.4.4 Aerosol Generation

The aerosol was generated using a Topas Condensation Aerosol Generator SLG 250. The generator uses a controlled condensation technique to produce monodisperse aerosols. Figure 3 shows the block diagram of this generator.

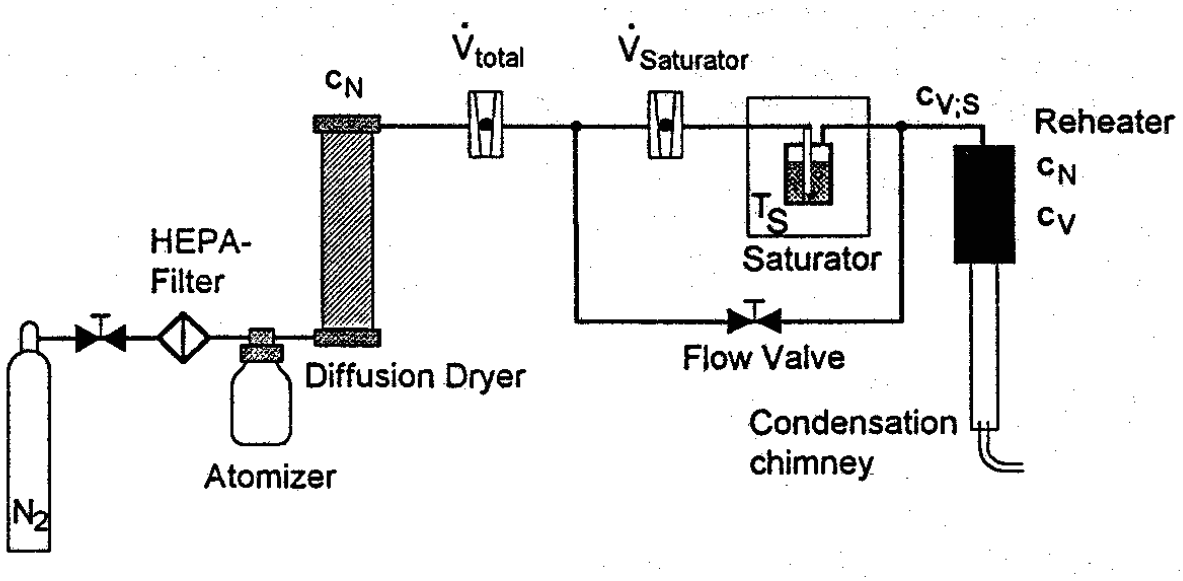

Fig. 1.4.3. Block diagram of the SLG 250

In the atomizer a NaCl solution is sprayed from a nozzle to produce droplets. Downstream a diffusion dryer removes the water from the droplets to produce small crystals, which have a size of 10-100nm, depending on the original concentration of the solution. The size of the aerosol particles to be produced is determined by the vapour concentration. The saturation of the nuclei aerosol takes place in the saturator. The aerosol bubbles through the aerosol material, which is held at constant temperature. Depending on the temperature and the vapour pressure a certain saturation concentration of the vapour is achieved in the bubbles. In the condensation chimney the vapour-nuclei mixture is cooled down in a laminar flow and the resulting super-saturation causes the vapour to condense onto the nuclei.

The aerosol material used was Di-2-ethyhexyl-sebacate (DEHS), a clear viscous liquid with a boiling point of 170ºC. The DEHS is labelled with a fluorescent dye, coumarin 6, to enable detection. Coumarin 6 is a fluorescent yellow tracer with an excitation wavelength of 444nm and has maximum emission at approximately 520nm. The aerodynamic size distribution of the output was measured with an Aerodynamic Particle Sizer (APS). Figure 1.4.4 shows the variation in particle size with saturator temperature and normalised flow rate. The normalised flow rate is the saturator flow rate divided by the total flow rate.

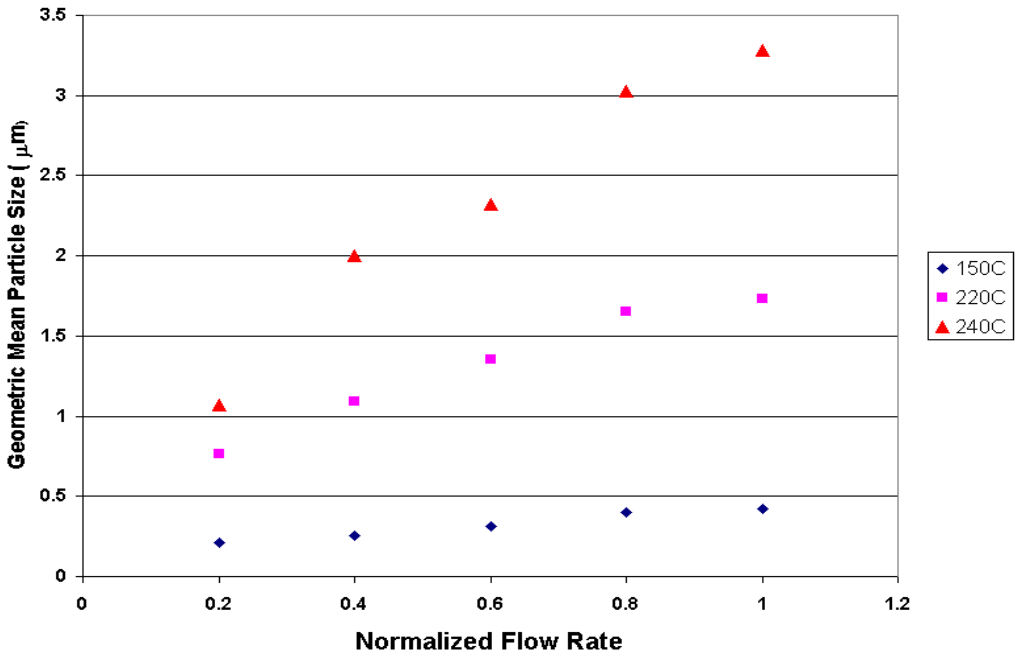

Fig. 1.4.4. Particle size change at 150ºC, 200ºC, and 240ºC under changing saturator flow rates

1.4.5 Results

A comparison of the deposition velocity for three different particle sizes onto vertical surfaces in simulated outdoor conditions was performed. For each particle size, the deposition velocity was determined six times. Table 1.4.2 lists the measured deposition velocities of 0.85µm, 3.0µm, and 6.0µm aerosol particles.

Table 1.4.2. Deposition velocities for each particle size.

Wind Speed, Turbulence Intensity	3m/s, 18.4% 0.85µm	3m/s, 18.4% 3.0µm	3m/s, 18.4% 6.0µm
V_d (cm/s)	7.74×10^{-2}	3.13×10^{-1}	3.59×10^{-1}
95% Confidence Interval (cm/s)	$5.66\text{-}9.81(\times 10^{-2})$	$2.60\text{-}3.66 (\times 10^{-1})$	$3.22\text{-}3.97(\times 10^{-1})$

With a mean velocity of 3.0 m/s and a turbulence intensity of 18%, the deposition velocity increased strongly with increasing aerodynamic diameter as can be seen in Figure 1.4.5.

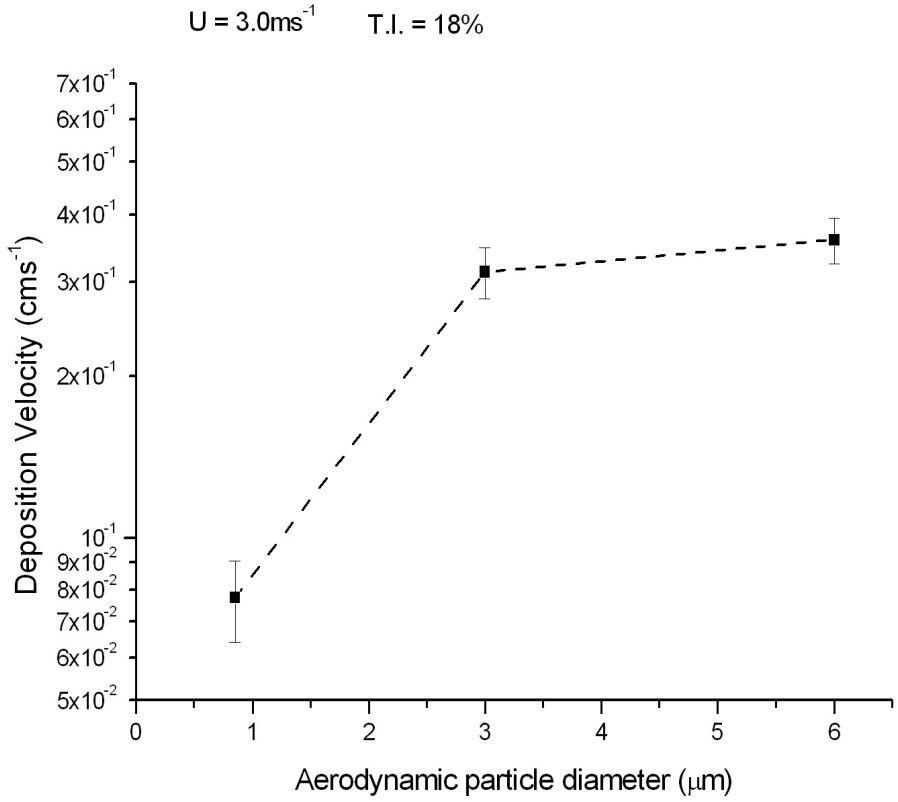

Fig. 1.4.5. The deposition velocity under conditions of a wind velocity of 3m/s and a turbulence intensity of 18%

There are many forces involved in particle deposition. The aerosol used consists of spherical, sticky particles of diameter 0.85μm – 6μm and have a density close to that of water or less. Thus, the transport by Brownian diffusion is negligible compared to the velocity of the mean flow and deposition due to gravity would be minor since it is deposition on a vertical surface that is under study. The phantom was not heated to mimic the human body. Normally, if the surface temperature of the human body is greater than the temperature of the surrounding air, upward convective air movements are formed. However, the significance of such air movements on the flow pattern around the body decreases with increasing surrounding air velocities. Therefore, with the relatively high velocities used in this study, such movements would have been small.

The increase in deposition velocity for the bigger particles is somewhat expected because of their larger inertia. When air carrying particles suddenly changes direction, the particles, because of their inertia, tend to continue along their original paths. If the change in air direction is cause by an object placed in the air-stream, particles with sufficient inertia will strike the object. This impaction combined with the stickiness of the aerosol in question, is expected to have resulted in a permanent deposition with little or no bounce. This may explain the higher deposition rates than those measured by Gudmundsson et al. (1997).

Other factors, which could affect the particle deposition and were not considered in this study, are surface roughness and electrophoresis.

A more in-depth study is necessary to determine the effect of changing wind velocity and turbulence intensity on a range of particle size. However, due to technical difficulties with regard to the wind tunnel facility at our disposal, we were unable to do this.

2 Clearance and penetration of contaminants deposited to humans

The clearance and percutaneous penetration processes of contaminants on the human body essentially determine the magnitude of the doses received from a given deposition. Preliminary studies of clearance parameters were made under the previous contract, relevant to a limited particle size range. It is expected that for instance in connection with a large nuclear power plant accident, the particles that would be of primary interest in the context of dose would have a size of only about one micron. Studies were therefore carried out to investigate the clearance processes for these small particles, and to verify the unexpectedly short clearance half-life of larger particles observed in the previous work. Penetration of contaminant particles across the skin surface barrier (stratum corneum) was examined in vitro for a range of particle sizes. Also the extent of contaminant penetration through clothing and onto skin was investigated.

2.1 Contaminant clearance from human body surfaces

Under contract FI4PCT950019, limited measurements of particle clearance from human skin were made, using filtered high-intensity white light to excite fluorescence in labeled silica particles, and a CCD camera and image processing system to detect this fluorescence. Results obtained indicated a clearance time from skin of several hours for supermicrometre particles. However, the reliability of the measurements was restricted by the sensitivity of the system- the physical size of the lighting arrangement required it to be at a large distance from the fluorescing surface in order to achieve correct focussing, and for this reason, the fluorescent signal was not maximized, and detection was limited to 2.5 mg of tracer particles cm^{-2}; this meant that the skin was still contaminated with particles when it appeared that complete clearance had occurred.

2.1.1 Fluorescent Scanning System Design

The recent availability of high-intensity light emitting diodes (LEDs) of suitable wavelengths has allowed the illumination system to be redesigned (Fig 2.1.1) and significantly improved. An array of blue light emitting diodes (LEDs), with their peak emission wavelength at 480nm, were arranged on a stand, as shown in Figure 2.1.1, and used to excite the fluorescence in the labelled silica particles, and a charge coupled device (CCD) camera and image analysis software were used to detect this fluorescence. The physically small size of the LEDs allows them to be positioned close to the fluorescing surface, thus maximizing the fluorescent signal that can be obtained. With this new system, the limit of detection has been improved by a factor of 50 to 0.05mg of tracer particles per cm^{-2}. In addition, the low cost of LEDs and their small size means that they can be easily exchanged for diodes of different excitation wavelengths if the use of alternative tracers requires this.

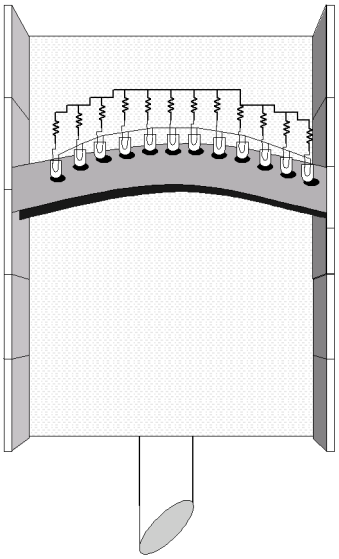

Fig. 2.1.1. Schematic diagram of the components of the fluorescent illumination system.

A Phillips FT12 (Starlight Express SXL8 range) CCD camera fitted with a 50mm lens was chosen to detect the fluorescent signal emitted by the labelled silica particles. The spectral response peaks in the blue-green light at 530nm, hence it is most sensitive at the wavelength of interest (i.e. 525nm). A Schott OG515 coloured glass filter was used as a blocking filter to ensure that no reflected or back-scattered illumination light entered the camera. With this filter, light of wavelength less than 500nm is very effectively blocked from entering the camera. The image processing software used to analyse the images containing the fluorescent signal emitted was Inspector v1.7 (Matrox, Quebec, Canada).

2.1.2 Tracer Particle Labelling

There are only a few dyes that fluoresce efficiently under visible light; the dye that was chosen was fluorescein isothiocyanate (Isomer I). Fluorescein isothiocyanate produces a bright green fluorescent signal at λ = 525nm when illuminated by blue light of approximately 480nm. The aerosol used for the clearance experiments is silica powder manufactured by Phase Separations Ltd. The labelling of the silica powder was achieved by adapting a technique described by Hodson et al. (1994), based on a protocol designed by van Blaaderen and Vrij (1992) to chemically bind organic dye molecules onto the silica molecular structure. A silane coupling agent, 3-aminopropyltriethoxysilane (APTS), was used to bond the dye, fluorescein isothiocyanate (FITC), to the monodisperse spherical particles. This produces a fluorescent dye compound with an attached silane "hook" which may be readily attached to the exposed hydroxy groups of the silica at the surface of the particle. The dry, dyed powder was an orange-yellow colour.

2.1.3 Results

To test the new fluorescence scanning system, experiments have been carried out to determine the clearance rates of 10µm and 3µm particles from skin and Table 2.1.1 shows the range of half-times (i.e. the time taken for the particle concentration to reach half of its initial value) and fall-off rates measured. In the absence of mechanical rubbing of the skin, the clearance of the supermicrometre particles is approximately exponential with time, with an average half-time of 1.5 to 7.8 hours; the range of half-times reflects the influence of the volunteer's arm hair concentration and activity pattern on the residence of particles on the skin. The results indicate that the efficiency of particle retention by the skin increases by a discernible degree as the particle size decreases.

Table 2.1.1. Measured range of fall-off rates and half-times for 3µm and 10µm particles

	10µm	3µm
Range of measured fall-off rates (hr^{-1})	$3.61x10^{-5}$ –$1.21x10^{-4}$	$2.47x10^{-5}$ – 1.28 x 10^{-4}
	Mean value: 8.10 $x10^{-5}$	Mean value: 6.40 x 10-5
Range of measured half-times (hr)	1.59-5.33	1.51-7.80
	Mean value: 2.62	Mean value: 3.79

Prior to application of the particles to the skin, images of the skin test area were recorded to be used as references or background counts. Volunteers, then, had the labeled silica particles applied to their skin using the Palas powder dispersion generator, with the arm positioned at such a distance so that the airflow to which the skin was subjected mimicked mild outdoor conditions (air speed range 0.1 – 0. 5 ms^{-1}). This procedure was followed to ensure that the particles adhered to the skin in a representative way. The subjects had their skin subsequently scanned at either 30 minute or 60 minutes intervals, whereby the camera was used to record the image of the test area. The amount of light emitted was detected by digitising the analogue camera signal and the software displayed the grabbed image. A known relationship between pixel values and the mass of tracer deposited enabled calculation of exposure to the tracer.

A typical decay curve representing the particle fall-off is shown in Fig 2.1.2. This experiment investigated the effect of the pattern of activity on the clearance rate. Low activity meant that for the duration of the experiment Volunteer A spent most of the time at a desk or performing sedentary tasks. The high activity of Volunteer B consisted of vigorous walking for 30-minute periods on a dry day with a light breeze. The analysis of the data from Volunteer A shows the characteristic exponential pattern of the rate of clearance of particles from the skin with time. The clearance of particles from the skin of Volunteer B's arm was not exponential and had reduced to a very low level after the first 30 minutes. Hence, the level of activity has a clear effect on the clearance rate.

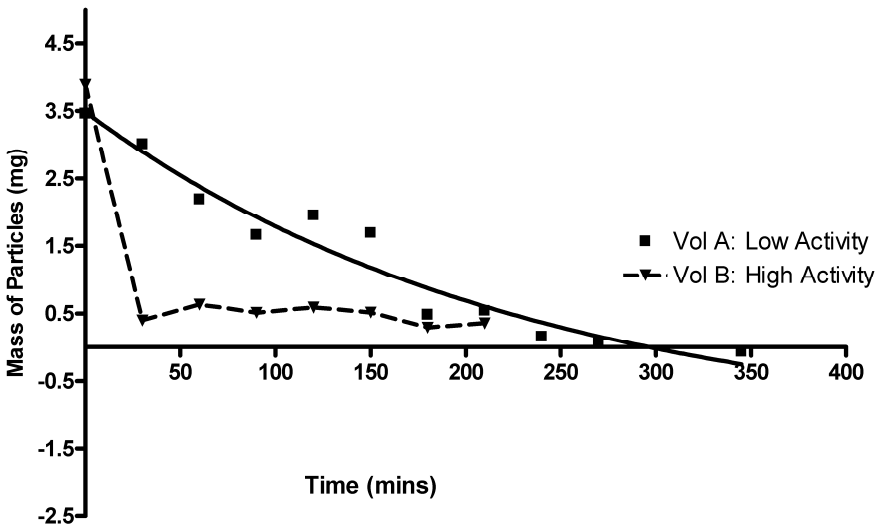

Fig. 2.1.2. Graph showing temporal variation in 10µm particle dermal contamination with varying levels of activity

In a further series of experiments, the effect of hair level on particle retention was investigated. The data generated indicate a difference in the particle fall-off rates from the hairy skin and relatively hairless skin, with hairy skin retaining particles for longer periods. Figure 2.1.3 presents results from one such experiment. Volunteer 1 is female with little arm hair; Volunteer 2 is a male with significant arm hair.

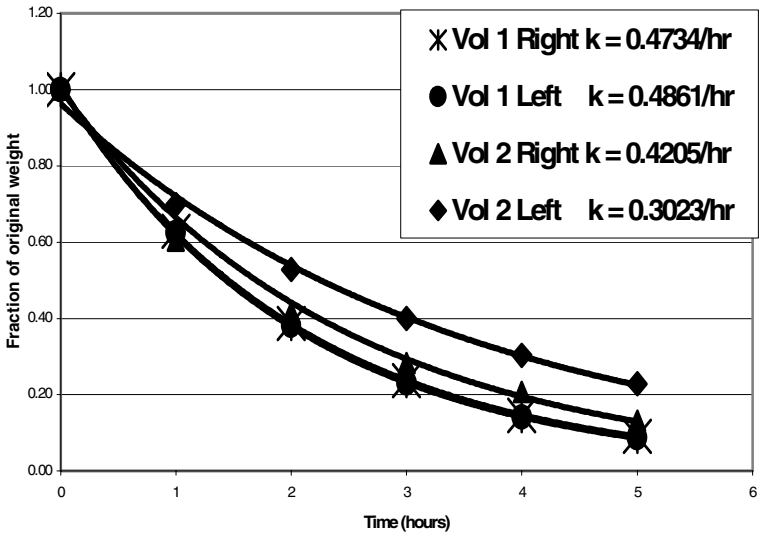

Fig. 2.1.3. Measured time variation in the concentration of 10μm particles on the skin of two volunteers with different levels of arm hair. Volunteer 1 is female with little arm hair; Volunteer 2 is male with significant hair.

It was considered that the loss of particles with time from Volunteer A, shown in Fig 2.1.2, would result from two contributions: particles falling from the skin and particle penetration into the skin. To separate these contributions, volunteers wore particle-coated patches made of latex, with no significant pores and crevices (and obviously, no hair follicles) adjacent to the areas of skin to which fluorescent particles had been applied. Figure 2.1.4 represents results from one such experiment. Over the duration of the experiment the percentage fall-off of the particles from the skin and latex patches differed by approximately only 4%. Taking error into account, the contribution due to penetration for the super-micrometre particles was found to be minor.

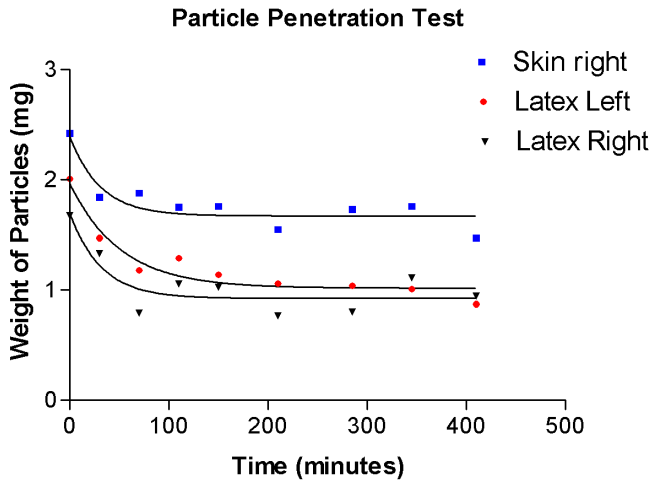

Fig. 2.1.4. Graph showing comparison in temporal variation in 10μm particle contamination of skin and latex patches

The clearance of sub-micrometre particles was investigated in a series of experiments. The particles used were 0.5 μm polystyrene latex micro-spheres that are commercially labeled with tracers that fluoresce at 408nm and are the same as those used in the in-vitro penetration measurements described in section 2.3 of this report. These particles were applied to latex patches which were attached to the skin, since the interference effect of the skin's auto-fluorescence, although reduced by the use of visible illumination, was still significant compared with the fluorescence of the sub-micrometre particles. For these smaller particles, a negligible fall-off rate was observed over a period of five hours of high activity. This is consistent with an earlier observation that small particles tend to be more tightly bound to a surface than larger ones once deposited (Nicholson, 1993).

These experiments indicate that the retention capability of skin for sub-micrometre particles is considerable, and this may imply that an important dose contribution is associated with skin-borne deposits, particularly as experiments described in Fogh et al (1999) indicate that the degree of penetration of particles into the skin structure is likely to increase with residence time. Penetration of toxic particles below the skin's outer layer has the dual effect of exposing deeper layers of the skin and making the particles more difficult to remove by any external means.

The findings described in this work have important dosimetric implications for persons unwittingly exposed to radioactive particles and who do not take steps towards active decontamination. In addition, a scanning system such as that described may also have uses in the occupational nuclear environment, where a need exists to test the efficacy of skin decontamination strategies that might be called into play in the aftermath of an accident.

2.2 Investigation of Chemical Parameters

The experiments described in section 2.3 (see below) attempted to determine the degree of penetration of particles into the skin structure. These experiments were carried out using fluorescent tracer-labelled polystyrene latex beads (of sizes 0.1 μm, 0.5 μm, and 1 μm), which are neither water soluble or fat soluble, so that their penetration (if any) would depend on physical characteristics of the particles and the skin. To complement these experiments, an objective for further work was to investigate the chemical factors governing particle penetration into skin. To this end, it was envisaged that skin would be exposed to particles with comparable size distributions to those produced for the other dermal penetration experiments (i.e. 1 μm or less), but which were fat-soluble. The feasibility of using (a) laboratory generated fluorescent tracer-labelled particles and (b) ambient particles with an identifiable marker was investigated, as outlined below.

2.2.1 Laboratory generated particles

Sub-micrometre fat-soluble particles were generated using the Topas condensation aerosol generator, as described in detail in section 2.3. In this case, the aerosol material used was solid carnauba wax, which had unit density, and a melting temperature of 82-86 ºC. The wax was labelled with the same dye described in section 2.3, Coumarin 6, but in this case, it was necessary to dissolve the dye in chloroform, and add it to the wax at 100^{o}C, whereupon the chloroform evaporated. The aerodynamic size distribution of the output was measured with an Aerodynamic Particle Sizer (APS). As shown in Figure 2.2.1, by holding the saturator temperature of the generator at ^{o}C, and varying the saturator flow rate, monodisperse particles of different sizes could be created. Three monodisperse particles of 0.6 μm, 0.8μm, and 1.0μm, respectively, were generated.

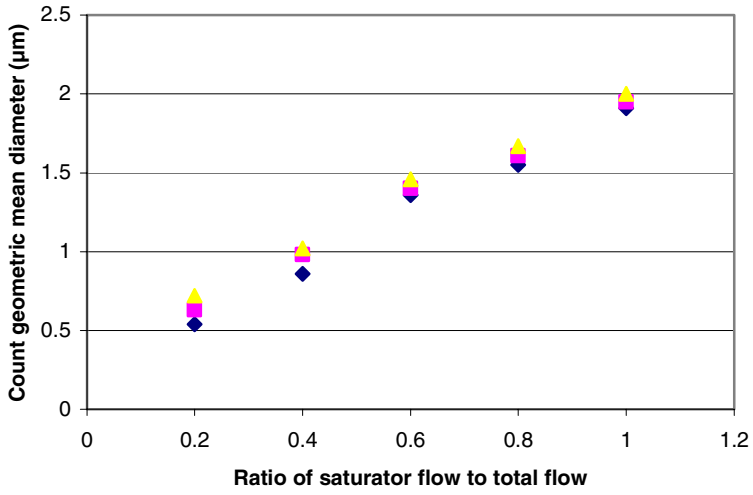

Fig. 2.2.1. Particle size variation with change in flow ratio.

2.2.2 Ambient tracer particles

Diesel exhaust particles generally have diameters between 0.05µm and 1.0µm. These particles consist of a carbonaceous core with a large surface area, onto which various chemical substances are adsorbed, including carcinogenic polycyclic aromatic hydrocarbons (PAHs), which are fat soluble. Investigations were carried out to determine whether suitable markers for diesel particles could be identified, so that, if successful, the penetration of these markers into skin could be studied. Black Carbon was one of the markers investigated. Black Carbon was analysed using an aethalometer (Model AE-8, manufactured by Magee Scientific) which employs the measurement of the attenuation of a beam of white light (due to its absorption by particles), which is transmitted through a sample collected on a quartz fibre filter. By measuring the light absorption for each filter sample before and after exposure, the light attenuation due to Black Carbon sampled on the filter can be deterimined.

A second series of markers that were studied were a selection of the PAHs attached to the surface of the diesel particles. Synchronous Fluorescence Scan (SFS), a known method for the simultaneous determination of multicomponent samples that has successfully been applied to mixtures of PAHs in water samples, was used to detect Chrysene, Benzo(b)Fluoranthene, and Benzo(k)Fluoranthene .

During a pilot study, particles originating from diesel exhaust, were studied by sampling airborne particles close to a diesel pump at a petrol station in Galway City, Ireland. In addition, a volunteer spent 3 hours walking along a busy road, with about 1800 vehicles per hour, in Galway City. In each experiment, three exposure pads, consisting of pre-fired quartz fibre filters (Whatman QM, 25mm diameter) were mounted on both upper (outside) arms, and the right chest, respectively. Airborne concentrations of particles were determined using an IOM total inhalable dust sampler. Based on these measurements, and subsequent analyses to determine Black Carbon concentrations and PAH concentrations, deposition velocities of the diesel particles to the arm and chest surfaces were determined, and were found to be in the range 9.5 x 10^{-5} ms^{-1} – 1.5 x10^{-4} ms-1. Good agreement was found between values determined by both analytical methods, and with the results of previous deposition velocity measurements for sub-micrometre particles to skin, indicating that PAHs and Black Carbon are both suitable markers for sub-micrometre diesel particles, and that their use in dermal penetration experiments could be pursued.

Although suitable particles were (a) successfully generated in the laboratory environment, and (b) successfully identified in the ambient environment for use in elucidating the chemical factors controlling particle penetration into skin, the actual penetration experiments were hindered by the tightening, during the course of the project, of the UK medical ethics requirements that allowed the acquisition of human skin for experimental purposes.

2.3 Dermal penetration rates

Prior to the INDOOR DOSE project, preliminary studies had suggested that when either human or mouse skin was exposed to aerosols of inert, fluorescent particles, that the particles penetrated the epidermis to be present in the underlying dermis. This finding indicated that particulate material could potentially cross the cutaneous barrier, enter into deeper tissues, and possibly redistribute to other sites. Experiments were carried out to examine this process in more detail. The general approach taken was that fresh human skin was exposed to aerosols of fluorescent beads of micrometre or sub-micrometre particles, the exposed skin was processed for histological sectioning, and skin sections were examined by confocal microscopy to determine the position of the particles.

2.3.1 Construction and characterisation of an exposure chamber

The initial part of the dermal penetration part of the project involved the design, construction and characterisation of a test chamber to expose samples of excised skin to aerosols in a reproducible and controlled manner (Fig. 2.3.1). The configuration of the chamber was an earthed stainless steel cylindrical drum with an aperture in the upper region of the wall to allow the introduction of the aerosols.

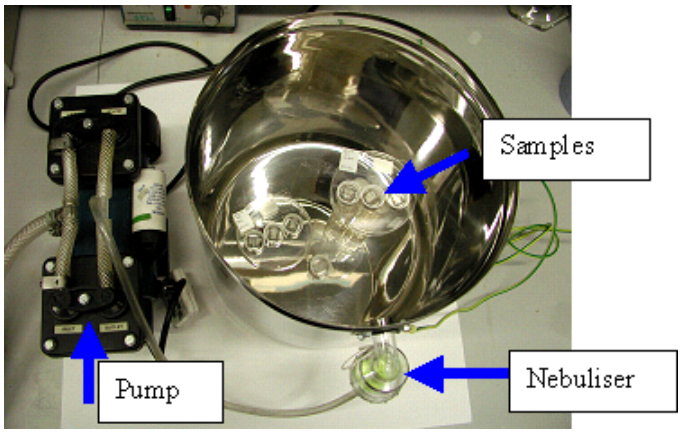

Fig. 2.3.1. The particle delivery apparatus

The pattern of deposition of nebulised particles was determined by introducing particles to the chamber when it contained short strips of adhesive tape at various positions on the flat circular base and curved walls (Fig. 2.3.2). Fluorescence deposited was measured by microscopic examination and image analysis of the tape from various positions in the chamber. A series of such experiments allowed us to determine the pattern of variability of particle deposition within the chamber, and enabled us to optimise our experiments with skin.

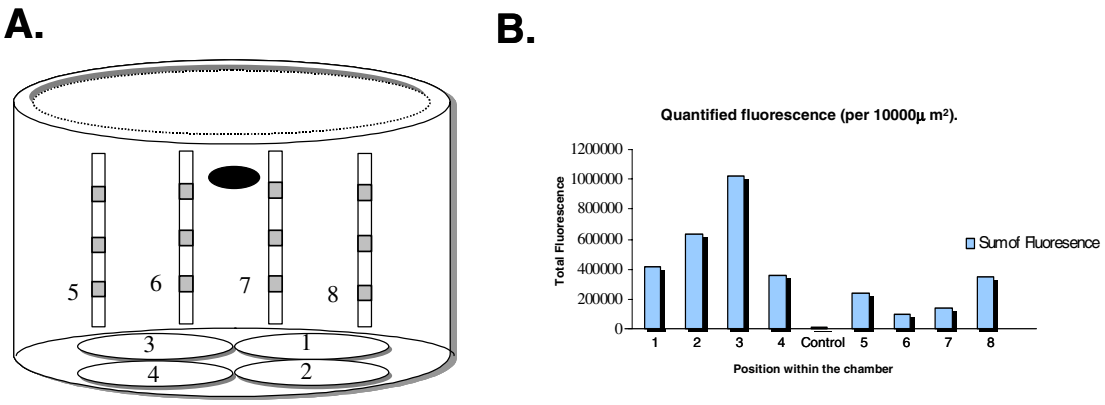

Fig. 2.3.2. Characterisation of the Particle Delivery Chamber: the results of a representative experiment. The graph (B) shows the sum of the fluorescence (arbitrary units) retained on adhesive strips placed at various positions within the chamber (A) (positions 1-4 on the chamber floor, and positions 5-8 (grey rectangles) on the lower regions of the chamber walls). No measurable fluorescence was detected on adhesive strips at higher levels on the chamber wall.

2.3.2 Exposure of excised skin to microparticles

Although some experiments were carried out on rat skin (two sets of particle exposure), the differences in skin thickness and density of hair follicles, compared to human skin, suggested that this may not prove to be a useful model of what may occur in human skin. For the remainder of the project, data was obtained from excised human skin. Human skin was obtained, with ethical approval, from individuals undergoing plastic surgical procedures such as breast or abdominal reduction. Five separate sets of experiments were carried out of skin from 5 different individuals. The skin was cleaned on the underside to remove the majority of the fibro-fatty hypodermis and placed in shallow Petri dishes such that the epidermis (outer layer) was uppermost. The dishes were transferred to the test chamber, which was then sealed. Suspensions of 0.1, 0.5 or 1 µm diameter green-fluorescent polystyrene monodisperse beads were nebulised and allowed to deposit onto the skin samples. After exposure, skin samples were frozen for cryo-sectioning. Sections 10-20 µm thick were taken and were mounted on microscope slides for examination by microscopy. A minimum of 10 sections (containing epidermis, dermis and hypodermis) from each treatment (i.e. time; particle size) was examined to determine the localisation of applied particles.

2.3.3 Microscopic analysis of particle distribution in skin

The tissue layers of the skin vary in density making cryo-sectioning problematic. When skin is sectioned for microscopic examination, it is normally sectioned so that the blade approaches the sample from the epidermal direction towards deeper layers. Initial examination of sections of particle-exposed skin suggested that the sectioning process could displace particles deposited on the epidermal surface such that they could appear in deeper skin layers, i.e. beads from the surface may have been "smeared" over the cut surface of sections and could appear to have penetrated. By altering the direction of sectioning from the standard method (across the layers from the epidermal direction), to along the layers or across the layers from the hypodermal direction, we did find evidence for particle displacement that could compromise the interpretation of particle localisation. Routine sectioning in directions other than surface-to-deep was not possible, as this disrupted the tissue integrity, therefore we had to take great care in the sampling process in our data acquisition.

Laser confocal scanning microscopy was used to determine the location of particles in exposed skin. This technique allows material to be optically sectioned (optical sections ~0.3 µm thick) by removing out-of-focus signal thereby allowing the exclusion of signals from any particles that have been dislodged from the skin surface to apparently deeper regions during handling and sectioning. Skin sections were examined using microscope filter

settings to excite the green fluorescence to visualise the polystyrene particles. Simultaneous phase contrast images of the tissue were acquired and overlaid to allow the determination of localisation of particles in the tissues.

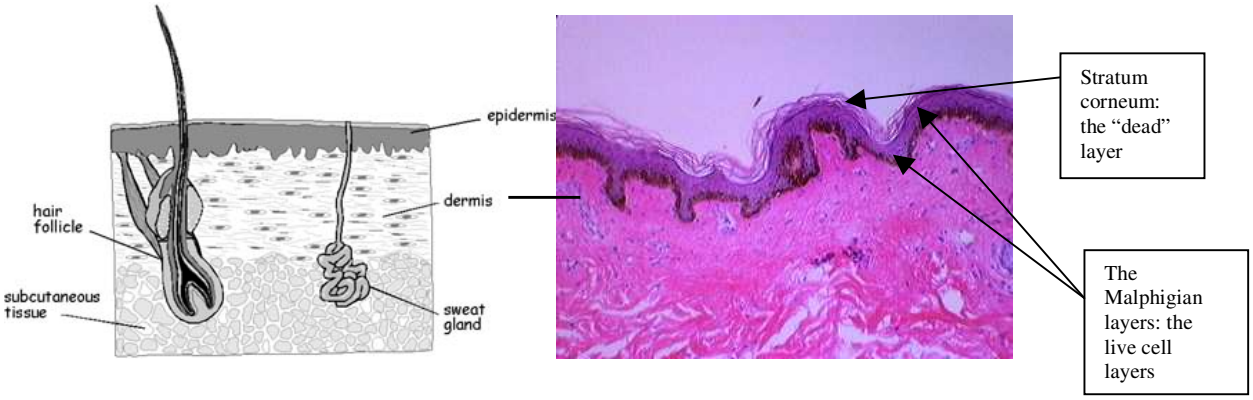

Fig. 2.3.3. Outer skin structure and constituents

The major barrier of the skin is formed by the stratum corneum (SC) of the epidermis (Fig. 2.3.3), the outermost layers of squamous, dead cells. Our observations of particle position within particle-exposed skin showed a consistent pattern, irrespective of particle size or time of exposure. Particles were evident on the surface of the epidermis (at the SC), but were not seen in the deeper layers of the epidermis or in the dermis (Fig. 2.3.4). Although the majority of particles were seen on the outer surface of the SC, some particles were observed to be lodged in spaces between squames of SC, i.e. still within the SC, but between the flakes that will detach from the surface during the normal turnover of the epidermis.

However, particles were found deep to the epidermal surface in hair follicles (Fig. 2.3.5). They were frequently found sandwiched in the space between the epidermis of the follicle, which is continuous with the surface epidermis, and the hair shaft. Though this is not strictly penetration, accumulation at these sites could allow particles to persist in the epidermis. It is also into this region that the lipidic secretions of the sebaceous glands, sebum, are secreted. It is possible that lodged particles could be flushed by such sebaceous secretions from the follicular regions to the epidermal surface.

An additional preliminary set of experiments were carried out where the skin was stretched after particle exposure to mimic natural movements, or damaged with a needle. No epidermal particle penetration was observed after stretching the skin, though a higher frequency of follicular particles was suggested. When the skin was pierced using a fine needle prior to particle exposure, particles were evident in the deeper layers (including the dermis), though the local damage to the tissue made interpretation difficult.

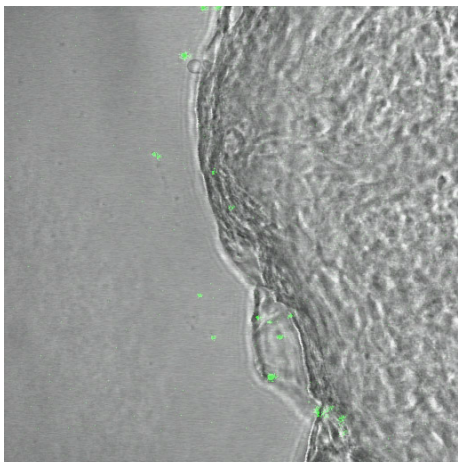

Fig. 2.3.4. This micrograph of particle-exposed skin is an overlay of the green-fluorescence channel and the phase contrast image. Human skin exposed to 0.5 µm beads (green) for 18hr. The particles have not penetrated the epidermal stratum corneum into deeper layers.

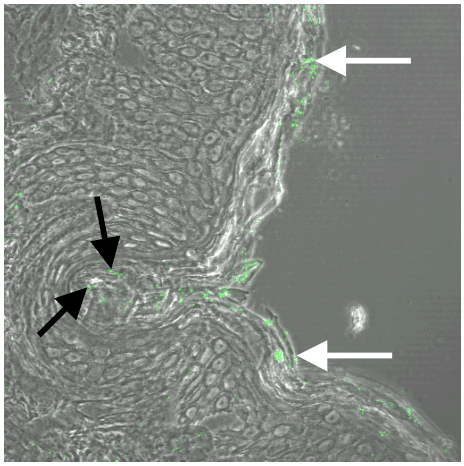

Fig. 2.3.5. An overlay of green particle fluorescence with the corresponding phase contrast image. 0.5 µm beads are evident at the stratum corneum surface (white arrows), but also in deeper regions in a hair follicle (black arrows).

2.3.4 Conclusion

This study examined the fate of aerosolised, inert, fluorescent microparticles deposited on excised human skin for periods of up to 18 hours. Deposited particles of diameters 0.1, 0.5 and 1 µm were observed at the stratum corneum of the epidermis, but were not seen in the deeper layers of the epidermis or in the dermis. The failure to find the particle penetration suggested by preliminary experiments is the result of a more careful detailed examination of the effects of the skin processing steps in producing artifactual displacement of particles

Inert microscopic particles do not appear capable of passively penetrating the stratum corneum of the epidermis. The particles do, however, lodge in hair follicles in the space between the shafts of hairs and the surrounding stratum corneum (which is continuous with the surface stratum corneum). These follicular particles could possibly persist, even after washing, to contribute to longer-term contamination.

2.4 Penetration through clothing

Penetration of contaminant particles through clothing fibres and onto skin is an aspect that has not previously been investigated. The purpose of the investigation was to determine the protective effect that clothing may have in preventing direct contamination of the human body. A series of tests were conducted, where volunteers wore various types of fabric of different materials and thicknesses (thick and thin pure cotton, thin 65 % polyester and 35 % cotton, thick 50 % wool and 50 % acrylic). The volunteers were exposed to tracer labelled 0.7 µm and 2.5µm particles. The penetration through these various types of clothing was examined both to the underlying skin (through wipes with filter paper soaked in ethanol) and to an underlying clothing sample material (cotton). The penetrated tracer concentrations were in none of the cases found to significantly differ from concentrations on the corresponding 'pre-samples' (wipes taken before the experiment or unexposed samples of same material type). This leads to a general conclusion that the penetration of particulate contaminants through clothing must be a pathway of contamination that has very little importance. Based on the measurements that were made, it can be concluded that if particles of the examined sizes deposit on clothing, the fraction of the particles that will penetrate through the clothing will be less than 5 %. In other words, the clothing reduces direct skin contamination by at least a factor of 20. For comparison, it can be mentioned that according to the modelling performed under the contract FI4PCT950019, beta ray attenuation through an ordinary cotton T-shirt will for, e.g., ^{137}Cs, ^{134}Cs and ^{131}I reduce the beta dose by significantly less than a factor of 20. This means that the contribution to beta dose from ^{137}Cs contamination on the outer surface of a contaminated T-shirt will at least be greater than the contribution from the ^{137}Cs that has penetrated through the T-shirt. In order to examine the influence on particle penetration of water (e.g., sweat or rain) added to the clothing-skin interface, an experiment was carried out, in which water was applied to a tracer particle exposed cotton T-shirt on a volunteer, giving rise to thorough wetting. However, skin wipe samples taken after various periods of contact time over one hour showed no significant tracer concentrations on the skin.

3 Redistribution of indoor contamination

This section of the report focuses on the redistribution of contamination through the processes of resuspension and contact transfer. Resuspended contaminants may impose a risk on people living in a contaminated area, both through inhalation and deposition on the body. Investigations were made to characterise resuspended contaminant aersols in the indoor environment, as well as to assess the magnitude of realistic indoor resuspension factors. Contact transfer between a contaminated surface and a human being is an other type of contaminant redistribution, which was under the previous contract deemed to be potentially important. Refined contact transfer investigations have been made, taking into account, e.g., the role of surface material differences and skin moisture.

3.1 Deposition to humans of resuspended particles

The potential for resuspension of deposited particles has traditionally been explained as the potential for aerodynamic forces on a particle to exceed the forces holding the particle to the surface it was deposited on (e.g., Reeks et al, 1988). For small particles in the size range that would typically be of major concern in connection with for instance a large accident at a nuclear power plant (less than 100 μm), inter-surface molecular adhesion (van der Waals forces) constitute a more effective restraint on resuspension than does gravity (Nicholson, 1988). The influence of gravity becomes negligible at particle sizes of less than 10μm. A sufficient condition for a particle to escape an adhesive force is that it be lifted a distance corresponding to twice the particle diameter (Phillips, 1980). At greater distances, adhesive forces will be of the order of thermal (Brownian) forces (Friedlander, 1976). It has been suggested that turbulent energy transfer to a particle on a surface builds up from the resuspending flow, through the agency of a fluctuating aerodynamic lift force (Reeks et al, 1988). This means that a particle in contact with a surface is in a constant state of vibration, and builds up energy until it reaches a level that permits detachment of the particle from the surface. An analogy is a vibrating spring, to which the impact of a series of comparatively small forces may build up a large vibration amplitude in the spring. Both the aerodynamically induced and the adhesive forces acting on a deposited particle increase with increasing particle size, but the aerodynamic forces have the greatest dependence on size (Phillips, 1980).

3.1.1 Size distribution of resuspended contaminant particles

In the context of indoor deposition it has been considered that resuspended particles may have a completely different size distribution from that of the initially deposited contaminants. Two experiment series have been carried out in office test rooms to examine this. Particles of two sizes (0.7µm and 2.5 µm), labelled with neutron activatable tracers (respectively indium and dysprosium), were released to the air in the test rooms, which had not previously been exposed to the applied tracers. The deposition to the floor as well as to surfaces at various heights (applying passive filter paper samples) and the initial size distribution of the emitted particles (by BLPI impactor measurement) were assessed. The following day, air concentrations of both particle sizes were found through impactor measurements to be below the limit of detection. Exactly 24 hours after the release, an effort was made over one hour to resuspend dust particles from the floor of the room. Vacuum cleaning has previously been demonstrated to be very efficient in resuspending house dust particles, although it would generally be expected to prove difficult to resuspend large proportions of small particles of the 0.7 µm range (Thatcher & Layton, 1994). To obtain results with as high accuracy as possible it was therefore decided to continuously 'vacuum clean' the floor of the test room, with no filter in the vacuum cleaner. This was done over a period of 1 hour, during which the size distribution of the resuspended aerosol was measured. Periodic (0.5 h) air samples were taken respectively 1, 2 and 3 hours after the vacuum cleaning was stopped, to examine the dynamics of the decline in the air concentration. After a further respectively 2 and 5 days the vacuum cleaning/ measurement session was repeated, to examine any changes over time in the fixation of the tracers to the floor of the test room. After a couple of weeks the experiment was repeated in a new, similar test room in an other building. The floor was in the first test room covered with linoleum and in the second with a wall-to-wall acrylic carpet.

Table 3.1.1 shows the relationship between air concentrations in the first test of particles labelled with respectively dysprosium and indium, during the initial emission session and during the resuspension session 24 h after the particle release. Throughout the experiment, the room temperature increased from 22.6 °C to 24.6 °C, and the relative humidity increased from 49.1 % to 52.5 %. As can be seen, the relationship between the tracer air concentrations increased by a factor of about 2, indicating that particulate represented by the dysprosium was most susceptible to resuspension. About 6 % of the particles associated with dysprosium could be resuspended by the vacuum cleaning, in comparison with only about 3 % of the particles associated with indium. This indicates that a significant proportion of the particles represented by the indium contamination was at this point still associated with the smaller particles that were originally dispersed in the room. The corresponding resuspension factors were recorded to be in the range of 0.01-0.02 m^{-1}, which ties in with the findings of Sehmel (1980) for vigorous sweeping. Differences in resuspension factor by various indoor activities (e.g., walking around or sitting) cover more than one order of magnitude, as described by Thatcher and Layton (1994), Lefcoe and Inculet (1975) and Sehmel (1980).

Table 3.1.1. Ratio of air concentrations of particles labelled with respectively dysprosium and indium, measured during the initial particle emission and during the subsequent resuspension by vacuum cleaning 24 h after the particle release. Test no. 1 with linoleum floor.

Regime	$C_{air}(Dy)/C_{air}(In)$
During initial particle emission	0.018
During particle resuspension	0.040

Table 3.1.2 shows the deposition velocities of particles labelled with dysprosium and indium to vertically oriented filter papers (passive) placed at heights of 50, 100 and 150 cm in test room 1. Results are shown for both the original tracer particle deposition and for particles resuspended 24 hours after deposition. As can be seen, there is no significant difference between deposition velocities of dysprosium labelled particles during the original deposition and during the first resuspension session. However, there is a tendency towards an increased

deposition velocity for particles labelled with indium. No clear variation in deposition velocity with height can be seen from these data.

Table 3.1.2. Deposition velocities of particles labelled with dysprosium and indium to vertically oriented filter papers placed at heights of 50, 100 and 150 cm of test room 1 (averages of 2 replicate filter samples). Values are given for the initially dispersed particles (ini) and for resuspended particles (res).

Height above ground	Dy_{ini} (m s^{-1})	In_{ini} (m s^{-1})	Dy_{res} (m s^{-1})	In_{res} (m s^{-1})
50 cm	$3.4\ 10^{-4}$	$1.8\ 10^{-5}$	$2.8\ 10^{-4}$	$2.5\ 10^{-5}$
100 cm	$3.8\ 10^{-4}$	$1.8\ 10^{-5}$	$2.7\ 10^{-4}$	$3.7\ 10^{-5}$
150 cm	$1.9\ 10^{-4}$	$1.4\ 10^{-5}$	$2.0\ 10^{-4}$	$3.5\ 10^{-5}$

From similar experimentation in the second resuspension test series, it was found that the deposition velocities of particles represented by the dysprosium to *horizontally* oriented passive filter paper samples were unchanged after resuspension, whereas it was found that the deposition velocity of the particles represented by indium increased by almost an order of magnitude. The average deposition velocity at the initial release was here $3.0\ 10^{-5}$ m s^{-1}, and the deposition velocity of the particles that were resuspended after a period of 5 days was $2.5\ 10^{-4}$ m s^{-1} (averages of 6 replicate filter samples). This data seems to suggest that much of the indium becomes associated with larger particles by the time of resuspension.

The ultimate test for any changes to the size distributions of the particles represented by the two tracers is the result of the neutron activation analysis of impactor foil samples taken immediately at the initial particle emissions and during each resuspension period. Figures 3.1.1 and 3.1.2 show the size distributions of the particles represented by dysprosium throughout the various stages of the two resuspension experiments (average fractions of tracer measured in air in each period). Through impactor measurements, it was assessed that the dysprosium and indium air concentrations in the room prior to any of the resuspension activities were negligible.

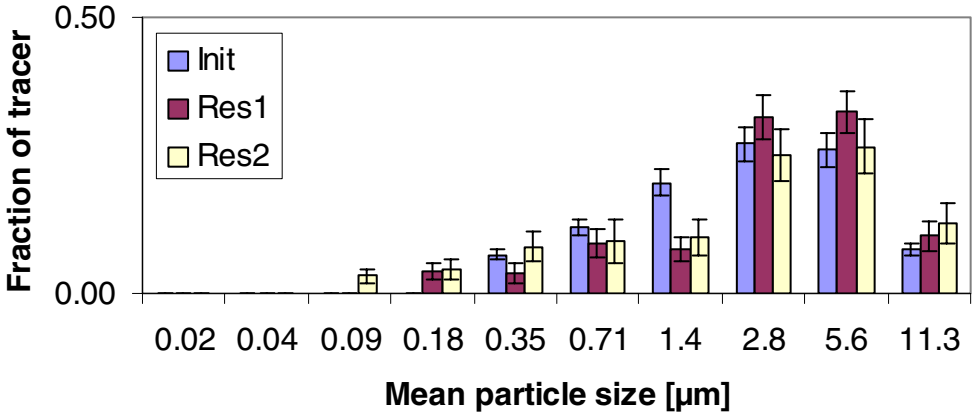

Fig. 3.1.1. Size distributions (fraction in each stage) of dysprosium attached aerosols measured in the various stages of experiment no.1 (linoleum floor). 'Init' is the distribution at the time of the initial particle emission in the room, whereas 'Res 1' is the result of the first particle resuspension after 24 hours, and 'Res 2' is the corresponding after 48 hours. Measurement standard deviations are shown as error bars.

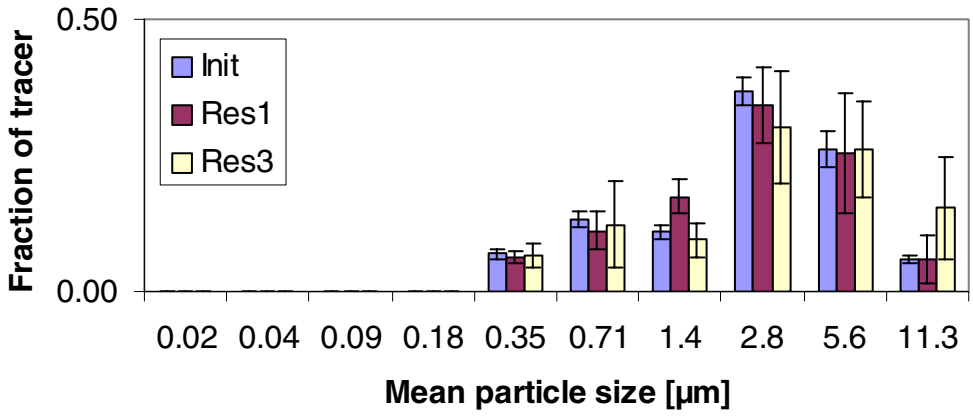

Fig. 3.1.2. Size distributions (fraction in each stage) of dysprosium attached aerosols measured in the various stages of experiment no.2 (floor with acrylic carpet). 'Init' is the distribution at the time of the initial particle emission in the room, whereas 'Res 1' is the result of the first particle resuspension after 24 hours, and 'Res 3' is the corresponding after 5 days. Measurement standard deviations are shown as error bars.

As can be seen from Figures 3.1.1 and 3.1.2, the particle size distribution is practically unaffected throughout the experiment series. The initially emitted dysprosium labelled particles had a mean particle size of about 2.5 µm, and so did the subsequently resuspended particles represented by the dysprosium.

Figures 3.1.3 and 3.1.4 show the corresponding size distributions of the particles represented by indium throughout the various stages of the two resuspension experiments (average fractions of tracer measured in air in each period).

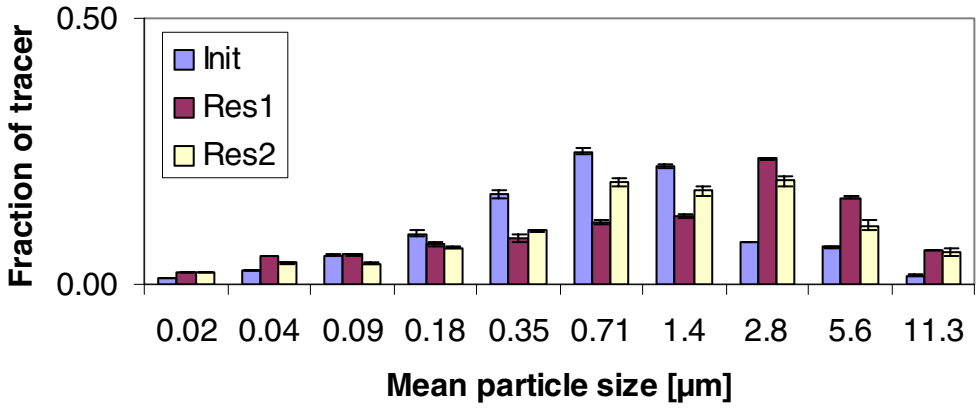

Fig. 3.1.3. Size distributions (fraction in each stage) of indium attached aerosols measured in the various stages of experiment no.1 (linoleum floor). 'Init' is the distribution at the time of the initial particle emission in the room, whereas 'Res 1' is the result of the first particle resuspension after 24 hours, and 'Res 2' is the corresponding after 48 hours. Measurement standard deviations are shown as error bars.

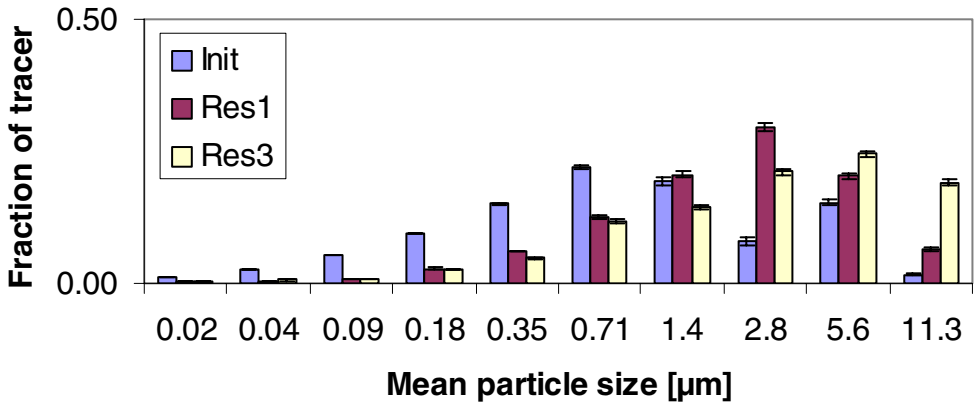

Fig. 3.1.4. Size distributions (fraction in each stage) of indium attached aerosols measured in the various stages of experiment no.2 (floor with acrylic carpet). 'Init' is the distribution at the time of the initial particle emission in the room, whereas 'Res 1' is the result of the first particle resuspension after 24 hours, and 'Res 3' is the corresponding after 5 days. Measurement standard deviations are shown as error bars.

As can be seen from Figures 3.1.3 and 3.1.4, the size distribution of indium-labelled particles was at the initial discharge centred around 0.7 µm, but at the first resuspension, the indium tracer was primarily associated with particles in the 2.8 µm range, and Fig. 3.1.4 shows that after 5 days, the highest indium concentration was found in the stage representing the 5.6 µm particles.

The fraction of the dysprosium tracer mass that could be resuspended from the linoleum floor after 48 hours was about 60 % of what could be resuspended after 24 hours. The fraction of the dysprosium tracer mass that could be resuspended from the floor with acrylic carpet after 5 days was also found to be about 60 % of what could be resuspended from this surface after 24 hours.

The fraction of the indium tracer mass that could be resuspended from the linoleum floor after 48 hours was about 60 % of what could be resuspended after 24 hours, but the fraction of the indium tracer mass that could be resuspended from the floor with acrylic carpet after 5 days was found to be only about 34 % of what could be resuspended from this surface after 24 hours.

Six months later, a further resuspension session was conducted in the carpeted test room, which had been closed off in the intermediate period. The resuspension process was carried out in the same manner as in the previous session. During this session it was found that the air concentration of dysprosium reached 48 % of that at the time of the first resuspension, whereas the indium air concentration reached 28 % of that at the time of the first resuspension.

From these results it seems evident that the contamination becomes more strongly attached to the surface with time. This is particularly the case for the smallest particles, which are the least susceptible to resuspension. However, this can not alone explain the changes to the size distribution of the particles represented by the indium tracer. The increase of the supermicroneous indium tagged particles with time must reflect the attachment of the initial submicron tracer particles to larger particles present in the environment.

Table 3.1.3 shows the decline in the aerosol concentrations over a relatively short period after the resuspension activity had ceased. The results are from the first experiment (linoleum floor). These figures give an image of the length of the time period after a reuspension event, where the resulting increased contaminant air concentration may lead to significant exposure of humans.

Table 3.1.3. Measured air concentrations respectively 1, 2, 3 and 24 hours after the resuspension activity had ceased. Percentages of the average air concentration measured during the resuspension.

	Dysprosium[1)]	Indium[1)]	Dysprosium[2)]	Indium[2)]
1 hour after resuspension	17	20	13	11
2 hours after resuspension	5	9	6	9
3 hours after resuspension	3	4	5	6
24 hours after resuspension	<1	<1	<1	<1

1) After the first resuspension on linoleum floor.

2) After the second resuspension on linoleum floor.

3.1.2 Resuspension of particles due to realistic mechanical disturbances

In an other test series, an experimental system was designed to study particle size-specific resuspension from individual surfaces. A cubic perspex chamber of volume 7600 cm^3 was constructed and a Palas RBG 1000 dry powder disperser was used to deliver aerosol particles to a test surface placed on a shelf at the bottom of the chamber. The particles used were polydisperse silica spheres, and were delivered into the chamber through an aluminium tube of length 41cm. To eliminate the effect due to particle charging two rings of Americium 241 sources were attached to the inside of the tube near the exit end of the tube. Following injection into the chamber, the particle size distribution was determined with an ULPC Laser Particle Counter, the sampling tube of which was inserted through an opening in the wall. The particles were found to have a count median diameter of 1.27 µm, a mass median diameter of 2.82 µm, and a geometric standard deviation of 1.68. The test surfaces used (in order of increasing roughness) were plastic sheeting, wooden board and knitted woollen fabric. Following dispersion into the chamber, particles were allowed to settle onto each test surface overnight.

The uniformity of particle loading of silica on the surface was estimated using fluorescently labelled silica deposited on eighty filter samples placed on the chamber floor. After deposition, each sample was analysed for a fluorescent signal using a Model LS 50B Luminescence Spectrometer and from a predetermined linear relationship between the mass of silica deposited and signal intensity, the mass deposited on each sample was determined. Using a statistical t-test, the difference in particle mass deposited on the test surfaces between trials was found not to be significantly different at the $\alpha = 0.05$ level of significance. For this reason, the output was considered to be reproducible.

Two rectangular metal blocks were chosen to represent a mechanical disturbance. Weight1: 0.110kg with dimensions 6.25cm x 4.40cm and Weight 2: 0.375kg with dimensions 7.55cm x 6.50cm; weights of similar magnitude were used in the resuspension studies of Kildeso et al. (1999). Each weight was dropped from a height of 20cm onto each contaminated surface (via an opening in the lid of the chamber). The concentration and size distribution of the resuspended particles were then determined using the Laser Particle Counter. This instrument classifies particles into six bins: 0.3 µm – 0.5 µm, >0.5 µm-1.0 µm, >1.0 µm-2.0 µm, >2.0 µm-3.0 µm, >3.0 µm-5.0 µm and >5.0 µm-10 µm. For each resuspension event, the particle counter sampled for 10 seconds and the volume of air sampled in that time period was $3.78 \cdot 10^{-3}$ m^3. For each surface, an uncontaminated sample was subjected to the disturbance of the dropped weight, and the resuspended particle distribution from this "background" sample was subtracted from that of the relevant contaminated sample. The aerosol particle counts due to ambient aerosol in the test chamber were also subtracted.

Concentrations of particles resuspended from the test surfaces of varying roughness (following subtraction of background counts) were not found to be significantly different; these results, averaged over five samples for each surface type, are shown for Weight 1 in Figure 3.1.5 and Weight 2 in Figure 3.1.6.

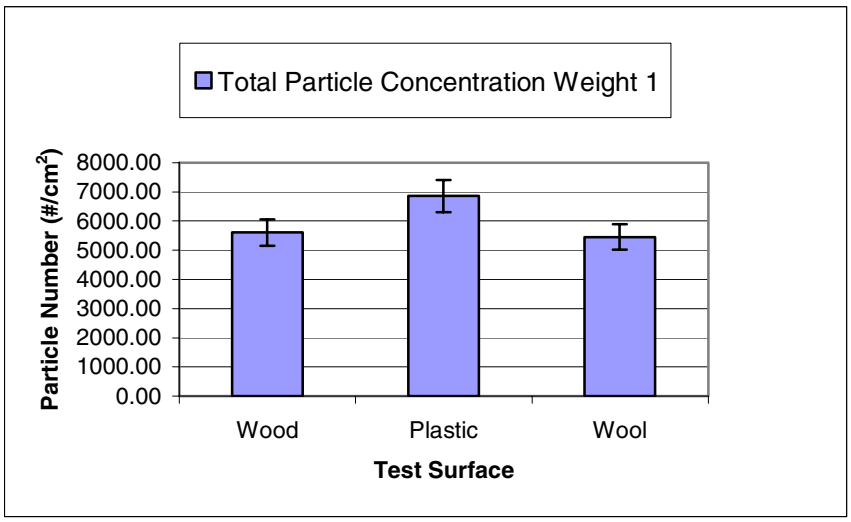

Figure 3.1.5. Total resuspension particle concentration from three test surfaces due to impact from Weight 1

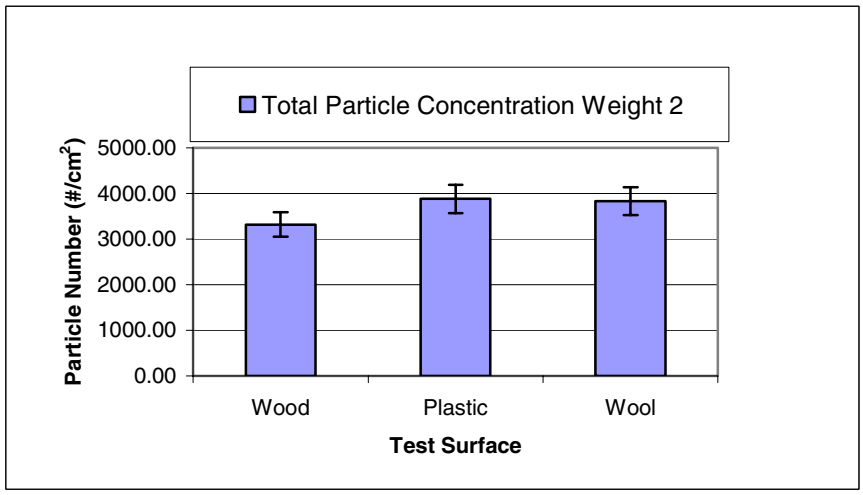

Figure 3.1.6. Total resuspension particle concentration from three test surface due to impact from Weight 2

A higher concentration of resuspended particles was expected from the impact of the heavier weight, however this was not the case and inconsistencies in the way in which the weights fell each time may be responsible for this discrepancy. The plastic surface in this work is the smoothest surface and appears to give the least resistance to resuspension, therefore giving off the highest concentration of particles in both cases. This is consistent with previous studies which found that resuspension is greater from smooth surfaces than rough (Braun et al. 2002).

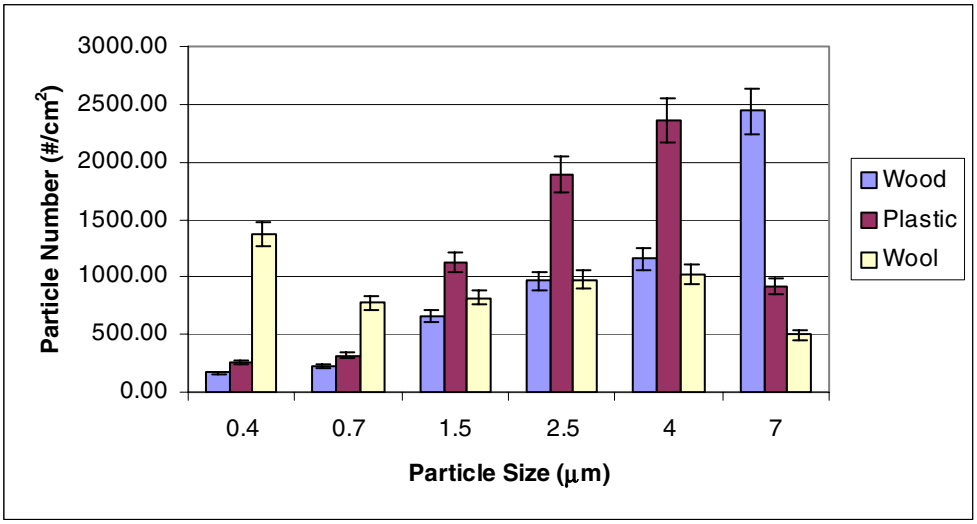

Figure 3.1.7. Resuspension particle concentration over each size range from each test surface due to impact from Weight 1.

Figures 3.1.7 and 3.1.8 illustrate the resuspension particle concentration over each size range for each surface for Weight 1 and 2 respectively. In the case of all three surfaces, there is a shift toward a larger count median diameter (CMD), relative to the depositing particles and the background deposits. It is known (Reeks et al., 1988) that the ratio of gravitational to van der Waal's forces acting on a particle, which is a function of particle size, is a determinant of resuspension potential. However, the ratio of gravitational forces to diffusive forces, which is a determinant of particle deposition on a surface, is governed by a different particle size function. For this reason, it is likely that the particle size spectrum of resuspending contamination will differ considerably from that of depositing, as is evident in these results. This shift is also an indication of the retention ability of the surface for small particles in particular.

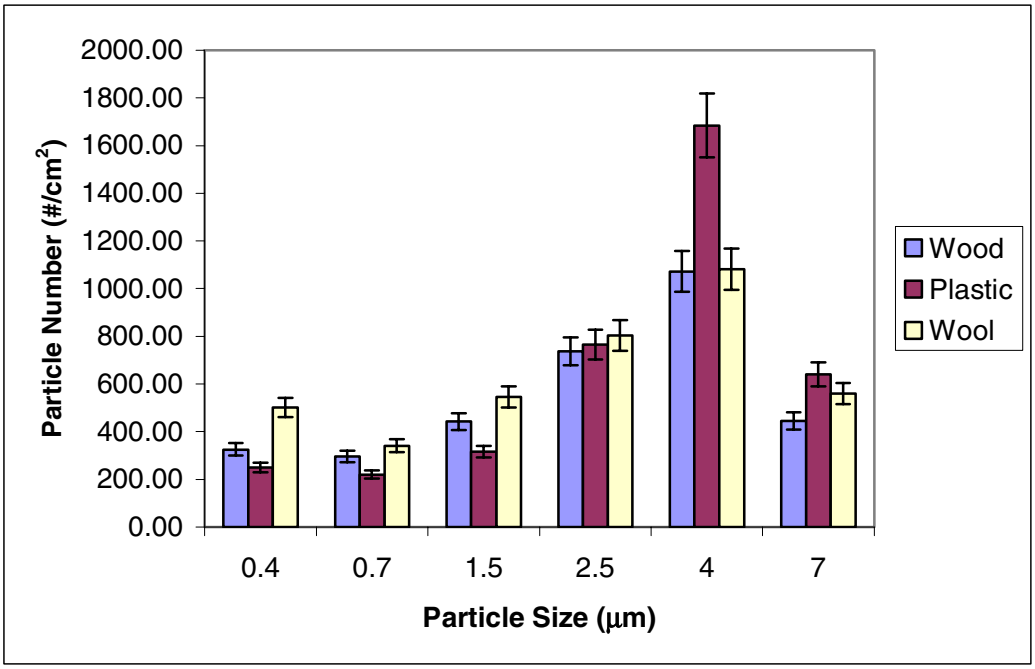

Figure 3.1.8. Resuspension particle concentration over each size range from each test surface due to impact from Weight 2.

For the plastic surface, resuspension is more efficient in moving the larger particles, which suggest that the submicron particles may be more influenced by the electrostatic nature of the surface. Small particles with smaller surface areas will have more surface contact with the plastic surface and adhesion bonds are harder to break (Reist, 1993).

Results for the wool surface show less of a shift towards larger particles than the other two surfaces. In fact, the resuspension results from this surface using Weight 1 indicate a high contribution from the smallest particles. One would expect such a rough surface to have a higher trapping or holding capacity than a smooth surface eg. particles settled into carpet, due to the pull of gravity are not easily removed by air currents within a room or through the action of walking. Quantitative results indicate that carpet can function in a filter-like capacity by trapping particulate matter (Braun, 2002). However, due to the "hairy" nature of the wool test surface used, it is thought that particles attached themselves to these hairs without actually settling on the surface. In this way, the surface area to which each particle is attached is reduced, thus reducing the adhesive force and the lift force required for resuspension to occur.

The wood test surface performed in a similar way to the plastic surface. Although having some grooves which could trap the smaller particles, it is relatively smooth overall and is likely to allow efficient resuspension of the larger particles, as is evident in the results.

Table 3.1.4 shows the measured count median diameters (CMDs), mass median diameters (MMDs) and geometric standard deviation of the particles resuspended from plastic, wood and wool.

Table 3.1.4. Comparison of the size distribution of deposited particles and resuspended particles, from wood, plastic and wool surfaces

	Count Median Diameter (μm)	Mass Median Diameter (μm)	Geometric Standard Deviation
Deposited Particles	1.27	2.82	1.68
Resuspended Particles – Wood 1	2.87	6.43	1.68
Resuspended Particles – Plastic 1	3.15	3.20	1.08
Resuspended Particles – Wool 1	1.47	2.01	1.38
Resuspended Particles – Wood 2	2.29	5.98	1.76
Resuspended Particles – Plastic 2	3.21	8.54	1.77
Resuspended Particles – Wool 2	2.22	5.56	1.74

Resuspension is described by a resuspension factor, R. R is the ratio of aerosol concentration at a reference height above a surface (gm^{-3}) to the aerosol particle loading per unit area of the surface (gm^{-2}).

The resuspension factors for the three different surfaces for both weights were calculated and are shown in Table 3.1.5.

Table 3.1.5. Comparison of the resuspension factors for wood, plastic and wool surfaces for two different weights

Surface Type	Weight 1	Weight 2
	Resuspension Factors (m^{-1})	Resuspension Factors (m^{-1})
Wood	$5.420 \times 10^{-6} m^{-1}$	$1.249 \times 10^{-5} m^{-1}$
Plastic	$2.918 \times 10^{-5} m^{-1}$	$3.987 \times 10^{-6} m^{-1}$
Wool	$1.484 \times 10^{-6} m^{-1}$	$3.228 \times 10^{-6} m^{-1}$

The resuspension factors are as expected with wood and plastic having greater values than that of wool. Again this is consistent with previous studies where the concentration of particles in the sample zone over a hard surface becomes significantly larger than that over a rough surface (Braun et al., 2002). Although the heavier weight (Weight 2) resuspended a lower concentration of particles, the resuspension factors are higher with the heavier weight for both the wood and wool surfaces. This can be attributed to the fact that there is a greater shift towards

larger particles in the wood and wool resuspension for Weight 2 than for Weight 1 i.e. there is a greater mass concentration.

The experiments described above represent an attempt at understanding size-specific particulate resuspension, from a range of surface types and under controlled conditions of surface loading. In agreement with earlier measurements, greater resuspended concentrations of particles have been measured from smooth surfaces than from rough surfaces. Smooth, hard surfaces offer little resistance to air motion and consequently particles on or near the hard surface are more readily resuspended into the air, the result being the potential for higher exposure of airborne particles in the breathing zone**.** An interesting feature of the data obtained is the observation of the shift in the particle size spectrum that occurs when deposited material undergoes resuspension, and the surface characteristics that influence this shift.

The calculated resuspension factors are also consistent with previous studies. Thatcher and Layton (2000) found resuspension rates of between $1.8 \cdot 10^{-5}$ and $3.8 \cdot 10^{-4}$ m^{-1} for light activity with four people in the residence. Also, Brodsky (1980) concluded that vigorous disturbance could produce resuspension factors higher than 10^{-6} m^{-1}.

In order to check that the disruptive forces to which the surfaces were subjected were realistic, the results were compared with the results of a small number of "real" resuspension events i.e. where the test surface was subjected to a footfall. Comparable resuspension factors were calculated, and the size spectrum of the resuspended particles was found to be similar.

3.2 Inhalation of resuspended and other particles

In addition to the results obtained under section 3.1, experiments were carried out to determine the influence of particle (re)suspension from the human body on breathing zone air concentrations.

A timber-framed chamber, with three plastic sheeting walls (and a plastic sheeting floor), and one wall composed of a high efficiency particle air (HEPA) filter was constructed. The dimensions of the chamber were 1.1m (l) x 1.47 m (w) x 2.6m (h). Drawing of air through the HEPA filter, using a pre-installed fan, provided an effective method of purging the chamber between trials.

A ULPC-500 Laser Particle Counter, capable of providing particle concentration data in six particle size ranges (midpoints 0.5 μm, 1.0 μm, 2.0 μm, 3.0 μm, 5.0 μm, 10.0 μm) was used. The 0.11m inlet sampling tube was inserted through a hole in the centre of the front face of the chamber, so that aerosol concentrations were consistently recorded at a distance of 1.47 m from the back wall and 1.12 m from the floor.

To assess the particulate contribution arising from various components of the body, a volunteer entered the chamber, and engaged in a repeatable activity pattern. Particle concentration measurements were made over a 1-minute period in the six particle size ranges while (a) the clothing, hair and hands were encased in plastic wrapping (b) the hair and hands were encased in plastic wrapping (c) the hair was encased in plastic wrapping and (d) the entire body was exposed. 5 repeat particle concentration measurements were made for each plastic wrapping pattern. It was ensured that the baseline particle concentration (achieved with the HEPA filter in operation) was re-established between trials.

5 volunteers participated in the experiments and their clothing and hair types were:

Volunteer 1: medium length hair, acrylic top, polyester trousers

Volunteer 2: Short hair, denim jeans, 65% polyester 35% cotton shirt

Volunteer 3: Long hair, woollen jumper, cotton trousers

Volunteer 4: Long hair, cotton top, denim jeans

Volunteer 5: Short hair, woollen jumper, denim jeans

Figure 3.2.1 shows the relative contributions to breathing zone particles, in six particle size ranges, arising from the body surfaces of Volunteer 3. These contributions arise from skin, hair and clothing fragments, and also from particles that have deposited on body surfaces and become resuspended. It can be seen (a) that the major contribution to particle number concentration occurs in the sub-micrometre size range and (b) the most significant contribution to total particle concentration arises from clothing, presumably because clothing covers a greater surface area of the body than hair or exposed skin. To obtain a clearer indication of the relative contributions of the other body surface components, Figure 3.2.2 shows particle concentrations arising from Volunteer 2, with the clothing contribution removed.

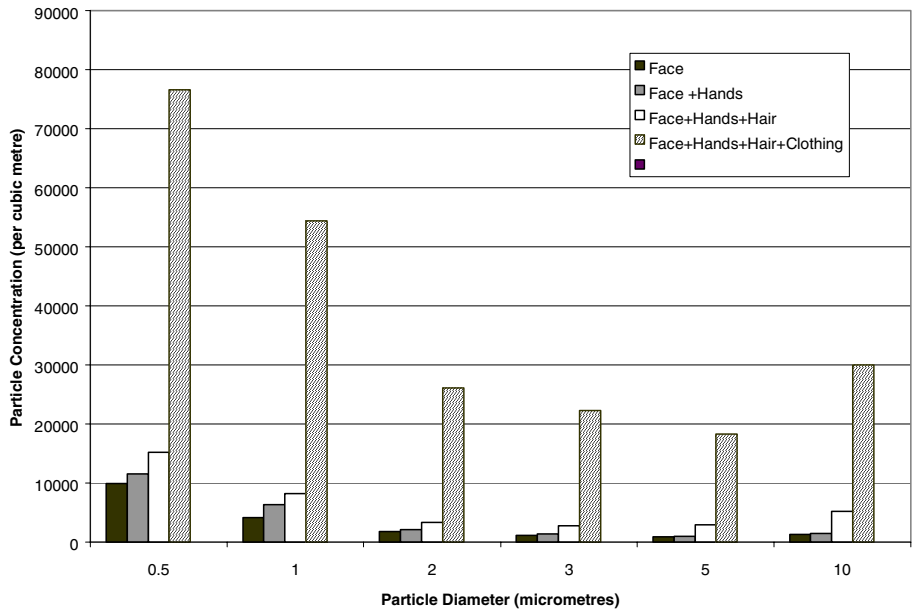

Fig. 3.2.1. Relative particle contribution from face, hands, hair and clothing: volunteer 3.

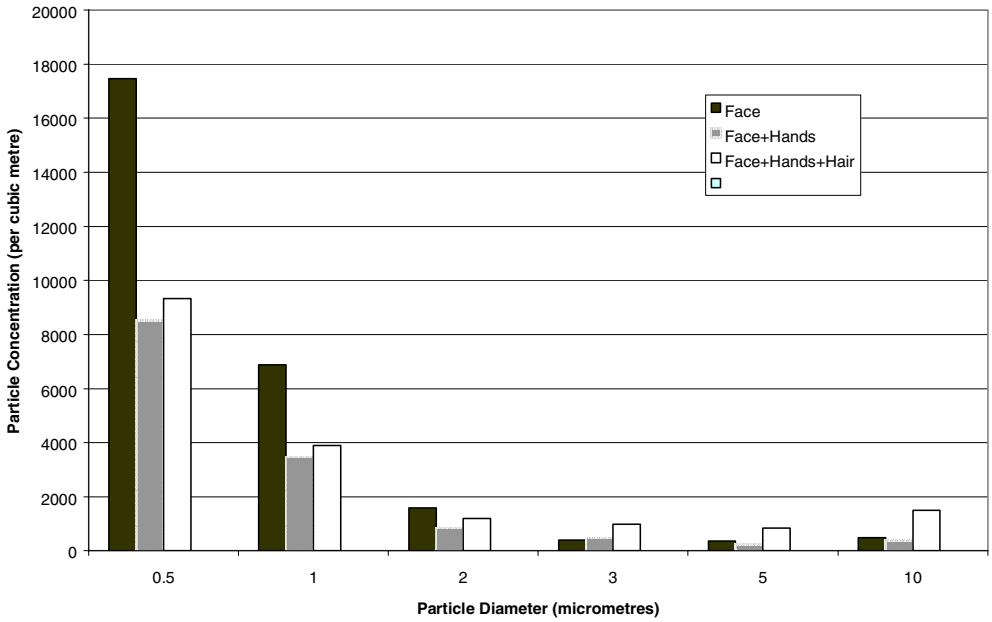

Fig. 3.2.2. Relative particle contribution from face, hands, hair and clothing: volunteer 2.

Figure 3.2.3 shows an inter-comparison of particle concentrations arising from two volunteers, and indicates that the type of clothing worn (natural vs. synthetic), and the length of hair are important governing factors.

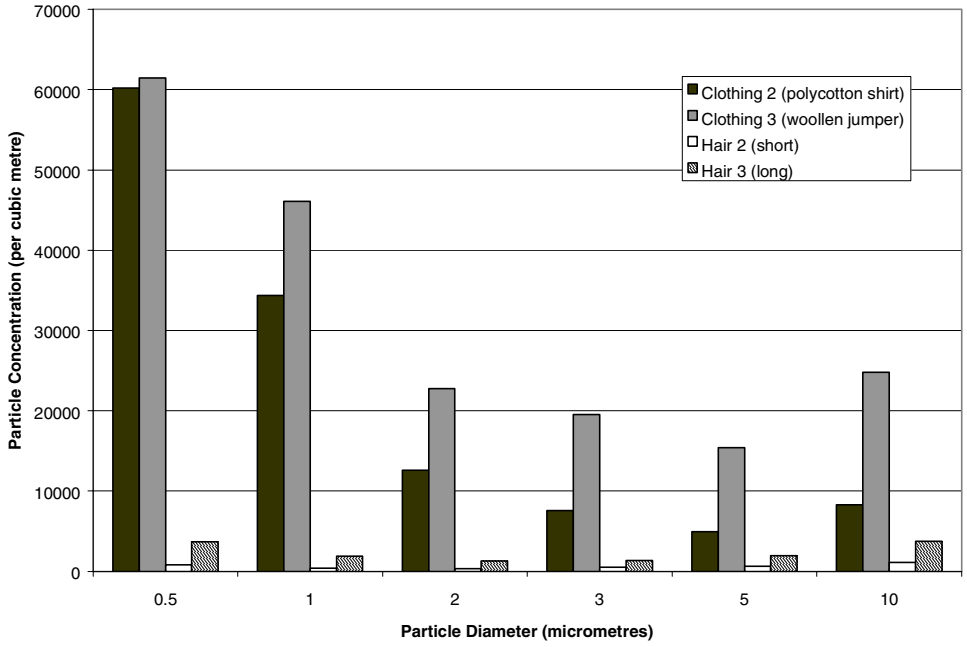

Fig. 3.2.3. Comparison of particulate contributions from hair and clothing between volunteers 2 and 3.

In the context of radiological risk assessment, it is the contribution of the re-suspended particulate component, and not the surface-generated component, to breathing zone concentrations that is of primary interest. In a series of experiments, two fabrics types (Fabric 1: 100% synthetic velvet-type fabric, Fabric 2: smooth cotton fabric) were washed and dried thoroughly (to remove any deposited particles), and then were exposed to "naturally-occurring" aerosol particles for several hours i.e. Fabric 1 was exposed to tobacco smoke particles, and Fabric 2 was exposed to house-dust. The fabrics were then introduced individually into the test chamber, and the degree of re-suspension resulting from each was observed. The results are shown in Figure 3.2.4, and indicate that there is a considerable difference between the re-suspended aerosol size distributions in the two cases, due (a) to differences in initial size distribution of the deposited material and (b) to different retention characteristics of the fabrics.

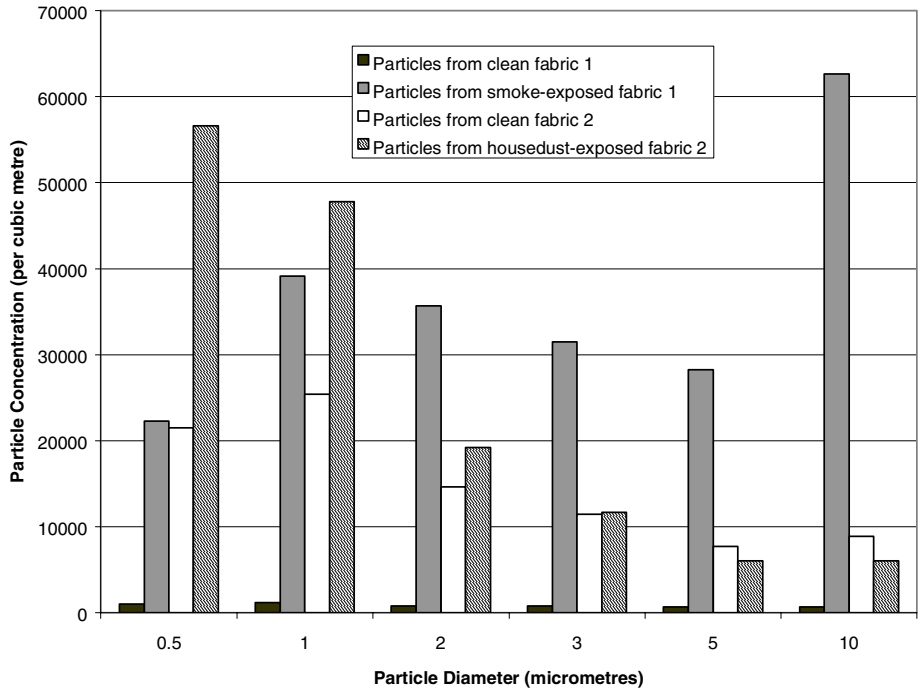

Fig. 3.2.4. Resuspended particles from fabric.

3.3 Skin contact transfer

To understand more completely the surface and particle related factors controlling contact transfer at low particle loadings (relevant to radioactive contamination scenarios), experiments have been carried out to significantly extend the range of particle sizes previously studied. Four new particle distributions were introduced: 0.026µm, 0.1µm, 0.5µm, and 1µm, and these are thought to be the first reported measurements of sub-micrometre particle contact transfer. The experimental strategy involved uniformly contaminating a test surface in a small exposure chamber (25cm x 25 cm x 21 cm) with fluorescent polymer particles using a De Vilbiss Model 45 nebuliser, touching the surface with a gloved hand in a repeatable way, and analysing the surface and the glove by using a

fluorimeter. The first series of experiments involved 0.1μm and 0.5 μm particles, dry gloves and damp gloves, single and double hand presses, and smooth plastic, smooth aluminium foil, and wooden workbench test surfaces and the results are summarised in Table 3.3.1. Percentage contact transfer efficiency, C, was evaluated using the following expression:

C = (Mass of fluorescent particles per unit gloved hand area/ mass of fluorescent particles per unit test surface area) x 100

Table 3.3.1. Percentage contact transfer efficiency (standard deviation and number of replicate experiments shown in parentheses).

	Plastic	Metal Foil	Wood
Dry gloves 1&2, 0.1μm particles	21.30% (2.58%, 5)	49.35% (6.65%, 5)	15.73% (1)
Dry gloves 1&2, 0.5μm particles	-	63.63% (3.81%, 5)	59.54% (7.67%, 5)
Damp gloves 1&2, 0.1 μm particles	70.17% (15.11%, 5)	63.43% (15.73%, 6)	59.54% (2.7%, 5)
Damp gloves 1&2 0.5 μm particles	-	65.48% (7.96%,5)	86.96% (2.67%,5)

A number of observations can be made, based on the results shown in Table 3.3.1. Firstly, the percentage contact transfer efficiency determined was large (albeit with a high standard deviation in some cases) for these smaller particles, relative to the earlier results obtained using 5μm and 10μm particles; the largest value recorded for the 5 μm particles was of the order of 30%. A second observation is that the effect of surface moisture on the gloves had an overall enhancing effect on the degree of contact transfer that occurred. Thirdly, it was observed that the transfer of 0.1 μm particles to dry gloves differed considerably according to whether the contaminated surface was smooth plastic or smooth metal foil. It is thought that the surface charges on the small polymer particles might enhance their adherence to the electrostatic plastic surface, whereas such charges would be dissipated when the particles deposited on the metal surface. Finally, it can be seen that, in general, contact transfer from the smooth foil and plastic surfaces was more efficient than transfer from the rougher workbench surface.

The second series of experiments introduced the significantly smaller 0.026 μm particles, and focussed on comparisons between contact transfer to gloves of different particle sizes. These results are summarised in Table 3.3.2 and in this case, transfer factors were calculated, where T, the percentage transfer factor is defined as:

T = (Mass of fluorescent tracer on glove/mass of fluorescent tracer on test surface) x 100

Table 3.3.2. Contact transfer factors (standard deviation and number of replicate experiments shown in parentheses)

	Plastic	Wood
Dry glove 1 1μm particles	35.2% (1.0%, 5)	-
Dry glove1 0.5μm particles	26.0% (4.8%, 3)	21.6% (4.5%, 3)
Dry glove 1 0.026 μm particles	22.9% (5.5%, 5)	16.8% (2.0%, 5)

The results shown in Table 3.3.2 indicate that the transfer efficiency of sub-micrometre particles decreases as particle size decreases. It is likely that surface adherence for the 0.026 μm particles is enhanced by electrostatic effects in the case of the plastic surface, and by roughness effects in the case of the wooden surface.

4 Dosimetric modelling

Various possibly significant contributions to dose from contamination in the indoor environment may be perceived. These may have varying importance in different types of contamination scenario. Figure 1 shows a flow diagram of how the contamination may migrate within the indoor environment, outlining a number of possible dose pathways. Contributions to dose from outdoor sources and anthropogenic indoor contamination from outdoor sources (e.g., tracking in under shoes) are not covered by the project. The events leading to the contamination may be as diverse as a release from a nuclear power plant, the detonation by a terrorist of a 'dirty bomb' contaminant dispersion device or a laboratory spillage of radioactive matter.

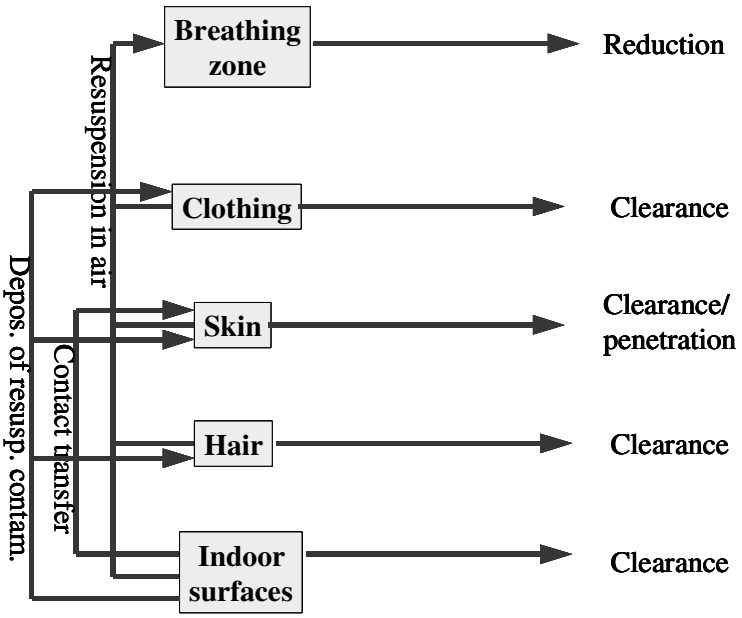

Fig. 4.1. Diagrammatic representation of the potential transfer of contamination within an indoor environment.

4.1 General methodologies

4.1.1 Contamination on humans

4.1.1.1. Generic formulae

Radioactive contamination on human skin, hair or clothing can result in both beta doses to the skin and gamma doses to the body.

The total deposition per unit of area to a human body surface is given by the following expression, incorporating contributions to the time-integrated air concentration of particles from both initial and resuspended contaminants:

(1) $M_h = \int v_{d,h} C_i dt + \int k v_{d,h} M_f dt$, where $v_{d,h}$ is the deposition velocity to the human surface in question, C_i is the air concentration of the released contaminant, M_f is the deposited amount of particles on the floor at the time of the resuspension, and k is the resuspension factor for contaminants of the relevant type. The integration covers the periods of time where the room is occupied by humans. Both gamma and beta doses due to the deposition of a contaminant radionuclide can be calculated from the following:

(2) $D = M_h \cdot \Gamma \cdot \frac{1}{\lambda_{nuclide} + \lambda_{clearance}}$ (Fogh & Andersson, 2000), where Γ is the conversion factor from surface contamination level to either gamma or beta dose rate to the human body part in question, $\lambda_{nuclide}$ is the radioactive decay rate constant of the nuclide, and $\lambda_{clearance}$ is the rate constant for clearance from the human surface.

Indoor-outdoor air concentration relationship:

If the source is of outdoor origin, but the exposed persons are indoors most of the time, as would for instance be expected in the event of a major nuclear accident, the following relationship would at equilibrium apply between indoor and outdoor contaminant air concentrations:

(3) $\frac{C_i}{C_o} = \frac{f\lambda_v}{\lambda_v + \lambda_d}$, where f is the filtering factor, and λ_v and λ_d are the rate coefficients of respectively ventilation and deposition. Typical value ranges for these three parameters for different sorts of dwellings are given in the final report of contract no. FI3P-CT92-0038 (Andersson et al., 1995). For European houses of good construction, the relationship between indoor and outdoor air concentrations at equilibrium would on this basis be expected to be of the order of 0.5 for 0.7 µm and 0.1 for 5µm particles, which have considerably higher indoor deposition velocities.

4.1.1.2. Deposition velocities

Estimates of dry deposition velocities of particles to skin, hair and clothing can be based on the experimental results obtained in the INDOOR DOSE project, which are supported by the findings of Fogh et al. (1999). No other relevant estimates of these parameter values are available from published literature. A number of different types of events may lead to considerable radioactive contamination of the human body, and a crucial factor governing the fate and impact of the contaminant aerosol is, as demonstrated in the previous paragraphs, its size. Table 4.1 shows a selection of best general estimates of the relationship between aerosol size and expected deposition velocity to human skin, hair and clothing, based on the measurements. As was found in the experimental work, fabric type has little influence on the deposition to clothing. Interpolations between the different data sets for the various examined aerosol sizes are allowable for estimates for other aerosol sizes, since the variation in the first derivative of the deposition velocity vs. particle size function is expected to be relatively little for sizes above 0.7 µm.

Table 4.1. Best general estimates of deposition velocities of particles on human body surfaces

Particle AMAD	0.7 µm	4 µm	10 µm
V_d (human skin) [m s^{-1}]	$1.0\ 10^{-3}$	$1.2\ 10^{-2}$	$3.0\ 10^{-2}$
V_d (human hair)[a)] [m s^{-1}]	$2.6\ 10^{-4}$	$3.0\ 10^{-3}$	-
V_d (human hair)[b)] [m s^{-1}]	$1.2\ 10^{-4}$	$1.5\ 10^{-3}$	-
V_d (clothing) [m s^{-1}]	$1.7\ 10^{-3}$	$2.7\ 10^{-3}$	$5.0\ 10^{-3}$

a) distal part of hair strand; b) proximal part of hair stand

It should be stressed that the above 'best general estimates' would not necessarily be applicable in situations where the deposition process is strongly influenced by certain physical mechanisms. As has been found within the project, electrophoretic effects near surfaces with high voltages may have a considerable effect on the deposition velocity to humans. However, this would only be expected to have importance for submicron particles and only in unusually strong electric fields, for instance in the vicinity of a TV screen. The actual influence on deposition would depend on the surface charge density of the particles and the influencing electric field in the given situation, but based on the experimental data, increases by more than an order of magnitude in deposition velocity could be realistic if the exposed persons are very near a TV screen.

In the INDOOR DOSE project, also skin moisture has been found to have a highly significant effect on the deposition / initial retention of particles on skin. The deposition velocities to very moist skin can be at least a factor of 2 greater than the values shown in Table 4.1, whereas deposition velocities to very dry skin may be more than a factor of 2 less than those given in Table 4.1. Contrary to electrophoresis, skin moisture has been found to affect both sub- and supermicron particles.

Natural variations in the temperature difference between humans and ambient air have been found to have little bearing on the deposition velocity to the humans. Also, the effect of sitting very near a heat source during the deposition process was found to be small unless the distance to the heat source is extremely small. However, any heat source will naturally add to the convective turbulent air streams that can significantly influence deposition.

The figures given in the table are for persons who are sitting still. The experimental results obtained within the project suggest that the deposition velocity to walking persons could be about a factor of 2 higher, both for sub- and supermicron particles.

In addition to particle deposition, also deposition of radioactive gases may lead to significant contamination of the human body. It has been demonstrated that specifically exposure to elemental ^{131}I gas may be a highly significant problem in connection with a major nuclear accident. This problem, which was investigated experimentally within the project, is described in detail in connection with the demonstration scenario in the next chapter.

Also the implications of contamination of humans by resuspension is described in detail in the demonstration scenario section.

4.1.1.3. Removal rates

For the dose calculation in the above formula no. 2, estimates are needed of the radioactive decay rate constant(s) of the nuclide(s) in question, and of the rate constants for clearance from the various contaminated human surfaces. Radioactive decay rate constants are tabulated in numerous standard references, such as the Chemical Rubber Publishing Co.'s Handbook of Chemistry and Physics.

Like deposition velocities, clearance half-lives of the various contaminants on humans are strongly dependent on the size of the aerosol (Andersson et al., 2002).

Experimental work carried out within the INDOOR DOSE project combined with earlier work by the same consortium to determine clearance half-lives from skin suggests a value of about 1.2 days for particles in the 2.5 µm AMAD range, but only about 0.16 days for particles with an AMAD of about 4.5 µm. Experimental work in the INDOOR DOSE project revealed that particles in the 0.5-1 µm range remain on the skin surface over much longer periods of time. Based on these results, it is considered that the clearance process will here be governed by the shedding of the stratum corneum (horny surface layer) with a half-life of some few weeks.

Particularly the smaller of the particles of interest have been found to have the ability to penetrate into crevices of the stratum corneum and deep into hair follicles, where they are to some extent immobilised. As described above, no particle penetration beyond the stratum corneum layer, which also lines the surface of hair follicles, has been observed in any of the experiments performed in this project. It has, however, recently been found by other workers using similar techniques that a small percentage of the applied 0.5-1 µm particles can in connection with motion of for instance a wrist penetrate the human stratum corneum and reach the epidermis, and, occasionally, even deeper than the epidermis (Tinkle et al., 2003). Consistent with the experimental results obtained in the project, these workers found no particle penetration in tissues that had not been flexed. The stratum corneum, which is the effective barrier of the human body for protection against the external environment, consists of a number of layers of stacked keratinocytes surrounded by lipids. These lipids form a tortuous, yet continuous channel between the skin surface and the deeper layers of the epidermis. The flexing force and its duration together with the particle size will essentially govern the possible extent of particle penetration through these channels. Flexing (at 45°, 20 flexes per minute) periods of 15 minutes have been reported to lead to observations of penetration of 0.5 and 1 µm particles, but not of supermicron particles, into the epidermis (Tinkle et al., 2003). However, if the applied external force is very strong, larger particles may also to some extent penetrate. In cases where individuals have walked barefoot, insoluble 0.5 µm particles could to a comparatively large extent penetrate the epidermis, and even 25 µm particles were occasionally found in lymph nodes of the exposed individuals (Blundell et al, 1989). Percutaneous penetration of particles can thus not be ruled out as a possibly significant source of inner body organ contamination, but the available data is at present far too sparse and not sufficiently quantitative to allow reliable consequence modelling.

It should be noted that even particles as large as several microns are not very easily removed from the skin surface by force. In the experiments it was found that thorough scrubbing with ethanol soaked filter paper to an extent that made the skin red only removes a limited fraction of the deposited particles.

Percutaneous absorption of dissolved contaminants is a different phenomenon, which clearly merits further investigation (Schaefer & Lademann, 2001). It must however be considered that for instance in connection with a reactor accident, the solubility of the refractory radionuclide aerosols would generally be low (Salbu & Oughton, 1995), and after the Chernobyl accident even the radiocaesium aerosol was found in Prague to have a range of different degrees of solubility (Tomasek et al., 1995). Most of the radiocaesium associated with this aerosol, which according to the findings of Rulik et al. (1989) had an AMAD of about 0.7 µm, was not in readily water-soluble form. As a consequence of the short time periods, over which the doses from contamination on skin are received, dissolved contaminants would be assumed to play a minor role in connection with a contaminant aerosol deposition. Also, from *in vitro* experiments it has generally been found that the mobility of a range of radionuclides (e.g., ^{137}Cs) in solution across skin barriers (primarily the stratum corneum) is low (Koprda et al., 2000).

Elemental iodine can be relatively easily removed by washing shortly after deposition on skin. However, if this is not done, the iodine will attach strongly to the skin surface and can also slowly become incorporated in the subsurface stratum corneum (Hendley & Ashe, 1991). The findings of Miller et al. (1985) suggest that part of the radioiodine deposited to skin may migrate into the body and give a dose to the thyroid. It is however here important to bear in mind that these experiments were carried out on rats, which have much higher density of hair follicles than humans, and it is believed that hair follicles constitute main transport channels of skin penetration by dissolved pollutant ions, because the stratum corneum lining is rather thin at the bottom of hair follicles (Schaefer & Lademann, 2001; Koprda et al., 2000; Koprda et al., 1998). On the background of the available literature it is not possible to give a reliable estimate of the doses that may be received by dermal penetration of elemental iodine, but a potential significance of this dose pathway can not be ruled out. Based on the findings of Cline et al. (1965) it appears that the process of reduction in elemental iodine contamination levels will be dominated by the short physical half-lives of these isotopes.

Based on experimental findings in connection with the INDOOR DOSE project together with the work of Fogh et al. (1999) and Thatcher & Layton (1995), the clearance half-life on clothes of the considered supermicroneous

particles is estimated to be of the order of 0.3 days. For the smaller particles the clearance is believed to be governed by the washing of the clothes. Estimates of clearance rate of submicroneous particles from clothes are based on experimental investigations of washing efficiencies (Fogh et al., 1999; Andersson et al., 1999) as well as on assumptions regarding the periods of time that clothes are worn before washing. It was found that ordinary washing of clothes would typically lead to a reduction in the contamination level by a factor of about 1.4. The washing effect did not appear to be greatly influenced by the particle size, although a tendency was observed towards a greater effect for the larger of the considered particles. If it is assumed that the clothes are washed at intervals of 2 days and then worn again, a washing reduction factor of 1.4 will correspond to a clearance half-life of about 4 days. Supermicroneous particles would be expected to be bound much less strongly, as is the case on the skin.

Investigations in the INDOOR DOSE project with various types of fabric have indicated that the transport of contaminant particles through clothing and onto skin is generally negligible. Most of the elemental iodine deposited on clothes can probably be assumed to remain on the clothing until it is washed, although some evaporation would be expected.

Clearance of particulate contaminants from hair was studied under the previous contract. It was here found that a simple hair wash was very efficient in removing practically all the tracer labelled particles, even as small as 0.5 µm. If the hair is not washed, most of the 0.5 µm particles would remain on the hair over a day.

4.1.1.4. Dose conversion factors

The last factors that are needed to calculate dose contributions from equation 2 are the conversion factors from surface contamination level to gamma or beta dose rate to the human body parts in question.

Estimates of the effective dose contribution to the whole body from gamma emission on skin were made, based on Monte Carlo calculations using the MCNP code from Los Alamos National Laboratory. A comparatively simple model was used, in which a tissue equivalent ICRU sphere was subjected to radiation from a surface contamination, which emitted photons of various energies. The sensitivity of this model to changes in sphere diameter was found to be very limited. In the model the sphere was placed at a height of 1 m above ground. The statistical uncertainty of the Monte Carlo calculations was in all cases less than 1%, and all statistical checks of MCNP were satisfied.

Calculations made by Rohloff and Heinzelmann (1996) clearly show that the dose rate contributions to the basal layer of the skin epidermis from gamma radiation are generally not significant in comparison with the contributions from beta radiation.

For beta radiation, estimates of the dose conversion factor, Γ, were required for a depth in human tissue corresponding to the basal layer of the epidermis, where it is generally believed that proliferating cells in the skin are predominantly located. This depth varies somewhat, for instance according to body sites. An investigation has shown it to be 50 ± 22 µm on the face, but 85 ± 26 µm on the back of hands (ICRP, 1992). Also a diurnal variation has been measured. This was explained by relocation of dermal fluid by gravity. Finally, a weak correlation between skin thickness and age was observed (Tsukahara et al., 2001). Recognising that deterministic effects may arise in deeper layers, the ICRP recommends that doses to skin be determined at a depth of 70 µm (ICRU, 1997). Nuclide-specific absorbed dose rates at a depth of 70 µm in water from various beta sources distributed over an area on the air-water boundary were derived from ICRU report 56 (1997). The ICRU figures were mostly based on the Monte Carlo calculations of Cross et al. (1992), and were found to be in reasonably good agreement with corresponding factors reported by Faw (1992).

On the parts of the body that are covered by clothes, the beta doses to skin are much lower due to the shielding effect of the clothing. The Tables in Appendix A of ICRU report 56 show that due to the similar beta attenuation

characteristics, it would be reasonable to assume that equal mass-thicknesses of cotton clothing and tissue are equivalent in dose considerations. From the dose rate factors given in ICRU 56 it follows that practically no beta doses would be received through 3 mm thick clothing. Doses have, however, been modelled for skin covered by cotton clothes of a thickness of 0.4 mm. This corresponds to the thickness of a T-shirt. The dose conversion factors applied for 0.4 mm cotton clothing are in reasonable agreement with those reported by Taylor et al. (1997) for a 26 mg cm^{-2} thick layer of cotton with a density of 0.7 g cm^{-3}.

As for beta doses from contamination on hair, it has been found from the experimental work in the project that the deposition velocity to the distal part of the hair is about twice as great as that to the proximal part of the hair. However, the beta dose per unit of contamination on the distal part of the hair is less than the corresponding from the proximal part. The most important reason for this is that the lower hair layers will attenuate the beta radiation. At the same time, also the air gap between the contamination on the distal hair end and the head will give a reduction in the beta dose, and the contamination on the distal end is slightly farther away from the head than that on the proximal part, which gives a slight difference in geometry. The latter geometry effect is generally not deemed to have importance unless the outer hair layers are unusually far from the head, but the air gap attenuation may typically give a reduction of the beta dose by a factor of 1.0-1.3, depending on the energy (Pushparaja et al., 1992). By far the most significant effect is that of the attenuation in hair. It has been measured that a representative hair mass-thickness of the test persons in the experimental part of the project is of the order of ca. 20-40 mg cm^{-2}. A mass-thickness of 40 mg cm^{-2} corresponds to a thickness of about 0.4 mm in hair or human tissue. It is for modelling purposes assumed, based on the experimental work in the project, that one third of the hair contamination will be found at the proximal part of the hair (very near the surface of the head), whereas two thirds will be at a distance corresponding to a mass-thickness of 40 mg cm^{-2}. The required beta dose factors for both of these geometries can be found in Appendix A of ICRU report 56.

Although subject to considerable variation according to for instance sex, season and climate, it is here assumed that the fraction of the human body that is not covered by clothing corresponds to the fraction constituted by the head and hands. Using the general methodology given in the report of the ICRP Task Group on Reference Man (ICRP, 1974), it can be found that this would for a fully grown person amount to some 15 %. Out of this, it is considered to be likely that one-third is covered by significant hair growth.

4.1.1.5. Age differences

Of course, the body size of young children differs significantly from those of adults. However, in connection with the calculations of gamma dose described above for the ICRU sphere it was found that the sensitivity of effective dose to changes in sphere diameter was low. A highly significant feature of very young children is the different proportions of the various body parts. At birth, the surface area of the head constitutes some 21 % of the total body area, but at the age of 5 it has decreased to about 13 %, and for an adult it is only about 7.5 % (ICRP, 1974). This means that the body parts taken to be uncovered by clothing (head and hands) would for a very young child not constitute 15 %, as assumed in the dose model of this study, but possibly as much as 30 %. However, with the above assumptions concerning clearance from skin, hair and clothing, it can be found that the resultant change in effective gamma doses would generally be by less than 30 %.

In the following some further considerations are made regarding differences in doses received from contamination on human surfaces by an adult, child or foetus.

The epidermis (the thin outer layer of human skin) essentially consists of three parts. The stratum corneum is the outermost horny layer consisting of dead cells. Deep to this are layers of living keratinocytes. These are generated in the basal layer and form new stratum corneum cells as the stratum corneum sheds from the outer surface. The deepest layer is the basal layer, where basal cells continuously divide and form new keratinocytes. The stratum corneum is the most important barrier to dermal absorption. There appears to be no major differences

in the structure and thickness of the stratum corneum in adults and young children (Snodgrass, 1992). However, until typically 3-5 days after birth, the epidermis is unkeratinised. This means that the skin permeability of particularly elemental iodine and contaminant ions in solution can in this period be expected to be somewhat higher, but after about 5 days differences in the skin absorption barriers of children and adults are small (Plunkett et al., 1992; Snodgrass, 1992).

It has been found that neonatal and adult epidermis have similar thicknesses (Hoeger & Enzmann, 2002). This implies that the mean depth of the epidermal basis layer is similar in infants and adults, and thus the beta dosimetric parameters used for adults would generally apply. Anyway, within the 20-100 µm depth range in skin, differences in dose will only be significant for very low-energy beta particles. The threshold energy for penetration to a depth of 20 µm is ca. 30 keV, and to a depth of 70 µm it is ca. 70 keV (ICRU, 1997).

Due to the generally short range in human tissue of the beta radiation from most radionuclides, beta doses to the foetus will in most cases be totally negligible. A main exception is ^{106}Ru/^{106}Rh, which emits very high-energy beta particles. However, even for this radionuclide, the beta dose to the surface tissue of the foetus will not exceed a few percent of that to the skin of the mother (ICRU, 1997).

As for the gamma dose to the foetus, it has been suggested that estimates of doses to the mother's uterus give a reasonable representation of the foetus dose, since it has been shown that there is a high correspondence between the dose in the uterus and in foetal tissues, particularly during the latest half of the pregnancy (ICRP, 1991). The energy-dependence of equivalent dose to various human organs (including the uterus) relative to kerma free-in-air has been reported by the ICRP for external gamma radiation incident on the human body in various geometries (ICRP, 1995). This reference also gives the corresponding energy-dependence of the effective dose to the human body relative to kerma free-in-air. This data clearly shows that for photons with energies higher than about 50 keV, which would in most thinkable scenarios be expected to give the main dose contribution, differences between the effective dose and the uterus equivalent dose are generally less than 20 %. For most energies the uterus equivalent dose appears to be slightly lower than the effective dose. This suggests that the effective gamma dose to the foetus is adequately represented by estimates of the effective dose to the mother. However, the foetus is considered to be more susceptible to radiation-induced effects than the mother (Chapple et al., 1994; ICRP, 1990). Nevertheless, in Japanese atomic bomb survivors, the dose-dependent excess of cancers in adult life appears to be similar after prenatal irradiation and after irradiation during the first ten years of life (ICRP, 1991).

It should be considered that the overall risk of radiation-induced cancer per unit of exposure is significantly greater in a child than in an adult. It should also be considered that the behaviour pattern of children is different from that of adults. For instance, the likelihood of children being outdoors during part of the deposition phase may well be greater.

4.1.2 Contamination on surfaces in the indoor environment

4.1.2.1. Generic formulae

The presence of airborne contaminants in dwellings will lead to a deposition on interior surfaces of the dwelling. These deposits will give rise to a dose contribution to persons staying in the dwellings. The dose contributions from contamination on building interior can be found from the following generic equation:

$$(4)\quad D = \sum_{nuclides} M_s \cdot \Gamma \cdot fr \cdot \frac{1}{\lambda_{nuclide} + \lambda_{removal}},$$

in which M_s is the total time-integrated deposition of each contaminant nuclide per unit of area of the surface in question, Γ is the dose conversion factor [Sv per Bq m^{-2}] for the nuclide and geometry in question, fr is the fraction of the exposed person's time that is spent in the contaminated location, $\lambda_{nuclide}$ is the radioactive decay rate constant of the nuclide, and $\lambda_{removal}$ is the rate constant for natural removal from the surface. If the contamination is of outdoor origin, M_s can be calculated from:

$$(5)\quad M_s = \int v_{d,s} C_o \frac{f\lambda_v}{\lambda_v + \lambda_d} dt + \int k v_{d,s} M_f dt ,$$

where $v_{d,s}$ is the deposition velocity to the indoor surface in question, C_o is the outdoor air concentration of the contaminant, f is the filtering factor, and λ_v and λ_d are the rate coefficients of respectively ventilation and deposition. M_f is the deposited amount of particles at the time of the resuspension, and k is the resuspension factor for contaminants of the relevant type. Typical parametric value ranges for λ_r, λ_d and f for dwellings of different qualities are given in the final report of contract no. FI3P-CT92-0038 (Andersson et al., 1995). It has been measured that the total deposition velocity to a furnished room may be higher than that to the same room without furniture, by a factor of about 1.3-2 (Lange, 1995). However, the furniture will also constitute structures that will shield against contamination on other surfaces in the indoor environment. As has been demonstrated by the resuspension experiments described above, even the most vigorous physical impact can only be expected to lead to resuspension of a very limited fraction of the contamination, and the redistribution of contaminants on the various indoor surfaces will thus have little importance in these dose contributions.

4.1.2.2. Dose conversion factors

For the purpose of estimating the dose conversion factor, energy dependent dose rate functions have been derived from photon transport modelling using the MCNP Monte Carlo code (Briesmeister, 1993). The gamma dose rate energy dependence relationships are shown in Appendix A, together with derived empirical functions, which can be used together with information on photon yield and energies for any gamma emitting radionuclide to determine the corresponding dose rate to a person from homogeneously contaminated indoor walls, floors or ceilings. As can be seen from the data in Appendix A, the energy dependence of dose rate can be accurately described by second order polynomial functions. Calculations have been made for persons staying in contaminated rooms in the following geometries:

In the centre of a 4m by 4m room with a ceiling height of 2.5 m.

In same room, very close to one wall but centred with respect to the perpendicular walls.

In the centre of a 10m by 10m room with a ceiling height of 2.5 m.

In the centre of a 2m by 2m room with a ceiling height of 2.5 m.

All dose rates were calculated to an ICRU sphere at a reference height of 1m above the floor. Since people spend much of their time lying in a bed or sitting on a chair at less height, a fifth geometry calculation was made, where the ICRU sphere was placed on top of a 45 cm high bed. The dimensions of the bed were 2 m (length) by 1 m (width), and it was modelled to consist of 2 cm thick wood covered by 10 cm of polyurethane foam with a density of 0.04 g cm^{-3}. Other than the bed, the room was in the fifth geometry calculations the same as in the first, and thus, only the dose rate contribution from the floor was recalculated.

The magnitude of beta doses to the skin from contaminated building interior very strongly depends on the distance between the contaminated surface and the exposed person. As an example, the beta dose from ^{137}Cs in water at a thickness of 0.04 cm is about one-fourth of the value at epidermal equivalent thickness (ICRU, 1997). If it is

assumed that equal mass-thicknesses lead to about equal attenuation, it would take 0.04 g cm^{-2} / 0.0012 g cm^{-3} = ca. 30 cm of air to provide the same beta attenuation. For some of the radionuclides that might arise from a major nuclear accident, such as ^{95}Zr, this distance provides a skin beta dose reduction by more than a factor of 10 (ICRU, 1997). At a distance of about one metre from the source, the beta dose from nearly all perceivable sources would be negligible. The closest contact between sources and exposed persons would be in situations where persons are sitting or lying on contaminated surfaces. In such cases, the beta doses can be compared with the corresponding contributions from the same source density deposited on skin/clothing on the body. Although the clearance half-life on skin is generally much shorter than that on most building interior surfaces, it has also generally been found that deposition velocities to for instance indoor walls are much lower than the corresponding to human skin. It should, however, be noted that for instance convective currents and rough and complex geometrical surface structures might possibly (subject to shielding geometries) lead to much higher levels of contamination than that on a smooth wall surface. Experimental investigations of such phenomena are beyond the scope of the INDOOR DOSE project. As even thin fabric shields well against beta radiation, the most critical situations would be those where unshielded skin comes into direct or close contact with a contaminated surface. One important situation is at night, when, e.g., the face is in direct contact with a possibly contaminated surface for hours. However, in European member states, it would be assumed that most people sleep with their head on a pillow. By washing the pillow case regularly, these doses would be limited to a short period of time after the contamination took place, as ordinary machine washing is efficient in removing the contaminants (Andersson et al., 2002). On the background of the available experimentally derived parameters from INDOOR DOSE and previous project work undertaken by the consortium partners, it can not be ruled out that frequent use of chairs or sofas, if contaminated, may give a beta dose that is not insignificant.

Many of the factors mentioned above for direct contamination of children would also apply in cases where children are exposed to radiation from building interior surfaces. Particularly, the dose contribution to toddlers from the floor could in some cases be up to about an order of magnitude higher than that to adults, depending, e.g., on the average height in the room of the toddlers and the dimensions of the room.

4.1.3 Skin contact transfer

Contamination may be transferred from a contaminated surface (for instance a piece of furniture or a wall) to human skin, by contact. The doses received in this way can be described by the formula:

(6) $$D = M_{sur} \cdot TF \cdot \Gamma \cdot \frac{1}{\lambda_{nuclide} + \lambda_{clearance}}$$, where M_{sur} is the total contamination per unit of area on the contaminated surface at the time that it is touched, TF is the contact transfer factor (the mass of contaminants per unit of area of the relevant human surface, as a fraction of the mass of contaminants per unit of area on the contaminated surface in question), Γ is as above the dose conversion factor for the radionuclide in question, and $\lambda_{nuclide}$ is again the radioactive decay rate constant of the nuclide, whereas $\lambda_{clearance}$ is the rate constant for clearance from the human surface.

Based on the experiments carried out in the INDOOR DOSE project as well as earlier investigations made by the same consortium, it can be concluded that the contact transfer factor does not normally vary greatly with particle size, although it would appear that it decreases slightly with size at submicroneous particle sizes. A typical value of the TF is about 0.2 – 0.3 for dry fingers. If fingers are very moist, the TF for submicron particles can be as much as 3 times as high, whereas moisture appears to have only little effect on the TF for supermicron particles. For supermicron particles there seems to be little dependence of TF on the type of material that the transfer occurs from. However, for very small particles in the 0.1 µm range, a dependence on material characteristics has been found, which is believed to be associated with the influence of surface charge densities. It was thus found that 0.1 µm particles had a TF that was 2-3 times lower on plastic than on metal.

It should be noted that the experiments that formed the background for the above evaluation of contact transfer employed tracers at comparatively low concentrations, approximately corresponding to those applied in the investigations of direct deposition to the skin. The results are thus applicable to scenarios involving airborne contamination after, e.g., an atmospheric release, but in a laboratory or a decommissioning facility, for instance, a spillage of contaminated powder from a container would generally be expected to lead to a much thicker, possibly visible, contaminant layer on an indoor surface. In such cases, where the contamination cover is very significantly thicker than a mono-layer, the TF would be expected to be significantly smaller than the above. It is assumed that the skin (e.g., a finger) touches the surface, but is not moved around on the surface to accumulate dust on the skin by smearing. Transfer by smearing would be likely to lead to much higher levels of skin contamination, but on the other hand, large heaps of small particles would most likely very rapidly be cleared off from the skin, leaving only a comparatively thin layer on the skin surface. The doses received from skin contact transfer may be strongly dependent on the time at which the transfer occurs, if the initially deposited surface contamination, or part of it, consists of short-lived radionuclides.

4.1.4 Inhalation of contamination (taking into account resuspension)

The doses received by an individual through inhalation of contaminants as the polluted plume passed over the area can reasonably be calculated with the assumption that people stayed indoors during virtually the whole period where the air concentrations were highest. The committed doses can be calculated from the following expression:

$$(7)\quad D = BR \cdot \Gamma \cdot \frac{f \cdot \lambda_v}{\lambda_v + \lambda_d} \cdot \int_{t=T_o}^{T_1} C_o(t)dt + BR \cdot k \cdot M_{floor,\mathrm{int}} \cdot \frac{1}{\lambda_{nuclide} + \lambda_{dilu}} \cdot f_r$$

Here BR is the breathing rate, which can, according to the results of a recently reported investigation (California Air Resources Board, 2004), on average be taken to be 12 litres per minute for young children, 15 litres per minute for females, and 18 litres per minute for males (averages of rest and walking breathing rates). Γ is the inhalation dose coefficient (tabulated in ICRP, 1995), C_o is the outdoor air concentration of the contaminant, f is the filtering factor, and λ_v and λ_d are the rate coefficients of respectively ventilation and deposition. The second half of the expression accommodates the contribution from inhalation of resuspended contaminated dust. Here, k is the resuspension factor, $M_{floor,int}$, on the floor (assuming that reuspension will primarily occur from the floor; see the section on contamination on indoor surfaces for parameter values), and λ_{dilu} and $\lambda_{nuclide}$ are rate constants for respectively the natural dilution of contaminated indoor dust and radioactive decay of the radionuclide in question, whereas f_r is the fraction of the time, where the resuspension occurs *and* the individual is present.

4.2 Demonstration scenario

4.2.1 Source term definition

In the following a demonstration scenario will be described, which has been constructed in order to show an example of evaluation of the various dose pathways from indoor contamination, as considered in the INDOOR DOSE project, based on the methodology described in the previous section. The demonstration scenario has been chosen to reflect a situation resulting from a major nuclear accident, such as that, which happened at Chernobyl on the 26th of April 1986. A scenario of this type will be complex and accommodate a large number of different

considerations and calculations, and is thus thought to be ideal to demonstrate large parts of the model methodology derived in the project.

Following a major accident at a nuclear power plant, the local variation in the absolute level of the dry deposited contamination of an area can be considerable (Roed, 1990). It has been reported that dry deposition from the Chernobyl accident has led to local ^{137}Cs ground contamination levels of as much as 1 MBq m^{-2} in the settlement of Vishkov in the Bryansk region, about 160 km away from the Chernobyl NPP (Stepanenko et al., 2002). Significantly smaller dry contamination levels have been reported for other areas in the Bryansk region, but the choice of this round figure for the contamination level on the grassed reference surface facilitates the scaling of the results of the demonstration scenario. Kryshev (1996) assessed the relative concentrations of the various contaminants from Chernobyl that could be found in near-ground air at a location about 25 km away from Vishkov. These relations have, together with the assumption of contamination levels that would result in a dry deposition of ^{137}Cs on short grass of 1 MBq m^{-2}, determined the source term for the demonstration scenario. It would be expected that people are indoors during much of the period where the contaminant air concentrations are highest. This is partly because it would be strongly recommended by the authorities, if these are given sufficient time to warn the public. Also, a number of independent surveys in Western Europe and in California (Jenkins et al., 1992; Andersson, 1996; Long et al., 2001; Kousa et al., 2002) have shown that people on average spend some 80-95 % of their time indoors. Formula no. 3 in the 'general methodology' section is thus applicable to identify the direct exposure of humans in the scenario.

In connection with the Chernobyl accident it was found that with respect to atmospheric transport and deposition, the released contaminant aerosol can be divided into two groups: a volatile group, which includes ^{137}Cs, ^{134}Cs, ^{103}Ru, ^{106}Ru, ^{132}Te and ^{99}Mo and a refractory group including ^{90}Sr, ^{89}Sr, ^{141}Ce, ^{144}Ce, ^{95}Zr and ^{140}Ba. Measurements made in various European countries after the Chernobyl accident rather consistently showed that outside the immediate vicinity of the Chernobyl NPP, the AMAD (Activity Median Aerodynamic Diameter) of the volatile radioactive aerosols was of the order of 0.7 µm, whereas a higher AMAD value of the order of 5 µm was found for those belonging to the refractory group (Reineking, Becker, Porstendörfer & Wicke, 1987; Tschiersch & Georgi, 1987; Rulik, Bucina & Malátová, 1989; Dorrian, 1997).

The Chernobyl accident also led to high air concentrations of both iodine in aerosol form, elemental (or other inorganic) iodine and organic iodine (notably CH_3I) (Roed, 1987). Measurements made in Sweden, Finland, Norway and Germany showed that the Chernobyl ^{131}I was mainly (ca. 90 %, which is also assumed in this scenario) in the gas phase, primarily as inorganic iodine (Devell et al., 1986; STUK, 1986; Jost et al., 1986; Pacyna et al., 1986). Practically the same distribution between iodine species was reported by Tomasek et al. (1992) for measurements in Prague and Budapest. It is therefore clear that in connection with estimates of the fate and doses from radioiodine, clear distinctions are necessary between the different physicochemical groups. The AMAD of aerosol iodine has after the Chernobyl accident been found to be similar to that of other volatile radionuclide aerosol (Tschiersch & Georgi, 1987). The deposition velocity of organic iodine is generally 3-4 orders of magnitude lower than that of elemental iodine (Atkins, Chadwick & Chamberlain, 1967; Tomasek, Wilhelmova & Horyna, 1992), and its influence on the doses from deposition to skin and other surfaces, or from inhalation, can be assumed to be negligible. The experimental studies of elemental iodine deposition to skin in the project confirmed that this species generally has a high deposition velocity, also to human skin. Based on default parameters applied in the European COSYMA standard model it is here assumed that all non-elemental iodine is of the organic form.

Dermal penetration has not been considered, for the reasons given in the general methodology section.

4.2.2 Indoor / outdoor air concentration relationship

The relationship between indoor and outdoor air concentrations at equilibrium can be calculated from formula no. 3 in the general methodologies section. Based on experience from comprehensive experimental work (e.g., Roed and Cannell, 1987; Roed, 1990; Fogh et al, 1997), the filtering factor can be assumed to be unity. A wide range of testing has shown that a realistic value of the rate coefficient of ventilation is of the order of 0.3-0.5 h^{-1} in relatively well-constructed buildings, and this parameter has for the demonstration scenario calculations been assumed to be 0.4 h^{-1}. In agreement with the values given in the modelling methodology section, the rate coefficient of deposition to indoor surfaces has been assumed to be 3 h^{-1} for aerosols of the refractory group and 0.4 h^{-1} for the volatile aerosol group, with the exception of ruthenium, for which a value of 1.1 h^{-1} is deemed to be reasonable, based on the work of Roed and Cannell (1987). Elemental iodine gas would have a high indoor deposition velocity, and based on the work of Cline et al. (1965), Roed & Cannell (1987) and Kocher (1980), the relationship between indoor and outdoor elemental iodine concentrations is estimated to 0.07. As for methyl iodine, the extremely low deposition velocity would mean that there would not be significant differences between indoor and outdoor air concentrations.

4.2.3 Contamination on humans

4.2.3.1. Deposition, removal and dose conversion

Concerning deposition velocities, the 'best general estimate' parameters given in Table 4.1 were applied for aerosols on the various human body surfaces. For elemental iodine, the values established through the experimental work in the project were applied.

Removal rates were assumed to be as estimated in the general methodology section. Clearance has been taken into account, but dermal penetration has not been considered in this case, as little of the contamination resulting from an accident of this type would be likely to be readily soluble, and only qualitative data currently exists which suggests a possibility of penetration of particles within the relevant size-range. It was assumed that the elemental iodine deposited on humans was not actively removed by washing, although this would to some extent be a possibility immediately after the deposition.

Dose conversion factors for gamma and beta radiation were assumed to be as given in the general methodology section. The effect of the air gap between hair and the head was assumed to be unimportant. However, in some cases, where contaminated distal hair parts are far from the head, this would have a small effect on the doses from particularly low energy beta emitters. The exclusion of this effect makes the estimate of doses from the distal part of the hair strand very slightly conservative.

4.2.3.2. Results

Table 4.2 shows the indoor to outdoor contaminant concentration relationships for the considered radionuclides, as calculated from formula no. 3. Together with the shown deposition velocity estimates and assumed time-integrated outdoor air concentrations, this forms the background material for calculation of the total deposition of the various radionuclides from the radioactive cloud on the different body surfaces, using formula no. 1.

Table 4.2. Typically observed relationships between indoor and outdoor contaminant air concentrations, contaminant deposition velocities to skin, clothing and distal as well as proximal parts of human hair. On the basis of the assumed integrated air concentrations of the various contaminants, the total amounts of deposited material on skin, clothing and the two parts of the hair are calculated and shown in the table.

Radio-nuclide	C_i / C_o	$V_{d,skin}$ [m s^{-1}]	$V_{d,clothing}$ [m s^{-1}]	$V_{d,dist.hair}$ [m s^{-1}]	$V_{d,prox.hair}$ [m s^{-1}]	Assumed integr. air conc. outdoors [Bq s m^{-3}]	Total deposit on skin [kBq cm^{-2}]	Total deposit on cloth. [kBq cm^{-2}]	Total deposit on distal hair* [kBq cm^{-2}]	Total deposit on prox. hair* [kBq cm^{-2}]
Te-132	0.5	1.0E-03	1.7E-03	2.6E-04	1.2E-04	2.3E+09	1.1E-01	1.9E-01	2.9E-02	1.4E-02
Cs-134	0.5	1.0E-03	1.7E-03	2.6E-04	1.2E-04	1.1E+09	5.6E-02	9.5E-02	1.4E-02	6.7E-03
Cs-137	0.5	1.0E-03	1.7E-03	2.6E-04	1.2E-04	2.2E+09	1.1E-01	1.9E-01	2.9E-02	1.3E-02
Ba-140	0.12	1.2E-02	2.7E-03	3.0E-03	1.5E-03	1.4E+09	1.9E-01	4.4E-02	4.9E-02	2.4E-02
Zr-95	0.12	1.2E-02	2.7E-03	3.0E-03	1.5E-03	3.3E+08	4.8E-02	1.1E-02	1.2E-02	6.0E-03
Mo-99	0.5	1.0E-03	1.7E-03	2.6E-04	1.2E-04	6.5E+08	3.2E-02	5.5E-02	8.4E-03	3.9E-03
Ru-103	0.27	1.0E-03	1.7E-03	2.6E-04	1.2E-04	1.1E+09	3.1E-02	5.2E-02	8.0E-03	3.7E-03
Ru-106	0.27	1.0E-03	1.7E-03	2.6E-04	1.2E-04	2.9E+08	7.7E-03	1.3E-02	2.0E-03	9.2E-04
Ce-141	0.12	1.2E-02	2.7E-03	3.0E-03	1.5E-03	4.0E+08	5.7E-02	1.3E-02	1.4E-02	7.1E-03
Ce-144	0.12	1.2E-02	2.7E-03	3.0E-03	1.5E-03	2.7E+08	3.9E-02	8.7E-03	9.6E-03	4.8E-03
Sr-89	0.12	1.2E-02	2.7E-03	3.0E-03	1.5E-03	1.7E+07	2.4E-03	5.4E-04	5.9E-04	3.0E-04
Sr-90	0.12	1.2E-02	2.7E-03	3.0E-03	1.5E-03	1.8E+06	2.5E-04	5.7E-05	6.4E-05	3.2E-05
Np-239	0.12	1.2E-02	2.7E-03	3.0E-03	1.5E-03	2.1E+09	3.0E-01	6.8E-02	7.6E-02	3.8E-02
I-131,e	0.07	1.0E-02	1.0E-02	1.0E-02	1.0E-02	2.2E+10	1.6E+00	1.6E+00	1.6E+00	1.6E+00

* Note: kBq cm^{-2} of skin covered by hair

As for the resuspension part of formula no. 1, the resuspension factor, k, would for the particle size range considered in the demonstration scenario be estimated to be of the order of 10^{-5} m^{-1} from a person walking in a room, and 10^{-3} m^{-1} from vigorous indoor activities, including sweeping (Sehmel, 1980). The experimental work performed in the project showed a limited effect of particle size on the resuspension factor, possibly because the smallest (submicron) particles agglomerate and by the time of resuspension seem to have become similar in size to the larger (supermicron) particles examined. The contribution of resuspended particles to the time-integrated indoor air contaminant concentration can be estimated by multiplying the resuspension factor, k, by the time-integrated contamination deposit concentration, $M_{floor,int}$, on the floor (see the section on contamination on indoor surfaces for parameter values), which is the surface, from which the indoor resuspension is likely to be significant, a time-factor accommodating the natural dilution of contaminated indoor dust (half-life: $\ln(2)/\lambda_{dilu}$) and the physical half-lives of the radionuclides ($\ln(2)/\lambda_{nuclide}$), and the fraction of time, f_r, during which resuspension occurs:

$$(8) \quad \int_0^\infty C_{resusp} \cdot dt = k \cdot M_{floor,\mathrm{int}} \cdot \frac{1}{\lambda_{nuclide} + \lambda_{dilu}} \cdot f_r ,$$

as the deposition to the floor occurs over a very short period of time, compared with the resuspension period.

If it is assumed that the half-life of the contaminated dust dilution process on the floor is about 0.5 year (as estimated from experimental data) and that the dominant resuspension is caused by walking in the room for one hour daily, it can be found that the time-integrated air concentrations of the various contaminants will increase by the fractions shown in Table 4.3.

Table 4.3. Estimated fractional increases of total time-integrated air concentrations through resuspension by walking in a room for 1 h every day.

Te-132	Cs-134	Cs-137	Ba-140	Zr-95	Mo-99	Ru-103	Ru-106	Ce-141	Ce-144	Sr-89	Sr-90	Np-239
4.1E-05	1.6E-03	1.8E-03	3.0E-04	1.2E-03	3.5E-05	2.3E-04	7.5E-04	6.9E-04	2.5E-03	9.8E-04	3.4E-03	5.9E-05

It is expected that iodine gas, due to its great chemical reactivity and resultant binding to surfaces, will not to any significant extent lead to resuspension of iodine in particle form. However, natural sublimation of iodine would occur, where the iodine has not formed a chemical compound with the surface material. The extent of this would be material-specific and depend on time as well as on temperature.

If it were instead assumed that vigorous indoor particle resuspending activities took place for one hour daily (which would hardly seem plausible), these fractions could increase by about a factor of 100, and further the radionuclides belonging to the volatile group are after resuspension bound to larger particles than the originally deposited particles. As the deposition velocity on skin of the resuspended 'volatile group' particles is about an order of magnitude greater than that of the initial 'volatile group' particles, this means that the contribution of resuspended material to the total time-integrated contamination on skin could be a factor 1000 higher than that given in Table 4.3. However, the clearance process of the larger resuspended radiocaesium particles from skin would be much faster than that of the original submicron radiocaesium particles, and the conclusion is that in connection with an accident of this type, it is the initial particles from the radioactive cloud that will govern the doses from contaminant deposition on humans.

Employing the total deposits on the different surface types, as given in Table 4.2, together with the relevant physical radionuclide half-lives and the assumptions on clearance half-lives given in the general methodology section (concerning hair, it was assumed that this was not washed for a week after the contamination – this would be expected to result in a dose estimate above the average), and gamma dose rate coversion factors calculated by Monte Carlo modelling (Andersson et al., 2002), the gamma doses to the body from the various contaminated body surfaces are calculated from formula no. 2, and presented in Table 4.4.

Table 4.4. Estimates of gamma dose contributions to the whole body from contamination on human skin, clothing, distal and proximal hair parts.

Radio-nuclide	General (without clearance) γ-dose rate conver-sion factor [Sv y^{-1} per Bq cm^{-2}]	γ-dose from skin contamination [mSv]	γ-dose from clothing contamination [mSv]	γ-dose from distal fraction of hair contamination [mSv]	γ-dose from proximal fraction of hair contamination [mSv]
Te-132	3.5E-05	4.6E-03	2.4E-02	4.0E-04	1.8E-04
Cs-134	2.3E-04	1.4E-01	1.7E-01	1.2E-02	5.8E-03
Cs-137	1.0E-04	1.3E-01	1.5E-01	1.2E-02	5.4E-03
Ba-140	2.4E-05	2.9E-04	4.5E-03	2.4E-05	1.2E-05
Zr-95	1.4E-04	4.1E-04	6.6E-03	3.4E-05	1.7E-05
Mo-99	2.7E-05	8.6E-04	4.7E-03	7.4E-05	3.4E-05
Ru-103	8.7E-05	1.8E-02	3.2E-02	1.6E-03	7.2E-04
Ru-106	3.2E-05	2.7E-03	3.2E-03	2.3E-04	1.1E-04
Ce-141	1.1E-05	3.9E-05	6.3E-04	3.3E-06	1.6E-06
Ce-144	3.2E-06	7.8E-06	1.2E-04	6.5E-07	3.2E-07
Sr-89	-	-	-	-	-
Sr-90	-	-	-	-	-
Np-239	1.2E-05	2.2E-04	3.3E-03	1.8E-05	8.9E-06
I-131,e	6.8E-05	2.6E-01	8.4E-01	8.7E-02	8.7E-02
Total	-	5.6E-01	1.2E+00	1.1E-01	9.9E-02

The corresponding beta doses are shown in Table 4.5. The shown dose conversion factors are here based on ICRU report 56 and the general underlying principles discussed in the general methodology section.

Table 4.5. Estimates of beta doses to human skin from contamination on skin, clothing, distal hair parts and proximal hair parts.

Radio-nuclide	Skin contamina-tion: β-dose conversion factor [Sv per Bq cm^{-2}]	Skin contamina-tion: β-dose [Sv]	Clothing contamina-tion: β-dose conversion factor [Sv per Bq cm^{-2}]	Clothing contamina-tion: β-dose [Sv]	Hair contamina-tion (distal): β-dose conversion factor [Sv per Bq cm^{-2}]*	Hair contamina-tion (distal): β-dose [Sv]	Hair contamina-tion (proximal): β-dose conversion factor [Sv per Bq cm^{-2}]*	Hair contamina-tion (proximal): β-dose [Sv]
Te-132	9.2E-05	1.0E-02	4.1E-07	7.8E-05	5.4E-07	1.6E-05	7.4E-05	1.0E-03
Cs-134	1.1E-03	6.2E-02	3.5E-05	3.3E-03	4.0E-05	5.6E-04	1.7E-04	1.1E-03
Cs-137	1.7E-03	1.9E-01	5.2E-05	9.9E-03	6.0E-05	1.7E-03	2.5E-04	3.3E-03
Ba-140	8.1E-06	1.5E-03	5.0E-06	2.2E-04	5.0E-06	2.5E-04	1.5E-05	3.6E-04
Zr-95	6.3E-06	3.0E-04	8.9E-07	9.8E-06	8.9E-07	1.1E-05	1.2E-05	7.2E-05
Mo-99	1.3E-04	4.2E-03	3.8E-05	2.1E-03	5.0E-05	4.2E-04	1.1E-04	4.3E-04
Ru-103	3.6E-04	1.1E-02	3.4E-06	1.8E-04	4.1E-06	3.3E-05	9.0E-05	3.3E-04
Ru-106	1.8E-03	1.4E-02	1.7E-04	2.2E-03	1.9E-04	3.8E-04	2.8E-04	2.6E-04
Ce-141	8.8E-06	5.0E-04	1.7E-06	2.2E-05	1.7E-06	2.4E-05	1.6E-05	1.1E-04
Ce-144	5.0E-06	2.0E-04	3.0E-07	2.6E-06	3.0E-07	2.9E-06	9.4E-06	4.5E-05
Sr-89	9.5E-06	2.3E-05	9.2E-06	5.0E-06	9.2E-06	5.4E-06	1.8E-05	5.4E-06
Sr-90	8.2E-06	2.1E-06	3.5E-06	2.0E-07	3.5E-06	2.2E-07	1.5E-05	4.8E-07
Np-239	8.9E-06	2.7E-03	0	0	0	0	1.6E-05	6.1E-04
I-131,e	3.0E-04	4.8E-01	2.7E-05	4.3E-02	3.5E-05	5.6E-02	1.6E-04	2.6E-01
Total	-	7.8E-01	-	6.1E-02	-	5.9E-02	-	2.7E-01

* Note: Sv per Bq cm^{-2} of skin covered by hair

As can be seen from Table 4.4, the gamma doses from contamination on the human body amount to about 2 mSv over a short period of time. Table 5 shows that the beta doses to unprotected skin were close to 1 Sv. Although this is below the threshold for non-stochastic radiation effects of the skin, the skin cancer mortality risk would at this dose be ca. 0.02 %, and the corresponding skin cancer morbidity risk would be about 10 % (ICRP, 1991). As can be seen, beta doses to skin covered by hair are somewhat smaller than those from contaminants deposited directly on the skin. Beta doses from contamination on clothing are about an order of magnitude lower than those from contamination on skin, but the contamination on the clothing gives the greatest single contribution to the gamma dose to the body, due to the large surface that is assumed to be covered by clothing. Both gamma and beta doses are dominated by the contributions from elemental iodine and caesium.

Several of the parameters applied in the above calculations are prone to variation, and the applied values reflect what is believed to be 'best estimates' of average conditions, unless specifically stated otherwise.

Probably, the doses received from contamination on clothes and hair are overestimated in the above calculations, since the washing frequency was assumed to be low. Also, it should be pointed out that an active effort in the early phase to remove elemental iodine from surfaces would be likely to have a significant effect on the doses from all the considered types of surface.

As has been found by experiments carried out within the project, the half-life of the process of natural clearance of particles from skin (and other human body surfaces) is for the largest particles strongly dependent on the level of physical movement of the exposed persons. However, the radionuclides that generally contribute the most to the

various doses from human exposure are associated with submicroneous particles, which are very strongly held on the human body, and appear to be invariant to influences of physical movement.

As discussed in the general methodology section, doses may also for several reasons vary according to the age of the exposed persons.

The relationship between indoor and outdoor contaminant concentrations depends on the ventilation and indoor deposition rate coefficients. In a rather leaky dwelling with high ventilation rate, the indoor/outdoor concentration relationship for the largest of the considered particles could possibly be a factor of 3 higher than assumed above. However, for the small contaminant particles that contribute the most to dose, the corresponding increase would only be by about a factor of 1.5. In very air-tight dwellings, a corresponding *decrease* in the relationship between indoor and outdoor contaminant concentrations by respectively a factor of 3 and 1.5, compared with the 'default' would be possible.

As was found from the experimental work in the project, the influences of strong electric fields could lead to very significantly higher deposition velocities of submicron particles. However, such strong fields would probably only exist close to TV sets (closer than one would normally be when watching TV), and the likelihood of this occurring over long periods of time would possibly be small.

An other effect that was found to have important bearing on the deposition of particles to skin is surface moisture. As mentioned above, this is partly individual-related and partly governed by external factors (e.g., heat). The deposition of the smallest particles to a very moist arm was found to be most of an order of magnitude higher than that to a very dry arm. The results above are based, also in this respect, on the assumption of a 'typically' observed value.

Finally, the experimental work in the project demonstrated a significant influence of air movement on deposition. This means that the deposition velocity of the important contaminants would be about a factor of two higher to a walking than to a sitting person. Outdoor aerosol deposition velocities could be even higher.

Further work is merited to investigate the potentially highly important effect of the solubilities of different contaminant particles on skin, while keeping track of skin parameters (e.g., moisture, pH). Also for instance the influence of age on particle behaviour on the skin is a topic that requires experimentation. The effects of various techniques for forced decontamination of contaminated human surfaces at different times is clearly an important matter that needs to be investigated in practice.

4.2.4 Contamination on surfaces in the indoor environment

Formula no. 5 can be used to calculate the total time-integrated deposition of each contaminant radionuclide per unit of area of each type of indoor surface. The integrated outdoor air contaminant concentrations as well as the relationships between indoor and outdoor air concentrations at equilibrium are given above in Table 2. Estimates of deposition velocities to indoor walls, floor and ceiling are given in Table 4.6, based on measured values (Lange, 1995). As previously mentioned, resuspension will generally have little importance in this context and this contribution can be neglected. Table 4.6 also shows the calculated total deposition on the three types of surface.

Table 4.6. Estimates of indoor deposition velocities on ceiling, floor and walls and estimates of the level of the total deposited contamination on these surfaces.

Radionuclide	$V_{d, ceiling}$	$V_{d, floor}$	$V_{d, wall}$	Ceiling contam. [Bq cm^{-2}]	Floor contam. [Bq cm^{-2}]	Wall contam. [Bq cm^{-2}]
Te-132	2.00E-05	5.00E-04	8.00E-05	2.26E+00	5.66E+01	9.05E+00
Cs-134	2.00E-05	5.00E-04	8.00E-05	1.12E+00	2.79E+01	4.47E+00
Cs-137	2.00E-05	5.00E-04	8.00E-05	2.23E+00	5.56E+01	8.90E+00
Ba-140	5.00E-04	4.00E-03	1.00E-03	8.10E+00	6.48E+01	1.62E+01
Zr-95	5.00E-04	4.00E-03	1.00E-03	2.00E+00	1.60E+01	4.01E+00
Mo-99	2.00E-05	5.00E-04	8.00E-05	6.48E-01	1.62E+01	2.59E+00
Ru-103	2.00E-05	5.00E-04	8.00E-05	6.14E-01	1.54E+01	2.46E+00
Ru-106	2.00E-05	5.00E-04	8.00E-05	1.54E-01	3.85E+00	6.16E-01
Ce-141	5.00E-04	4.00E-03	1.00E-03	2.38E+00	1.90E+01	4.76E+00
Ce-144	5.00E-04	4.00E-03	1.00E-03	1.61E+00	1.28E+01	3.21E+00
Sr-89	5.00E-04	4.00E-03	1.00E-03	9.90E-02	7.92E-01	1.98E-01
Sr-90	5.00E-04	4.00E-03	1.00E-03	1.06E-02	8.46E-02	2.12E-02
Np-239	5.00E-04	4.00E-03	1.00E-03	1.26E+01	1.01E+02	2.52E+01
I-131,e	5.00E-03	5.00E-03	5.00E-03	7.74E+02	7.74E+02	7.74E+02

The above total contamination levels can be used together with information on natural removal and physical half-lives of the contaminants, the fraction of the time spent in the indoor environment (fr) and a dose rate conversion factor, to calculate the contributions to dose from contamination on indoor surfaces, using formula no. 4. The dose rate conversion factors were derived from the Monte Carlo dose rate calculations presented in Appendix A. As mentioned above, people generally seem to spend some 80-95 % of their time indoors. It was therefore assumed in the scenario calculations that fr is 0.9. Based on experimental work carried out by the consortium partners over the years, it is assumed that the natural removal process on walls as well as on the ceiling has a half-life of some 10 years for 1 µm particles and 3 years for 5 µm particles. The natural removal from the floor is assumed to generally occur with a half-life of about 0.5 years. Much shorter half-lives have been reported for Chernobyl contamination on a floor (Allott et al., 1994). However, the indoor contamination was here almost exclusively associated with large soil particles that had inadvertently been brought in from the garden. The calculated doses received per Bq cm^{-2} of each contaminant on the various surfaces in the modelled geometries (see general methodology section) are shown in Tables 4.7 and 4.8.

Table 4.7. Gamma dose conversion factors (D/M_s in formula no. 4) for the various contaminants and surfaces considered. Results for geometries 1 and 2. Doses from walls are per wall.

Radio-nuclide	Geometry 1			Geometry 2				
	Dose conversion factor (wall) [µSv per Bq cm^{-2}]	Dose conversion factor (floor) [µSv per Bq cm^{-2}]	Dose conversion factor (ceiling) [µSv per Bq cm^{-2}]	Dose conversion factor (far wall) [µSv per Bq cm^{-2}]	Dose conversion factor (near wall) [µSv per Bq cm^{-2}]	Dose conversion factor (each other wall) [µSv per Bq cm^{-2}]	Dose conversion factor (floor) [µSv per Bq cm^{-2}]	Dose conversion factor (ceiling) [µSv per Bq cm^{-2}]
Te-132	0.04	0.12	0.09	0.02	0.24	0.04	0.10	0.08
Cs-134	48.33	33.59	103.99	20.67	285.40	40.99	27.16	87.43
Cs-137	93.49	18.25	201.02	39.91	549.89	79.68	14.76	169.27
Ba-140	0.11	0.29	0.23	0.04	0.61	0.09	0.24	0.19
Zr-95	2.67	6.23	5.74	1.14	15.80	2.25	5.04	4.82
Mo-99	0.02	0.07	0.05	0.01	0.13	0.02	0.05	0.04
Ru-103	1.13	2.77	2.42	0.48	6.55	0.98	2.24	2.05
Ru-106	3.73	4.03	8.02	1.59	21.83	3.20	3.26	6.77
Ce-141	0.15	0.37	0.31	0.06	0.83	0.13	0.30	0.27
Ce-144	0.35	0.50	0.74	0.15	1.99	0.30	0.40	0.63
Sr-89	0.00	0.00	0.00	0.00	0.00	0.00	0.00	0.00
Sr-90	0.00	0.00	0.00	0.00	0.00	0.00	0.00	0.00
Np-239	0.01	0.03	0.03	0.00	0.07	0.01	0.03	0.02
I-131,e	0.18	0.51	0.39	0.08	1.03	0.16	0.41	0.33

Table 4.8. Gamma dose conversion factors (D/M_s in formula no. 4) for the various contaminants and surfaces considered. Results for geometries 3, 4 and 5. Doses from walls are per wall.

Radio-nuclide	Geometry 3			Geometry 4			Geometry 5
	Dose conversion factor (wall) [µSv per Bq cm^{-2}]	Dose conversion factor (floor) [µSv per Bq cm^{-2}]	Dose conversion factor (ceiling) [µSv per Bq cm^{-2}]	Dose conversion factor (wall) [µSv per Bq cm^{-2}]	Dose conversion factor (floor) [µSv per Bq cm^{-2}]	Dose conversion factor (ceiling) [µSv per Bq cm^{-2}]	Dose conversion factor (floor) [µSv per Bq cm^{-2}]
Te-132	0.02	0.25	0.20	0.07	0.06	0.04	0.08
Cs-134	21.61	68.68	229.99	76.95	16.79	42.28	20.26
Cs-137	41.98	37.27	443.68	148.89	9.14	81.89	11.05
Ba-140	0.05	0.60	0.50	0.17	0.15	0.09	0.18
Zr-95	1.19	12.75	12.72	4.25	3.11	2.33	3.75
Mo-99	0.01	0.14	0.11	0.04	0.03	0.02	0.04
Ru-103	0.51	5.63	5.31	1.80	1.39	0.99	1.70
Ru-106	1.69	8.23	17.64	5.95	2.03	3.27	2.46
Ce-141	0.07	0.75	0.68	0.23	0.19	0.13	0.23
Ce-144	0.16	1.01	1.62	0.55	0.25	0.31	0.31
Sr-89	0.00	0.00	0.00	0.00	0.00	0.00	0.00
Sr-90	0.00	0.00	0.00	0.00	0.00	0.00	0.00
Np-239	0.01	0.07	0.05	0.02	0.02	0.01	0.02
I-131,e	0.08	1.02	0.84	0.29	0.26	0.16	0.31

For the considered scenario, the doses can be found by multiplying the dose conversion factors in Tables 4.7 and 4.8 by the contamination levels given in Table 4.6. These results are shown in Tables 4.9 and 4.10.

Table 4.9. Gamma doses received from the various contaminants and surfaces considered. Results for geometries 1 and 2. Also estimates of the sum of the various radionuclide contributions to the dose from a surface and the total dose from the indoor surfaces are shown.

Radio-nuclide	Geometry 1			Geometry 2				
	Dose (each wall) [mSv]	Dose (floor) [mSv]	Dose (ceiling) [mSv]	Dose (far wall) [mSv]	Dose (near wall) [mSv]	Dose (each other wall) [mSv]	Dose (floor) [mSv]	Dose (ceiling) [mSv]
Te-132	3.9E-04	6.9E-03	2.1E-04	1.6E-04	2.2E-03	3.5E-04	5.6E-03	1.8E-04
Cs-134	2.2E-01	9.4E-01	1.2E-01	9.2E-02	1.3E+00	1.8E-01	7.6E-01	9.8E-02
Cs-137	8.3E-01	1.0E+00	4.5E-01	3.6E-01	4.9E+00	7.1E-01	8.2E-01	3.8E-01
Ba-140	1.7E-03	1.9E-02	1.8E-03	7.3E-04	9.9E-03	1.5E-03	1.5E-02	1.6E-03
Zr-95	1.1E-02	1.0E-01	1.2E-02	4.6E-03	6.3E-02	9.0E-03	8.1E-02	9.7E-03
Mo-99	5.8E-05	1.1E-03	3.1E-05	2.5E-05	3.4E-04	4.9E-05	8.7E-04	2.6E-05
Ru-103	2.8E-03	4.3E-02	1.5E-03	1.2E-03	1.6E-02	2.4E-03	3.4E-02	1.3E-03
Ru-106	2.3E-03	1.6E-02	1.2E-03	9.8E-04	1.3E-02	2.0E-03	1.3E-02	1.0E-03
Ce-141	7.0E-04	7.1E-03	7.5E-04	2.9E-04	3.9E-03	6.3E-04	5.7E-03	6.4E-04
Ce-144	1.1E-03	6.4E-03	1.2E-03	4.7E-04	6.4E-03	9.8E-04	5.2E-03	1.0E-03
Sr-89	0	0	0	0	0	0	0	0
Sr-90	0	0	0	0	0	0	0	0
Np-239	3.0E-04	3.4E-03	3.2E-04	1.2E-04	1.7E-03	2.6E-04	2.8E-03	2.7E-04
I-131,e	1.4E-01	3.9E-01	3.0E-01	5.9E-02	8.0E-01	1.2E-01	3.2E-01	2.5E-01
SUM	1.2E+00	2.5E+00	8.8E-01	5.1E-01	7.1E+00	1.0E+00	2.1E+00	7.4E-01
TOTAL		8.2E+00				1.2E+01		

Table 4.10. Gamma doses received from the various contaminants and surfaces considered. Results for geometries 3, 4 and 5. Also estimates of the sum of the various radionuclide contributions to the dose from a surface and the total dose from the indoor surfaces are shown.

Radio-nuclide	Geometry 3			Geometry 4			Geometry 5
	Dose (each wall) [mSv]	Dose (floor) [mSv]	Dose (ceiling) [mSv]	Dose (each wall) [mSv]	Dose (floor) [mSv]	Dose (ceiling) [mSv]	Dose (floor) [mSv]
Te-132	1.8E-04	1.4E-02	4.5E-04	6.2E-04	3.5E-03	8.6E-05	4.3E-03
Cs-134	9.6E-02	1.9E+00	2.6E-01	3.4E-01	4.7E-01	4.7E-02	5.7E-01
Cs-137	3.7E-01	2.1E+00	9.9E-01	1.3E+00	5.1E-01	1.8E-01	6.2E-01
Ba-140	7.8E-04	3.9E-02	4.0E-03	2.7E-03	9.6E-03	7.5E-04	1.2E-02
Zr-95	4.8E-03	2.0E-01	2.5E-02	1.7E-02	5.0E-02	4.7E-03	6.0E-02
Mo-99	2.6E-05	2.2E-03	6.9E-05	9.3E-05	5.4E-04	1.3E-05	6.5E-04
Ru-103	1.3E-03	8.6E-02	3.3E-03	4.4E-03	2.1E-02	6.1E-04	2.6E-02
Ru-106	1.0E-03	3.2E-02	2.7E-03	3.7E-03	7.8E-03	5.0E-04	9.5E-03
Ce-141	3.3E-04	1.4E-02	1.6E-03	1.1E-03	3.6E-03	3.1E-04	4.5E-03
Ce-144	5.1E-04	1.3E-02	2.6E-03	1.8E-03	3.2E-03	4.9E-04	4.0E-03
Sr-89	0	0	0	0	0	0	0
Sr-90	0	0	0	0	0	0	0
Np-239	1.4E-04	6.9E-03	6.9E-04	4.7E-04	1.7E-03	1.3E-04	2.1E-03
I-131,e	6.4E-02	7.9E-01	6.5E-01	2.2E-01	2.0E-01	1.2E-01	2.4E-01
SUM	5.4E-01	5.2E+00	1.9E+00	1.9E+00	1.3E+00	3.6E-01	1.5E+00
TOTAL		9.3E+00			9.3E+00		-

As can be seen from Tables 4.9 and 4.10, the total doses are fairly invariable, regardless of the dimensions of the room and the position of the person in the room, although the contributions from the individual surfaces vary considerably. The estimated doses, of the order of 10 mSv in total, are high, although they are received over a

period of several years. The main contributions to these doses are generally from the radiocaesium contaminants. As can be seen by comparing the dose from the floor contamination for geometries 1 and 5, an ordinary bed provides significant shielding against the radiation from the floor. Although the person in geometry 5 lies in a bed only 45 cm above the ground, whereas the dose is in geometry 1 received at a height of 1 m, the shielding effect is still pronounced. This work is believed to represent the first ever detailed account of gamma dose contributions from indoor contamination. To strengthen the model, there is a need, in particular, for investigations of the possible factor influences on the deposition velocities to the indoor surfaces, and of variations in the natural removal processes of the relevant contaminants in the indoor environment. Also parameters determining beta doses from indoor contamination constitute an area, which merits experimental investigations.

4.2.5 Skin contact transfer

As discussed above, the significance of doses from contact transfer of pollutants from a contaminated indoor surface to the skin strongly depends on the time when the contaminated surface is touched. The 'worst case' would be one, where the total contamination of the surface through airborne deposition has occurred, and the surface has not to any significant extent been subjected to natural clearance or forced cleaning processes. As the deposition in this case occurred over a period of several weeks, this would not be considered to be very likely in reality, but the results of a calculation based on the assumption would form a suitably conservative estimate of the doses that could be received through contact transfer. Estimates of the levels of total time-integrated deposition on a horizontal surface (e.g., a table or the floor) are given in Table 4.11, based on the time-integrated air concentrations assumed in the scenario. The contact transfer factors given in the table reflect a situation where the skin is moist and the contamination forms a very thin layer on the surface that is touched. This has importance for the smaller particulates and for elemental iodine. The transferred contamination per unit of area of skin are compared with the corresponding total airborne skin deposition. As can be seen, the relationship is about 0.3 for the radionuclides that generally contribute most to dose in this scenario. However, it is likely that this relationship would in most realistic cases be significantly less than 0.3. It should also be taken into account that a fraction of the smallest particles would, by the time that the contact transfer occurs, be associated with larger dust particles, which would have considerably shorter retention half-life on the skin than would the directly deposited skin contamination.

Table 4.11. Conservative estimates of total contamination levels on a horizontal surface that comes into contact with skin shown together with contact transfer factors (TF) for moist skin, and calculated skin contamination through contact transfer and through airborne deposition.

Radionuclide	Contamination on horizontal surface [Bq cm^{-2}]	TF (moist)	Transferred skin contamination [Bq cm^{-2}]	Corresp. direct skin contamination [Bq cm^{-2}]	Relationship (transfer to skin/ deposition to skin)
Te-132	57	0.6	34	110	0.31
Cs-134	28	0.6	17	56	0.30
Cs-137	56	0.6	33	110	0.30
Ba-140	65	0.3	19	190	0.10
Zr-95	16	0.3	5	48	0.10
Mo-99	16	0.6	10	32	0.30
Ru-103	15	0.6	9	31	0.30
Ru-106	4	0.6	2	8	0.30
Ce-141	19	0.3	6	57	0.10
Ce-144	13	0.3	4	39	0.10
Sr-89	1	0.3	0	2	0.10
Sr-90	0.1	0.3	0.0	0	0.10
Np-239	101	0.3	30	300	0.10
I-131,e	774	0.6	465	1600	0.29

Although the contact transfer contribution to dose in this case is not highly significant compared with that of the airborne skin contamination, skin contact transfer may be highly important in other scenarios, such as handling/spillage of open sources or decommissioning.

4.2.6 Inhalation of contamination (taking into account resuspension)

For the calculation of doses from inhalation during the plume passage and inhalation of resuspended contaminated dust, formula no. 7 was applied. The relevant integrated air concentrations were calculated as above in connection with the other dose contributions in the scenario. The assumed inhalation rates are mentioned in the 'general methodology' section. Age-dependent dose coefficients (see Table 4.12) were taken from ICRP 72 (1995). It was assumed that contaminants associated with condensation particles are relatively quickly absorbed, whereas the non-volatile contaminants are taken to be absorbed over a moderately long period. ICRP publication 72 also contains dose coefficient parameters for elemental iodine gas. To illustrate some age-dependent differences in the doses, committed inhalation doses were calculated for 5-year-old children, as well as for what was considered to be 'typical' adult males and females. As can be seen in Table 4.12, these doses are to a large extent dominated by the contributions from elemental ^{131}I.

The above Table 4.3 clearly shows that the contribution of resuspended contaminants to the total time-integrated pollutant air concentration – and thereby to the inhalation dose – will under normal circumstances be rather insignificant in this type of scenario.

Table 4.12. Assumed inhalation rates, committed inhalation dose coefficients and calculated committed inhalation dose in the scenario, for 5 year old children, male and female adults.

Radionuclide	Inhalation rate (5 year old child) [m^3 s^{-1}]	Inhalation rate (Female adult) [m^3 s^{-1}]	Inhalation rate (Male adult) [m^3 s^{-1}]	Committed inhalation dose coeff. (5-year old) [Sv Bq^{-1}]	Committed inhalation dose coeff. (Adult) [Sv Bq^{-1}]	Committed inhalation dose (5-year old) [mSv]	Committed inhalation dose (Female adult) [mSv]	Committed inhalation dose (Male adult) [mSv]
Te-132	2.0E-04	2.5E-04	3.0E-04	8.50E-09	1.80E-09	2.0E+00	5.2E-01	6.2E-01
Cs-134	2.0E-04	2.5E-04	3.0E-04	5.20E-09	6.60E-09	5.7E-01	9.1E-01	1.1E+00
Cs-137	2.0E-04	2.5E-04	3.0E-04	3.60E-09	4.60E-09	7.9E-01	1.3E+00	1.5E+00
Ba-140	2.0E-04	2.5E-04	3.0E-04	1.10E-08	5.10E-09	3.7E-01	2.1E-01	2.6E-01
Zr-95	2.0E-04	2.5E-04	3.0E-04	9.70E-09	4.80E-09	7.7E-02	4.8E-02	5.7E-02
Mo-99	2.0E-04	2.5E-04	3.0E-04	7.70E-10	2.20E-10	5.0E-02	1.8E-02	2.1E-02
Ru-103	2.0E-04	2.5E-04	3.0E-04	1.50E-09	4.80E-10	8.9E-02	3.6E-02	4.3E-02
Ru-106	2.0E-04	2.5E-04	3.0E-04	2.60E-08	7.90E-09	4.1E-01	1.5E-01	1.9E-01
Ce-141	2.0E-04	2.5E-04	3.0E-04	6.30E-09	3.20E-09	6.0E-02	3.8E-02	4.6E-02
Ce-144	2.0E-04	2.5E-04	3.0E-04	8.80E-08	4.00E-08	5.7E-01	3.2E-01	3.9E-01
Sr-89	2.0E-04	2.5E-04	3.0E-04	1.30E-08	6.10E-09	5.3E-03	3.1E-03	3.7E-03
Sr-90	2.0E-04	2.5E-04	3.0E-04	6.50E-08	3.60E-08	2.8E-03	1.9E-03	2.3E-03
Np-239	2.0E-04	2.5E-04	3.0E-04	2.00E-09	9.30E-10	1.0E-01	5.9E-02	7.0E-02
I-131,e	2.0E-04	2.5E-04	3.0E-04	5.00E-08	2.00E-08	1.5E+01	7.7E+00	9.2E+00
Total	-	-	-	-	-	2.0E+01	1.1E+01	1.4E+01

4.3 Dosimetric modelling – discussion

The above modelling scenario serves as an illustrative example of how the developed methodology can be used to assess the significance of an emergency situation involving contamination in the indoor environment. It was found that contributions from contaminant deposition on humans and indoor surfaces may give rise to considerable doses to inhabitants of areas contaminated through dry deposition. Each of these gamma dose contributions would be comparable with the external gamma dose from contaminated outdoor surfaces over one or even several years (Andersson & Roed, 2004), and should obviously be considered in connection with preparedness planning. Also the committed dose from inhalation of contaminants during the passage of the contaminated cloud is important, stressing the need for investigations of methodologies to achieve optimal protection in this context (e.g., application of vacuum-cleaners in forced air cleaning). The subsequent contribution to inhalation dose from resuspended radioactive matter appears to be insignificant in most cases involving a release of this type, but could well be important in other scenarios. Finally, the beta dose contribution from deposition on humans and possibly also from deposition on indoor building surfaces can add significantly to the skin cancer risk. Contact transfer of contaminants to skin was found to play a minor role in the scenario dose assessment, but could be highly significant in other contexts. Generally, elemental iodine and the radiocaesium isotopes contribute most to the doses received in the scenario.

In the following some viewpoints are given regarding other types of thinkable contamination scenarios, where the model methodology may be of use. As stated above, a crucial parameter determining both the deposited concentration and the natural and forced clearance rates of the contaminants on skin and other surfaces is the aerosol size. It is therefore important to characterise the contaminants arising from these other types of incidents with respect to their particle size.

Releases and deposition on humans of radioactive aerosol may also occur in the nuclear working environment. A survey has been conducted of published values of AMAD's of radioactive aerosols measured in working environments (Dorrian & Bailey, 1995). The results covered 52 publications and included a wide variety of industries and other work places. The results were found to be well fitted by a log-normal distribution with a median value of 4.4 µm, supporting the choice of the ICRP Task Group on Human Respiratory Tract Models of a 5 µm default AMAD for occupational exposure. However, obviously, perceivable radiocontaminant aerosols in the working environment may be of different sizes according to the processes that led to their release.

Over the years the world has witnessed a couple of plutonium weapons accidents leading to generation of radioactive atmospheric aerosol. Examples are the Palomares accident in 1966 (Stradling et al., 1998) and the Thule accident in 1968 (Eriksson, 2002). The contamination was in the Thule case found to be in the form of oxide particles with a log-normal size distribution with a median value of about 2 µm (Eriksson, 2002). A small number of hot particles were found to be much larger (of the order of 20 µm or more), but the clearance half-life of such particles from skin or clothing would be extremely short, so that the doses associated with deposition of these particles on, e.g., skin would be expected to be of comparatively minor importance (Andersson et al., 2002). Accidents of this type, which can spread radioactive matter over a considerable area of land (including its inhabitants) have strong parallels to the terrorist radioactive dispersal devices commonly termed 'dirty bombs' (Bunn and Braun, 2003). For instance, bombs containing large amounts of pure beta emitters, such as ^{90}Sr, would be comparatively unproblematic to transport in shielding. If a bomb of this type went off in a city area, the main radiological concern would be related to contaminant inhalation and deposition to humans.

Also non-radioactive dermal exposure may have serious detrimental implications on health. For instance, dermal contact with a range of biocides is known to potentially lead to skin cancer, and dermal exposure to biocides may also lead to dermatoses (Spiewak, 2001). Further, skin penetration of biocides may be great, since some of these contain compounds, which increase absorption by plants, and, adversely, also dermal penetration (Brand & Mueller, 2002). For instance fogger application of pesticides in greenhouses has been reported to lead to generation of aerosol in the ca. 1-10 µm range (Giles et al., 1995). Many of the reported results in this project

would be valuable also in this context, where there is an equal shortage of for instance deposition and clearance parameters.

In the non-radioactive workplace environment, occupational skin disease annually accounts for several million lost working days across Europe. The results of the project may contribute to initiatives for re-organising workplaces within the EU in a way that minimises dermal contamination, by direct and indirect routes. Ultimately, this should result in the eventual reduction of healthcare spending on treatment of skin disease and the reallocation of those resources to the treatment of other important ill-health issues.

The obtained data on resuspension give information relevant to the specialised workplace environment of the clean-room, where micro-electronic components and medical products are manufactured, and where the greatest potential source of product contamination are the clean-room operators themselves.

5 Conclusions

A series of experimental investigations were made to define parameters that may have an important bearing on the doses received from deposition of radioactive contaminants to human skin, hair and clothing. Further, the influences of a number of factors on these parameters were examined, in order to pinpoint the primary sources of variations. This will enable decision makers to estimate a set of parameters that would adequately reflect the specific conditions in a given scenario of interest, and distinguish between parametric variation and uncertainty. Investigations of relevance to doses from contamination on indoor surfaces (e.g., internal walls, floor and ceiling) were also made for different types of indoor scenery. The obtained knowledge was applied in a dose model for the entire contaminated indoor environment, incorporating also contributions from inhalation of primary contaminant particles as well as resuspended contaminated indoor dust. This model is the first of its kind. A modelling scenario demonstrated the developed modelling methodology and showed that a major nuclear power plant accident may lead to rather high doses from contamination on humans as well as from contamination on indoor surfaces and inhalation. The doses were here found to be dominated by the contributions from ^{131}I, ^{137}Cs and ^{134}Cs. In other cases, for instance the transfer of contamination from an indoor surface to human skin by contact may give a highly significant dose. The implications of the findings in relation to a number of different types of contamination scenarios, including non-radioactive aerosol releases, were discussed, and a number of parameters, which merit further investigation, were identified.

References

Allott, R.W., Kelly, M., & Hewitt, C.N. (1994). A model of environmental behaviour of contaminated dust and its application to determining dust fluxes and residence times. *Atmospheric Environment*, 28(4), 679-687.

Andersson, K.G. (1996). Evaluation of Early Phase Nuclear Accident Clean-up Procedures for Nordic Residential Areas, NKS Report NKS/EKO-5(96)18, ISBN 87-550-2250-2.

Andersson, K.G. & Roed, J. (2004). Doses received in a dry-contaminated living area in the Bryansk Region, Russia, since the Chernobyl accident, submitted for publication in J. Environmental Radioactivity, 2004.

Andersson, K.G., Fogh, C.L., Byrne, M.A., Roed, J. & Goddard, A.J.H. (1999). Radiation doses from contaminant aerosol deposition to the human body, Proceedings of the 12th ordinary meeting of the Nordic Society for Radiation Protection, Skagen, Denmark, ISBN 87-550-2617-6, pp. 177-180.

Andersson, K.G., Fogh, C.L., Byrne, M.A., Roed, J., Goddard, A.J.H. & Hotchkiss, S.A.M. (2002). Radiation dose implications of airborne contaminant deposition to humans, Health Physics 82(2), pp. 226-232.

Andersson, K.G., Roed, J., Paretzke, H.G. & Tschiersch, J. (1995). Modelling of the radiological impact of a deposit of artificial radionuclides in inhabited areas, in: Deposition of radionuclides, their subsequent relocation in the environment and resulting implications, J. Tschiersch (editor) EUR 16604 EN, ISBN 92-827-4903-7, pp. 83-94.

Atkins, D.H.F., Chadwick, R.C. & Chamberlain, A.C. (1967). Deposition of radioactive methyl iodide to vegetation, Health Physics 13, pp. 91-92.

Blichmann, C.W. and Seerup, J. (1988). Assessment of skin moisture, Acta Derm Venereol (Stockh.) 68, pp. 284-290.

Blundell, G., Henderson, W.J., Price, E.W. (1989). Soil particles in the tissues of the foot in endemic elephantiasis of the lower legs, Ann. Trop. Med. Parasitol. 83, pp. 381-385.

Braun, W.X., Cicciarelli, B.A., Davidson, D.L., Hart, E.H., Luedtke, A., McIntosh, K., Peoples, P.R. (2002). Indoor pollutant measurement and modelling, comparing impact of surface characteristics. Proceedings of Indoor Air 2002, the 9th International Conference on Indoor Air Quality and Climate, July 2002, Monterey, California, pp 885-890.

Briesmeister, J. (Ed.) (1993). MCNP - A general Monte Carlo N-particle transport code. Users manual. Report LA-12625, Los Alamos National Laboratory, Los Alamos, New Mexico, USA.

Brodsky, A. (1980). Resuspension Factors and Probabilities of Intake of Material in Process (Or "Is 10^{-6} a Magic Number in Health Physics?"). Health Phys. 39(6):992-1000.

Bunn, G. & Braun, C. (2003). Terrorism potential for research reactors compared with power reactors - Nuclear weapons, "dirty bombs", and truck bombs, American Behavioral Scientist 46(6), pp. 714-726.

California Air Resources Board. (2004). www.arb.ca.gov/research/resnotes/notes/94-11.htm.

Camuffo, D. and Bernardi, A. (1996). Deposition of urban pollution on the Ara Pacis, Rome, The Science of the Total Environment 189/190, pp. 235-245.

Cermak, J. E., Cochran, Leighton S. and Leflier, Russ D. (1995). Wind-tunnel modelling of the atmospheric surface layer. Journal of Wind Engineering and Industrial Aerodynamics, Volumes 54-55, pp 505-513.

Chapple, C.-L., Faulkner, K., Marshall, N.W. & Rawlings, D.J. (1994). The implications of ICRP 60 on the monitoring of pregnant hospital staff, Rad. Prot. Dosimetry 54 (3/4), pp. 299-302.

Cline, J.F., Wilson, D.O. & Hungate, F.P. (1965). Effect of physical and biological conditions on deposition and retention of ^{131}I on plants, Health Physics 11, 713-717.

Counihan, J., Armitt, J. (1968). Simulation of Atmospheric Boundary Layer in a Wind Tunnel. Atmospheric Environment 2 (1): pp 49-62.

Cross, W.G., Freedman, N.O. & Wong, P.Y. (1992). Beta ray dose distributions from skin contamination, Rad. Prot. Dosimetry vol. 40, no.3: 149-168.

Devell, L., Tovedal, H., Bergström, U., Appelgren, A., Chyssler, J. & Andersson, L. (1986). Initial observations of fallout from the reactor accident at Chernobyl, Nature 321, pp. 192-193.

Dorrian, M.D. (1997). Particle size distributions of radioactive aerosols in the environment, Rad. Prot. Dosimetry 69 (2), pp. 117-132.

Dorrian, M.D. & Bailey, M.R. (1995). Particle size distributions of radioactive aerosols measured in workplaces, Radiation Protection Dosimetry 60, No. 2, pp. 119-133.

Eriksson, M. (2002). On weapons plutonium in the Arctic environment (Thule, Greenland)", Riso report Riso-R-1321, ISBN 87-550-3006-8, Riso National Laboratory, Denmark.

Faw, R.E. (1992). Absorbed doses to skin from radionuclide sources on the body surface, Health Physics 63 (4), pp. 443-448.

Fogh, C.L. & Andersson, K.G. (2000). Modelling of skin exposure from distributed sources, Ann. Occup. Hyg. vol. 44 (7), pp. 529-532.

Fogh, C.L., Byrne, M.A., Andersson, K.G., Bell, K.F., Roed, J., Goddard, A.J.H., Vollmair, D.V., and Hotchkiss, S.A.M. (1999). Quantitative Measurement of Aerosol Deposition on Skin, Hair and Clothing for Dosimetric Assessment. R-1075 (EN), Riso National Laboratory, Roskilde, Denmark

Fogh, C.L., Byrne, M.A., Roed, J. & Goddard, A.J.H. (1997). Size specific indoor aerosol deposition measurements and derived I/O concentration ratios. Atmospheric Environment, vol. 31, No. 15, pp. 2193-2203.

Friedlander, S.K. (1977). Smoke, dust and haze. John Wiley, New York.

Giles, D.K., Welsh, A., Steinke, W.E. & Saiz, S.G. (1995). Pesticide inhalation exposure, air concentration, and droplet size spectra from greenhouse fogging, Transactions of the ASAE 38(5), pp. 1321-1326.

Gudmundsson, A., Schneider, M., Bohgard, M., Vinzents, P. and Akselsson, K.R. (1997). Deposition of airborne particles onto the human eye: human tunnel studies of the deposition velocity onto the eyes of a mannequin. *J. Aerosol Sci. Vol. 28, No. 6, pp. 1085-1100,.*

Hawley, C.A. (1966). Controlled environmental tests at the National Reactor Testing Station, 1965 progress report, IDO-12047.

Hawley, C.A., Sill, C.W., Voelz, G.L., Islitzer, N.F. (1964). Controlled environmental radioiodine tests, National Reactor Testing Station, IDO-12035.

Hendley, J.O. & Ashe, K.M. (1991). Effect of topical antimicrobial treatment on aerobic-bacteria in the stratum-corneum of human skin, Antimicrobial Agents and Chemotherapy 35 (4), pp. 627-631.

Hodson, M.J., Smith R.J., van Blaaderen A., Crafton T. and O'Neill, C.H. (1994). Detecting Plant Silica Fibres in Animal Tissue by Confocal Fluorescence Microscopy. *Annals of Occupational Hygiene,* 38, No. 2, 149-160.

Hoeger, P.H. & Enzmann, C.C. (2002). Skin physiology of the neonate and young infant: A prospective study of functional skin parameters during early infancy, Pediatric Dermatology 19 (3), pp. 256-262.

Holdstock, P. (1997). The damaging effects of electrostatic discharges from textile surfaces, Journal of Electrostatics 40-1: 529-534.

Hollander, W. and Pohlmann, G. (1991). Measurement of the influence of directed particle motion on the turbulent particle deposition velocity by means of laser-doppler anemometry. Particle & Particle Systems Characterisation 8(1):12-15.

ICRP (1974). Report of the task group on Reference Man, ICRP Publication 23, International Commission on Radiological Protection, Pergamon Press, Oxford.

ICRP (1990).: 1990 recommendations of the International Commission on Radiological Protection, ICRP Publication 60, ISBN 0 08 041144 4, International Commission on Radiological Protection, Pergamon Press, Oxford.

ICRP (1991). Risks associated with ionising radiations - Five papers prepared by the Task Group of Committee 1 of the International Commission on Radiological Protection, International Commission on Radiological Protection, Pergamon Press, Oxford.

ICRP (1992). The biological basis for dose limitation in the skin, ICRP Publication 59, ISBN 0 08 041143 6, International Commission on Radiological Protection, Pergamon Press, Oxford.

ICRP (1995). International Commission on Radiological Protection, Publication 72: Age-dependent doses to members of the public from intake of radionuclides: part 5 – compilation of ingestion and inhalation dose coefficients, Pergamon Press, ISBN 0 08 042737 5.

ICRU: "Report 56 - Dosimetry of External Beta Rays for Radiation Protection", International Commission on Radiation Units and Measurements, 7910 Woodmont Avenue, Bethesda, Maryland, USA, ISBN 0-913394-55-6, 1997.

Jenkins, P.L., Phillips, T.J., Mulberg, E.J. & Hui, S.P. (1992). Activity patterns of Californians: Use of and proximity to indoor pollutant sources, Atmospheric Environment vol. 26A (12), pp. 2141-2148.

Jost, D.T., Gäggeler, H.W., Baltensperger, U., Zinder, B. & Haller, P. (1986) Chernobyl fallout in size-fractionated aerosol, Nature 324, pp. 22-23.

Kildeso, J., Vinzents, P., Schneider, T. (1999) A simple method for measuring the potential resuspension of dust from carpets in the indoor environment. Textile Research Journal. 69(3), 169-175.

Kocher, D.C. (1980). Effects of indoor residence on radiation doses from routine releases of radionuclides to the atmosphere, Nuclear Technology, vol. 48, pp. 171-179.

Koprda, V., Harangozó, M. & Bohácik, L. (1998). Permeation of Cs+ ions across skin barriers, J. Radioanalytical and Nuclear Chemistry 229 (1-2), pp. 91-93.

Koprda, V., Harangozó, M. & Kassai, Z. (2000). Transfer of radionuclides across skin barriers of animal skin models in vitro, J. Radioanalytical and Nuclear Chemistry 246 (3), pp. 505-509.

Kousa, A., Kukkonen, J., Karppinen, A. Aarnio, P. & Koskentalo, T. (2002). A model for evaluating the population exposure to ambient air pollution in an urban area, Atmospheric Environment 36, pp. 2109-2119.

Kreyling, W.G. (1992). Intracellular particle dissolution in alveolar macrophages, Environ. Health Persp. 97, pp. 121-126.

Kryshev, I.I. (1996). Dose reconstruction for the areas of Russia affected by ^{131}I contamination, *Radiation Protection Dosimetry* 64 (1/2), 93-96.

Lange, C. (1995). Indoor deposition and the protective effect of houses against airborne pollution, Risø-R-780, Risø National Laboratory.

Lefcoe, N.M. and Inculet, I.I. (1975). Particulates in domestic premises, Arch. Environ. Health, 30, pp. 565-570.

Long, C.M., Suh, H.H., Catalano, P.J. & Koutrakis, P. (2001). Using time- and size-resolved particulate data to quantify indoor penetration and deposition behaviour, Environ. Sci. Technol. 35 (10), 2089-2099.

Miller, K.L., White, W.J., Lang, C.M. & Weidner, W.A. (1985). Skin exposure to I blocks thyroid uptake of ^{131}I, Health Physics 49, pp. 791-794.

Nicholson, K.W. (1988). A review of particle resuspension, Atmospheric Environment 22 (12), pp. 2639-2651.

Nicholson, K.W. (1993). Wind tunnel experiments on the resuspension of particulate material. *Atmospheric Environment.* 27A, No. 2, 181-188.

Opiolka, S. Schmidt, F. and Fissan, H. (1994). Combined effects of electrophoresis and thermophoresis on particle deposition onto flat surfaces, J. Aerosol Science 25(4), pp. 665-671.

Otani, Y., Emi, H., Kanaoka, C. and Kato, K. (1989). Determination of deposition velocity onto a wafer for particles in the size range between 0.03 and 0.8 µm. J. Aerosol Science 20(7), pp. 787-796.

Pacyna, J.M., Johansen, O., Saltbones, J. & Semb, A. (1986). Air radioactivity at selected stations in Norway after the Chernobyl reactor accident, Norwegian Institute for Air Research, Report E-8642, ISBN 82-7247-735-1.

Panofsky, H.A. & Dutton, J.A. (1984). Atmospheric Turbulence. Models and Methods for Engineering Applications, John Wiley & Sons, NY, USA.

Phillips, M. (1980). A force balance model for particle entrainment into a fluid stream, J. Phys. D: Appl. Phys. 13, pp. 221-233.

Plunkett, L.M., Turnbull, D. & Roderiks, J.V. (1992). Differences between adults and children affecting exposure assessment", In: P.S. Guzelian (ed.): Similarities and Differences between Children and Adults: Implications for Risk Assessment", ILSI Press, Washington DC, ISBN 0944398073.

Pushparaja, K.L., Popli, K.L., Kher, R.K., Iyer, M.R. (1992). Evaluation of beta-exposure in a natural uranium processing plant and the beta-dose attenuation of various shielding materials, Radiation Protection Dosimetry 42 (4): 301-305.

Rapp, G.M. (1973) Convective heat transfer and convective coefficients of nude man, cylinders and spheres. ASHRAE Transactions, Vol. 79, part 1, pp 75-87.

Reeks, MW, Reed, J, Hall, D. (1988). On the resuspension of small particles by a turbulent flow, *J. Phys. D: Appl. Phys* 21: 574-589.

Reineking, A., Becker, K.H., Porstendörfer, J. & Wicke, A. (1987). Air activity concentrations and particle size distributions of the Chernobyl aerosol, Rad. Prot. Dosimetry 19 (3), pp. 159-163.

Reist, C.R. (1993). Aerosol Science and Technology. Second Edition, McGraw-Hill, Inc.

Roed, J. (1987). Dry deposition on smooth and rough urban surfaces, Presented at the Post-Chernobyl Workshop, Brussels, 3-5 February, 1987, NKA/AKTU-245(87)1.

Roed, J. (1990). Deposition and removal of radioactive substances in an urban area, Final report of the NKA project AKTU-245, Nordic Liaison Committee for Atomic Energy, Roskilde, Denmark, ISBN 87 7303 514 9.

Roed, J. & Cannell, R.J. (1987). Relationship between indoor and outdoor aerosol concentration following the Chernobyl accident, Radiation Protection Dosimetry 21(1/3), pp. 107-110.

Rohloff, F. & Heinzelmann, M. (1996). Dose rate by photon radiation to the basal layer of the epidermis in the case of skin contamination", Rad. Prot. Dosimetry 63 (1), pp. 15-28.

Rulik, P., Bucina, I. & Malátová, I. (1989). Aerosol particle size distribution in dependence on the type of radionuclide after the Chernobyl accident and in the NPP effluents", Proceedings of the XVth Regional Congress of IRPA, Visby, Gotland, Sweden, pp. 102-107, ISBN 3-88585-668-9, TÜV Verlag Rheinland GmbH, Köln.

Salbu, B. & Oughton, D.H. (1995). Processes affecting the uptake of radioactive species into the environment", Rad. Prot. Dosimetry 62 (1/2), pp. 1-4.

Schaefer, H. & Lademann, J. (2001). The role of follicular penetration, Skin Pharmacol. Appl. Skin Physiol. 14, pp. 23-27.

Sehmel, G.A. (1980). Particle resuspension: A review, Environ. Int. 4, pp. 107-127.

Semwal, S. K. and J. J. Hallauer (1994). Biomechanical modeling: Implementing line-of-action algorithm for human muscles and bones using generalized cylinders. Computers & Graphics, Volume 18, Issue 1, pp 105-112.

Snodgrass, W.R. (1992). Physiological and biochemical differences between adults and children affecting exposure assessment", In: P.S. Guzelian (ed.): Similarities and Differences between Children and Adults: Implications for Risk Assessment, ILSI Press, Washington DC, ISBN 0944398073.

Spiewak, R. (2001). Pesticides as a cause of occupational skin diseases in farmers. Annals of Agricultural and Environmental Medicine, 8(1), pp. 1-5.

Stepanenko, V.F., Gavrilin, Yu.I., Snykov, V.P., Shevchuk, V.E., Göksu, H.Y., Voillequé, P.G. & Orlov, M.Yu. (2002). Elevated exposure rates under inclined birch trees indicate the occurrence of rainfall during radioactive fallout from Chernobyl, *Health Physics* 82(2), 240-243.

Stradling, G.N., Hodgson, S.A., Hodgson, A., Fell, T.P., Iranzo, C.E., Espinoza, A. & Aragon, A. (1998). Dose coefficients and assessment of intake after inhalation of contaminated dusts from Palomares", Radiation Protection Dosimetry 79, No. 1-4, pp. 179-182.

STUK (1986). Second interim report on radiation situation in Finland from 5 to 16 May 1986, STUK report STUK-B-VALO 45, ISBN 951-46-9578-x, Helsinki.

Taylor, D.C., Hussein, E.M.A. & Yuen, P.S. (1997). Skin dose from radionuclide contamination on clothing, Health Physics 72(6): 835-841.

Thatcher, TL, Layton, DW. (1995). Deposition, resuspension and penetration of particles within a residence. *Atmos. Environ.* 29: 1487-1497.

Tierney, M.J. and Quarini, G.L. (1997). Mass transfer by simultaneous dropwise condensation and particle deposition. International Journal of Heat and Mass Transfer 40(3), pp. 727-735.

Tinkle, S.S., Antonini, J.M., Rich, B.A., Roberts, J.R., Salmen, R., De Pree, K. & Adkins, E.J. (2003). Skin as a route of exposure and sensitization in chronic beryllium disease. Environmental Health Perspectives 111 (9): 1202-1208.

Tomasek, M., Rybacek, K. & Wilhelmova, L. (1995). Chemical fraction of radioactive cesium in atmospheric aerosol in Prague after the Chernobyl accident, J. Radioanal. Nucl. Chem., Letters 201 (5), pp. 409-416.

Tomasek, M., Wilhelmova, L. & Horyna, J. (1992). A possible mechanism of airborne CH3131I formation, Proceedings of the CEC/IUR/SCR International Symposium on Radioecology at Znojmo, Czech Rep., pp. 140-142.

Tsai, R. & Liang, L.J. (2001). Correlation for thermophoretic deposition of aerosol particles onto cold plates, J. Aerosol Science, 32 (4), pp. 473-487.

Tschiersch, J. & Georgi, B. (1987). Chernobyl fallout size distribution in urban areas, J. Aerosol Sci. 18 (6), pp. 689-692.

Tsukahara, K., Takema, Y., Moriwaki, S., Fujimura, T. & Imokawa, G. (2001). Diurnal variation affects age-related profile in skin thickness, J. Cosmetic Science 52 (6), pp. 391-397.

Van Blaaderen, A. and Vrij, A. (1992). Synthesis and characterisation of colloidal dispersions of fluorescent monodisperse silica spheres. *Langmuir,* 8, 2921-2931

Appendix A.

Gamma dose conversion factors for contamination on building interior

In this appendix, the results are shown of a series of calculations to determine the dependence on gamma energy of gamma dose rates received from contamination on building interior surfaces. This relationship has been estimated on the basis of photon transport modelling using the MCNP Monte Carlo code. For different dwelling geometries, empirical functions have been derived describing the energy dependence of dose rate contributions originating from contamination on walls, floor and ceiling. Together with information on photon yield and energies for gamma emitting radionuclides this can, according to the following formula be applied to determine the corresponding gamma dose conversion factor for each contaminant radionuclide from homogeneously contaminated indoor walls, floors or ceilings:

$$\Gamma = \sum_{i=energy} D_i y_i ,$$

where y_i is the photon yield for photons with energy i emitted from a given contaminant nuclide, and D_i is the dose rate per photon with energy i emitted per unit of time and area from the contaminant nuclide in question.

Calculations of D have been made for persons staying in contaminated rooms in the following geometries:

In the centre of a 4m by 4m room with a ceiling height of 2.5 m.

In same room, very close to one wall but centred with respect to the perpendicular walls.

In the centre of a 10m by 10m room with a ceiling height of 2.5 m.

In the centre of a 2m by 2m room with a ceiling height of 2.5 m.

All these dose rates were calculated to an ICRU sphere at a reference height of 1m above the floor. However, a further calculation was made, where the ICRU sphere was modelled to be placed on top of a 45 cm high bed.

A.1. D in the centre of a 4m by 4m room with a ceiling height of 2.5 m

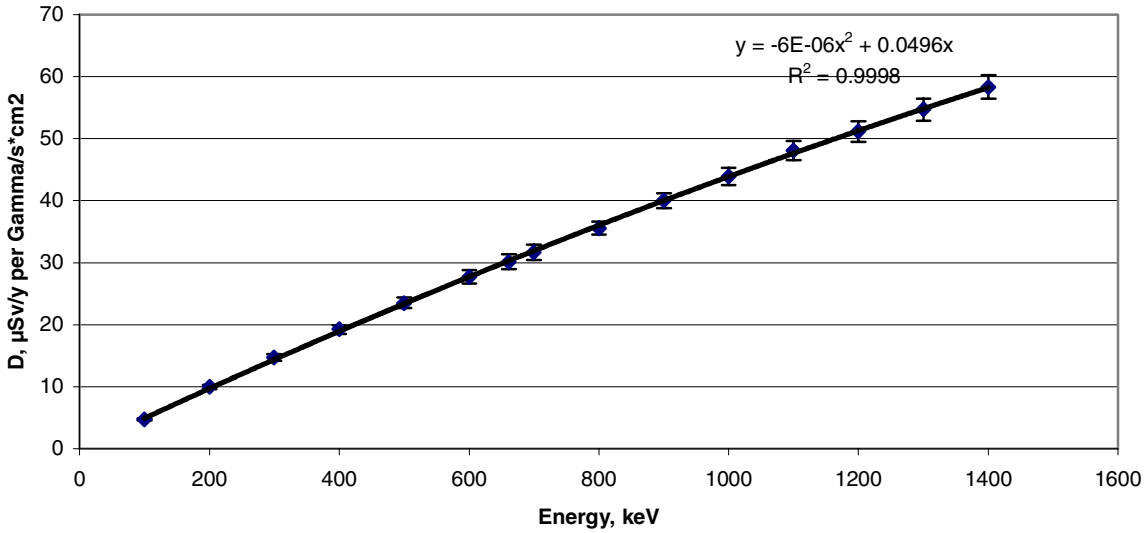

Fig. A.1.a. Geometry 1. Dose rate per gamma photon emitted from each unit of area of the floor, as a function of photon energy. A second order polynomial fit is shown.

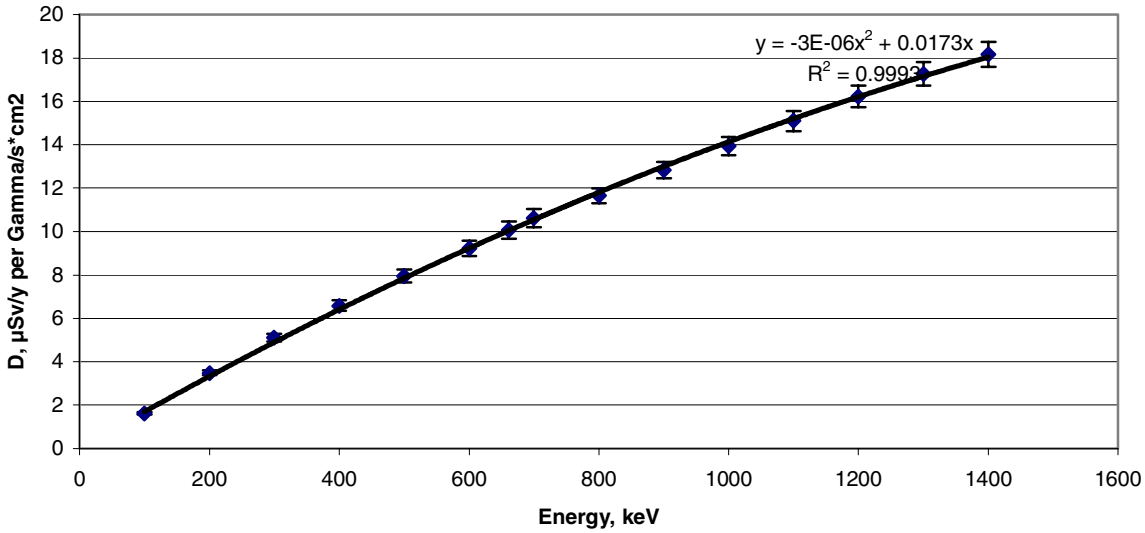

Fig. A.1.b. Geometry 1. Dose rate per gamma photon emitted from each unit of area of a wall, as a function of photon energy. A second order polynomial fit is shown.

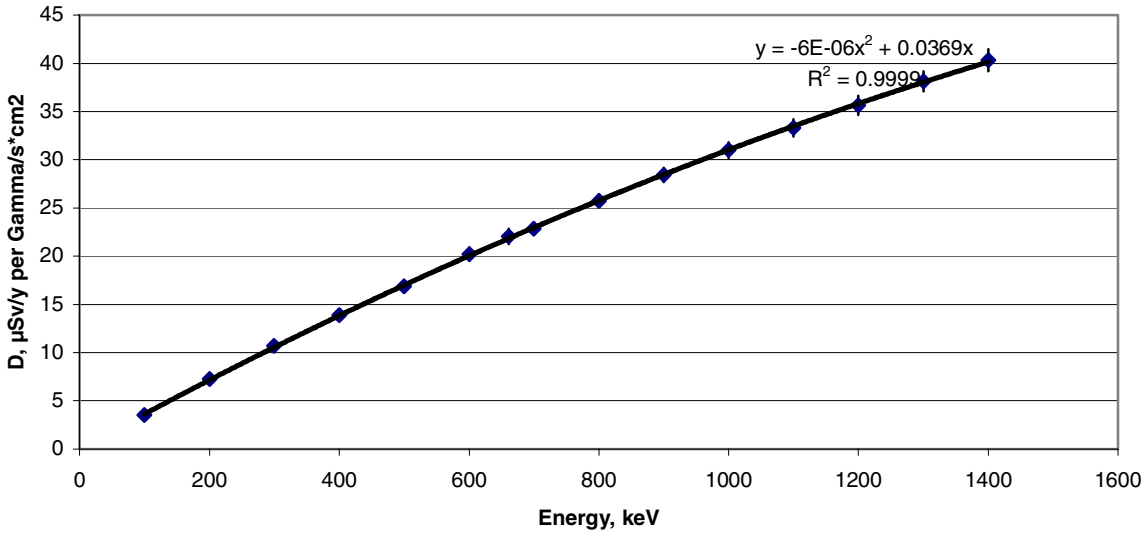

Fig. A.1.c. Geometry 1. Dose rate per gamma photon emitted from each unit of area of the ceiling, as a function of photon energy. A second order polynomial fit is shown.

A.2. D very close to one wall but centred with respect to the perpendicular wall in a 4m by 4m room with a ceiling height of 2.5 m

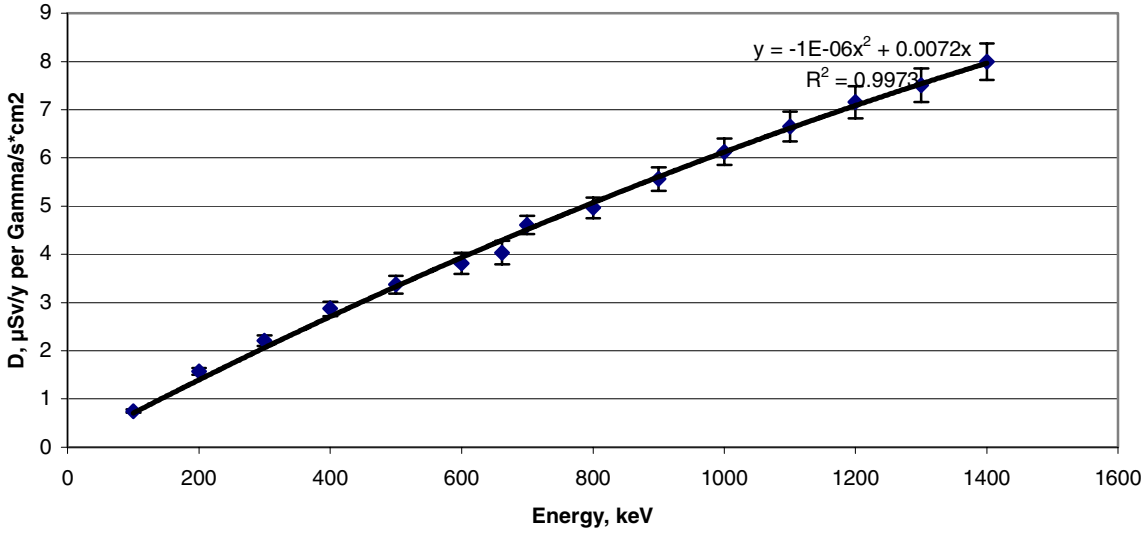

Fig. A.2.a. Geometry 2. Dose rate per gamma photon emitted from each unit of area of the most distant wall, as a function of photon energy. A second order polynomial fit is shown.

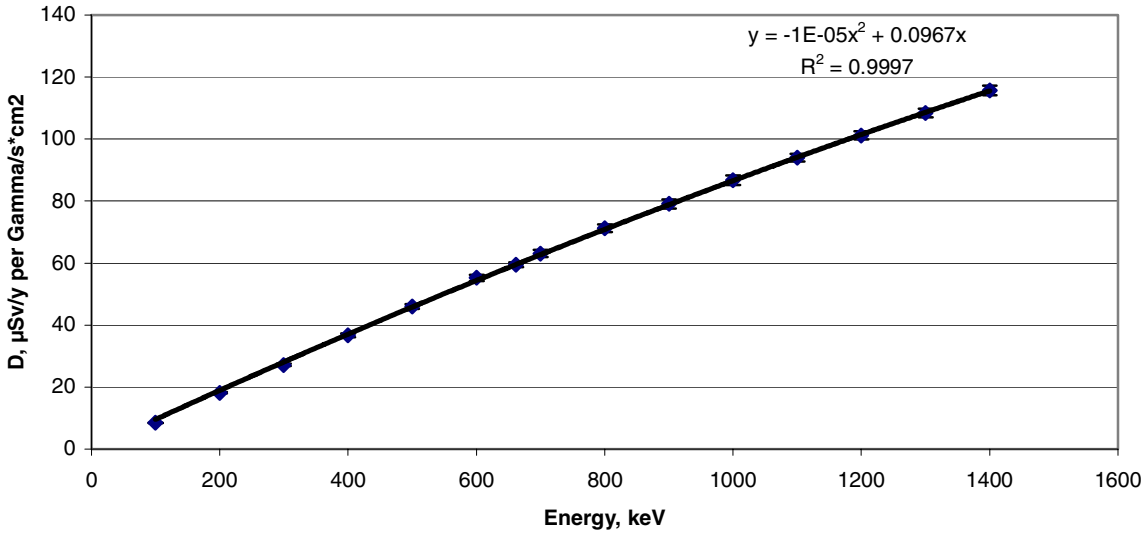

Fig. A.2.b. Geometry 2. Dose rate per gamma photon emitted from each unit of area of the nearest wall, as a function of photon energy. A second order polynomial fit is shown.

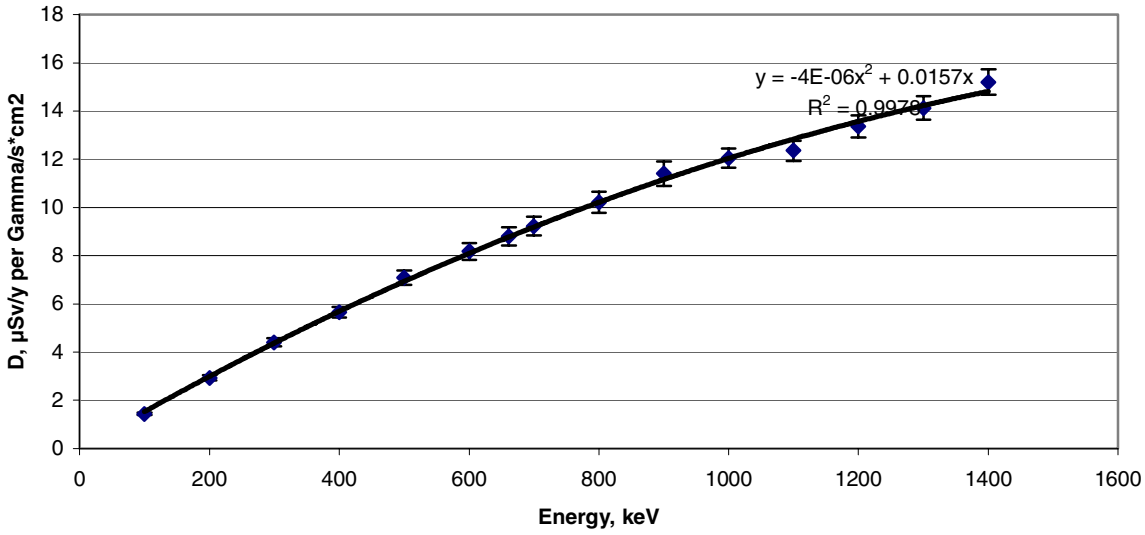

Fig. A.2.c. Geometry 2. Dose rate per gamma photon emitted from each unit of area of one of the other two walls, as a function of photon energy. A second order polynomial fit is shown.

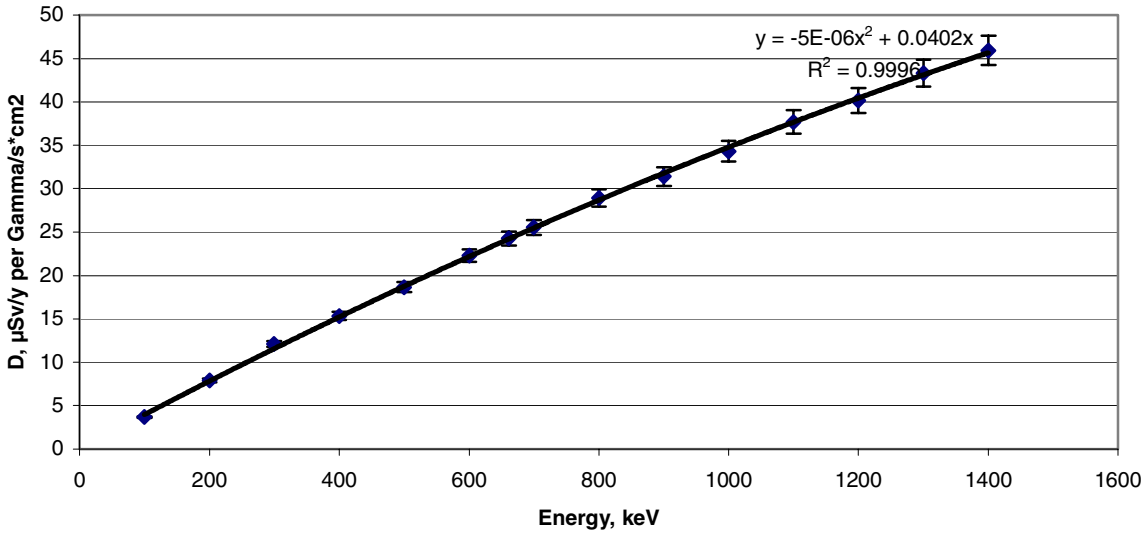

Fig. A.2.d. Geometry 2. Dose rate per gamma photon emitted from each unit of area of the floor, as a function of photon energy. A second order polynomial fit is shown.

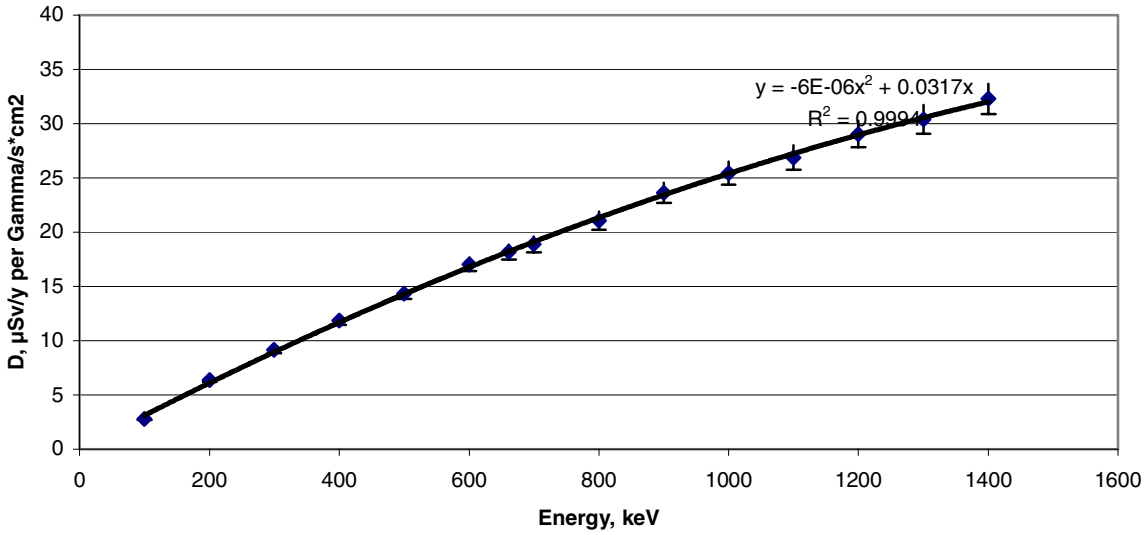

Fig. A.2.e. Geometry 2. Dose rate per gamma photon emitted from each unit of area of the ceiling, as a function of photon energy. A second order polynomial fit is shown.

A.3. D in the centre of a 10m by 10m room with a ceiling height of 2.5 m

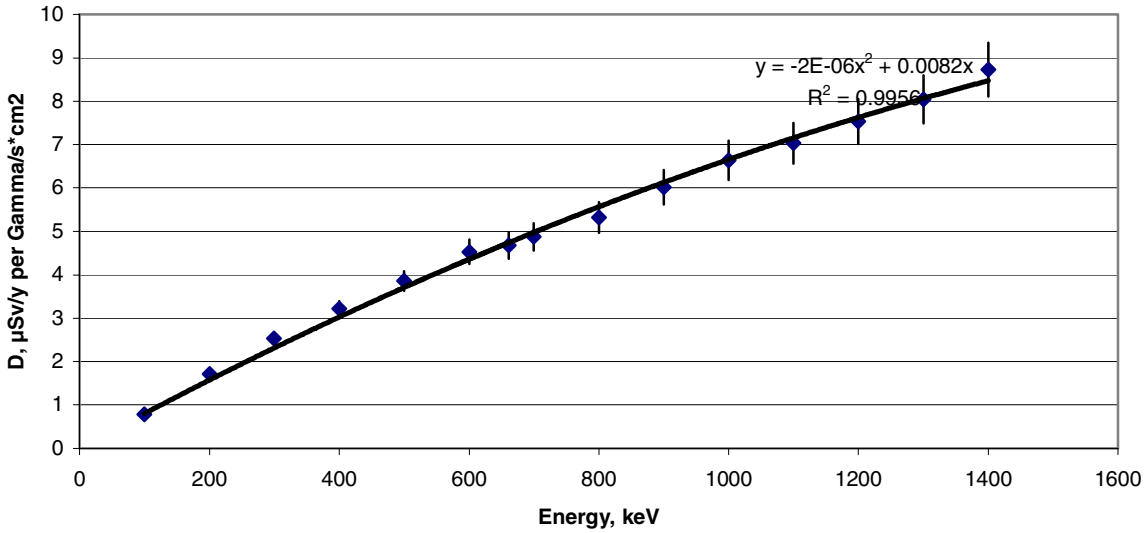

Fig. A.3.a. Geometry 3. Dose rate per gamma photon emitted from each unit of area of a wall, as a function of photon energy. A second order polynomial fit is shown.

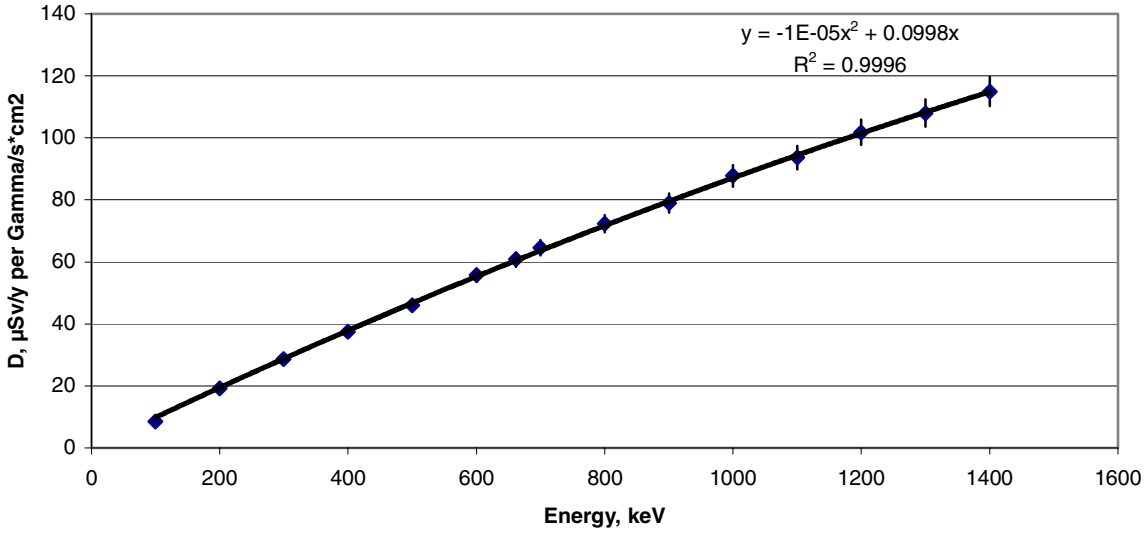

Fig. A.3.b. Geometry 3. Dose rate per gamma photon emitted from each unit of area of the floor, as a function of photon energy. A second order polynomial fit is shown.

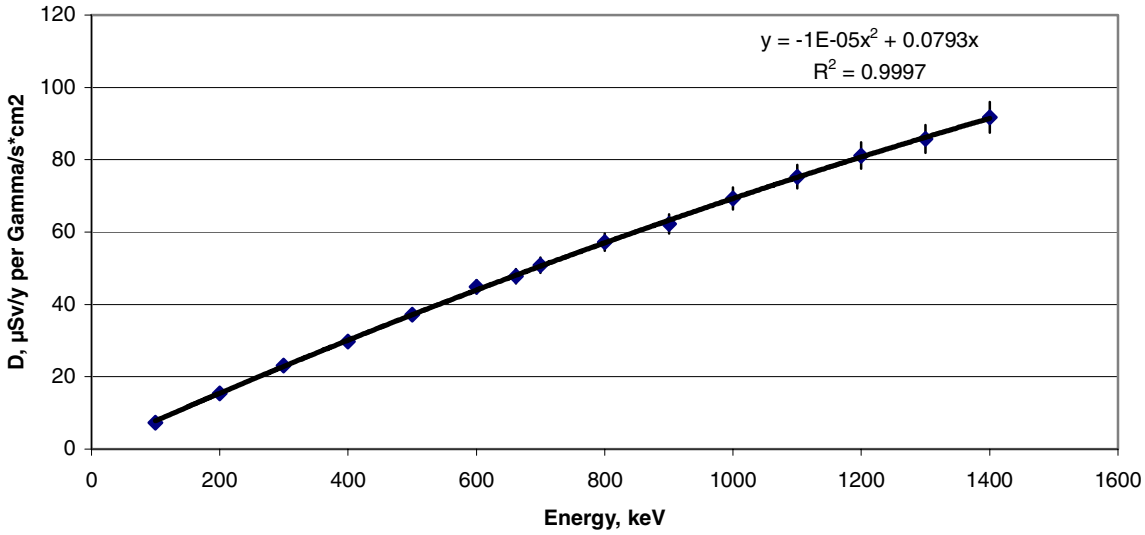

Fig. A.3.c. Geometry 3. Dose rate per gamma photon emitted from each unit of area of the ceiling, as a function of photon energy. A second order polynomial fit is shown.

A.4. D in the centre of a 2m by 2m room with a ceiling height of 2.5 m

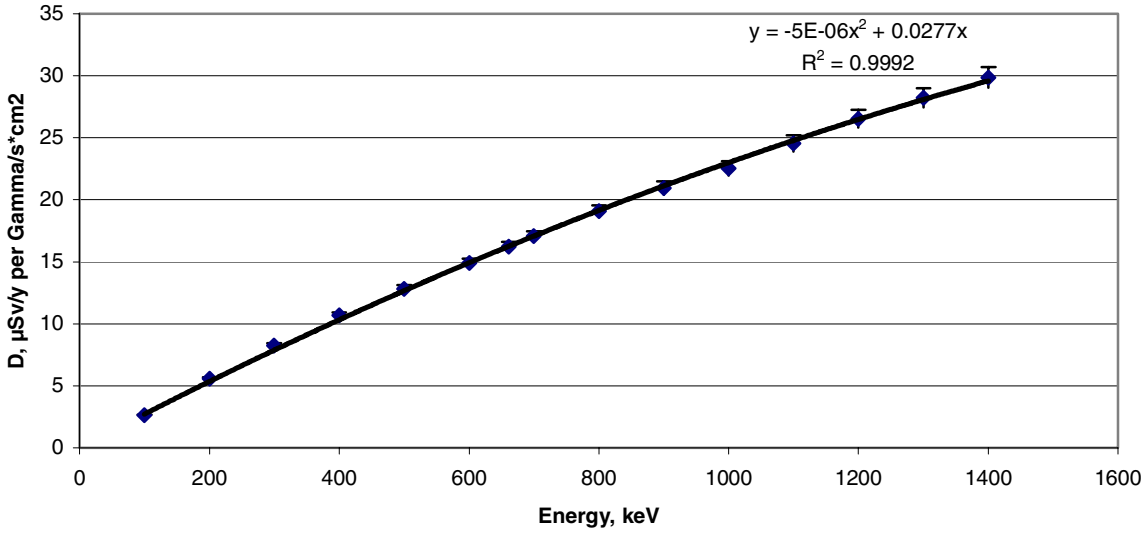

Fig. A.4.a. Geometry 4. Dose rate per gamma photon emitted from each unit of area of a wall, as a function of photon energy. A second order polynomial fit is shown.

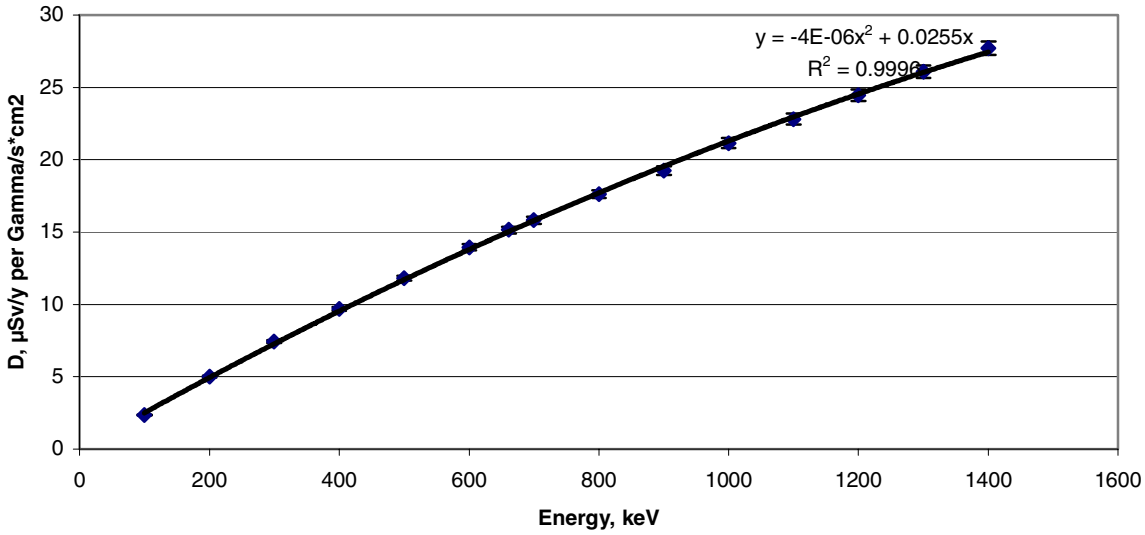

Fig. A.4.b. Geometry 4. Dose rate per gamma photon emitted from each unit of area of the floor, as a function of photon energy. A second order polynomial fit is shown.

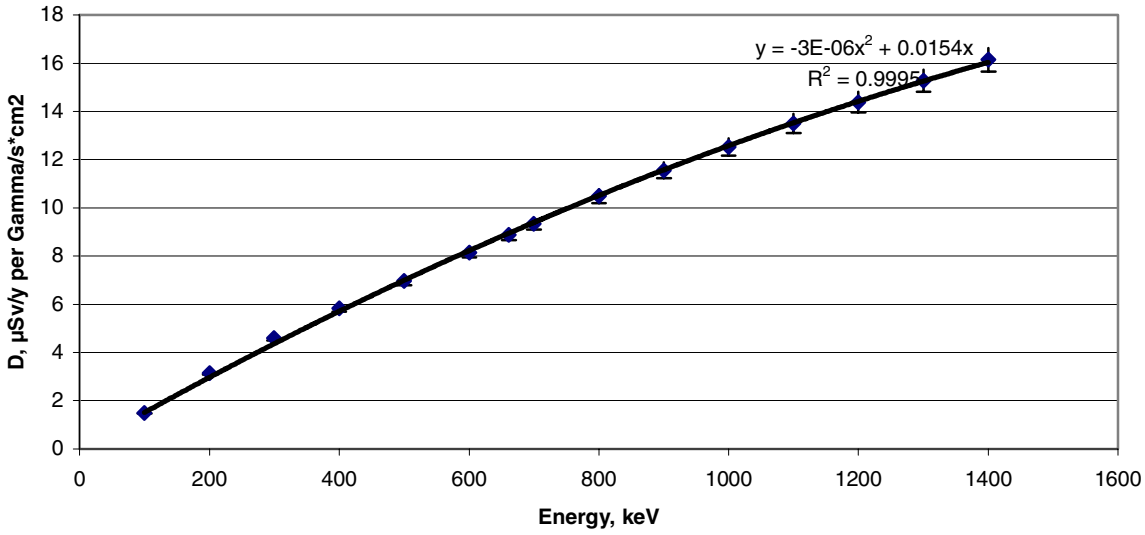

Fig. A.4.c. Geometry 4. Dose rate per gamma photon emitted from each unit of area of the ceiling, as a function of photon energy. A second order polynomial fit is shown.

A.5. D from the floor to a person in a bed in the centre of a 4m by 4m room with a ceiling height of 2.5 m

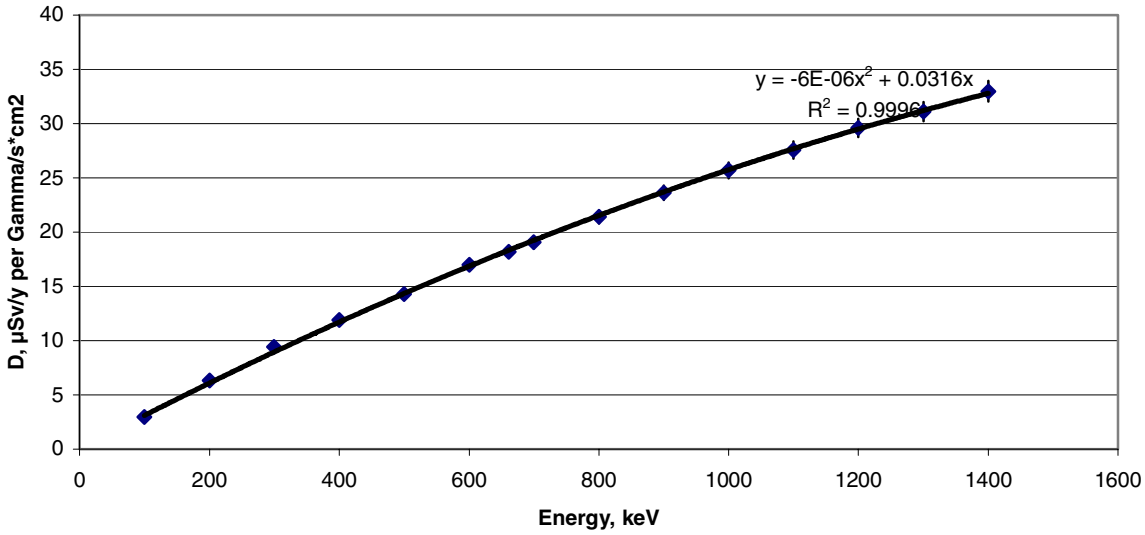

Fig. A.5. Geometry 5. Dose rate per gamma photon emitted from each unit of area of the floor, as a function of photon energy. A second order polynomial fit is shown.

Mission

To promote an innovative and environmentally sustainable technological development within the areas of energy, industrial technology and bioproduction through research, innovation and advisory services.

Vision

Risø's research **shall extend the boundaries** for the understanding of nature's processes and interactions right down to the molecular nanoscale.

The results obtained shall **set new trends** for the development of sustainable technologies within the fields of energy, industrial technology and biotechnology.

The efforts made **shall benefit** Danish society and lead to the development of new multi-billion industries.